Appendix A.17:

Sandown Cres – CPT 15498

Table 1: Site Description for Sandown Crescent (CPT 15498 – CC LIQ 11).

Attribute	Yes/No			Description/Date	Symbol in Figure 1
	10-m Buffer	20-m Buffer	50-m Buffer		
Near a body of surface water or other free face features?	No	No	No	The site is situated on the inside of the meander of the Avon River and its center is 504 m away from the nearest free-face feature, which is ~2.5 m high and oriented in the NW-SE direction.	NA
Lateral spreading observed during the CES?	No	No	No	Absence of ground cracks indicates no lateral spreading, as observed by the mapping team.[1]	NA
Nearby buildings or structures?	Yes	Yes	Yes	Building coverage of the 10-m, 20-m, and 50-m buffers is 22%, 15%, and 22%, respectively. Buildings are in the E portion of the 10-m and 20-m buffers and in all quadrants of the 50-m buffer.	White Fill + Brown Outline
Sloping land?	No	No	No	Flat land, residential area.	NA
Step changes in the ground surface?	No	No	No	NA	NA
Retaining walls?	No	No	No	NA	NA
Vegetation?	Yes	Yes	Yes	Trees and bushes cover 33% of the 10-m buffer, 25% of the 20-m buffer and 24% of the 50-m buffer. They are in all quadrants of the three buffers.	White Fill + Green Outline
Manmade changes to the site between the LiDAR surveys?	No	No	Yes	Removal of a building in the SE quadrant of the 50-m buffer between Jan 2015 and Jun 2015 and addition of a new building at the same property by Sep 2015.	Building Removal in 2015: Orange Crossline
Other important factors?	Yes	Yes	Yes	Low-motor-vehicle-volume roadway occupies 23% of the 20-m buffer and 12% of the 50-m buffer and stretches throughout the E half of the 20-m buffer and throughout all quadrants of the 50-m buffer. Drying rack is in the N portion of the 10-m and 20-m buffers. Swing is in the NW quadrant of the 50-m buffer. The road is at a lower elevation than the surrounding properties by ~0.5 m.	Road: Gray Fill + Red Outline; Drying Rack: White Fill + Purple Outline; Swing: White Fill + Yellow Outline

Note: Buffer is the area within a circle of a specified radius with CPT investigations done at its center (172.708479°, -43.509917°).

[1] Canterbury Geotechnical Database. (2012). "Observed Ground Crack Locations", Map Layer CGD0400 - 23 July 2012, retrieved July 09, 2018 from https://canterburygeotechnicaldatabase.projectorbit.com/

Figure 1: Site plan with areas where LiDAR survey data is considered.

Note 1: Six patches (outlined in red) in the free field were initially selected for settlement assessment as areas free of vegetation and structures. Further analyses such as proximity of a patch to a CPT, proximity of a patch to a property subjected to addition and/or demolition of a structure, front yard/backyard alterations (e.g., ploughing, rubble, scrap), aerial distribution of sediment ejecta, and density of LiDAR points for 2003 resulted in Patches A and B being selected for detailed settlement assessment and other patches being discarded in detailed settlement assessment. In addition, since significant amounts of ejecta were observed on roads in the CES, the entire portion of the road within the 50-m buffer was considered for settlement assessment. Roads as hard, relatively flat surfaces provide many ground-classified points. Therefore, it is very useful to compare settlement estimates on roads with settlement estimates for the unpaved patches.

Table 2: LiDAR flight error adjustments, global adjustments for the difference between average LiDAR point elevations and benchmark survey elevations, and vertical tectonic movement adjustments.

	Adjustments (mm)		
Earthquake Event(s)	LiDAR Flight Error	Global Offset[2]	Tectonic Vertical Movement
Sep-10	-100	-3	0
Feb-11	0	16	-20
Jun-11	0	38	-50
Dec-11	0	-65	10
CES	-100	-14	-60
Post Sep 2010 LiDAR survey affected by ejecta?*			Yes

Note: The negative sign indicates the subtraction from the ground surface subsidence, while the positive sign indicates the addition to the ground surface subsidence; * indicates the presence of ejecta on the road at the time of March 2011 (and potentially May 2011) LiDAR survey based on the satellite image from 8 March 2011, which resulted in the underestimate of the ground surface subsidence due to the Feb-11 EQ hence 30 mm for Road will be added to the raw LiDAR-based ground surface subsidence for the Feb-11 EQ and subtracted from the raw LiDAR-based ground surface subsidence for the Jun-11 EQ.

Table 3a: LiDAR Measurement Error for Patch A.

Surveys	Buffer	Area Averaged Difference Indicating Repeat Measurement Error (mm)	$\sigma^*_{\text{individual LiDAR points}}$ (mm)	%Reduction in σ due to Area Averaging of LiDAR Points
Post Feb 2011: Mar 2011 and May 2011	10-m	81	59	[137,137]
	20-m	81		
	50-m	81		
Post Dec 2011: Feb 2012 and Oct 2015	10-m	15	70	[21,21]
	20-m	15		
	50-m	15		

*Standard deviation.

[2] Russell, J., & van Ballegooy, S. (2015). *Canterbury Earthquake Sequence: Increased liquefaction vulnerability assessment methodology*. New Zealand: Tonkin & Taylor Ltd.

Table 3b: LiDAR Measurement Error for Patch B.

Surveys	Buffer	Area Averaged Difference Indicating Repeat Measurement Error (mm)	$\sigma^*_{individual\ LiDAR\ points}$ (mm)	%Reduction in σ due to Area Averaging of LiDAR Points
Post Feb 2011: Mar 2011 and May 2011	10-m	NA	59	[144,144]
	20-m	NA		
	50-m	85		
Post Dec 2011: Feb 2012 and Oct 2015	10-m	NA	70	[20,20]
	20-m	NA		
	50-m	14		

*Standard deviation.

Table 3c: LiDAR Measurement Error for Road.

Surveys	Buffer	Area Averaged Difference Indicating Repeat Measurement Error (mm)	$\sigma^*_{individual\ LiDAR\ points}$ (mm)	%Reduction in σ due to Area Averaging of LiDAR Points
Post Feb 2011: Mar 2011 and May 2011	10-m	NA	59	[176, 180]
	20-m	104		
	50-m	106		
Post Dec 2011: Feb 2012 and Oct 2015	10-m	NA	70	[14, 79]
	20-m	10		
	50-m	55		

*Standard deviation.

Table 4a: Ground surface subsidence adjustments for Patch A due to LiDAR measurement error.

Earthquake Event(s)	$\sigma_{pre\text{-}EQ\ LiDAR\ survey}$ (mm)	$\sigma_{post\text{-}EQ\ LiDAR\ survey}$ (mm)	σ_{total} (mm)	Area Average Adjusted σ (mm) **
Sep-10	158	56	134	±184
Feb-11	56	59	59	±81
Jun-11	59	61	62	±85
Dec-11	61	70	87	±119
CES	158	70	124	±171

**Based on the highest %Reduction in Table 3a.

Table 4b: Ground surface subsidence adjustments for Patch B due to LiDAR measurement error.

Earthquake Event(s)	$\sigma_{\text{pre-EQ LiDAR survey}}$ (mm)	$\sigma_{\text{post-EQ LiDAR survey}}$ (mm)	σ_{total} (mm)	Area Average Adjusted σ (mm) **
Sep-10	158	56	134	±193
Feb-11	56	59	59	±106
Jun-11	59	61	62	±112
Dec-11	61	70	87	±156
CES	158	70	124	±224

**Based on the highest %Reduction in Table 3b.

Table 4c: Ground surface subsidence adjustments for Road due to LiDAR measurement error.

Earthquake Event(s)	$\sigma_{\text{pre-EQ LiDAR survey}}$ (mm)	$\sigma_{\text{post-EQ LiDAR survey}}$ (mm)	σ_{total} (mm)	Area Average Adjusted σ (mm) **
Sep-10	158	56	134	±241
Feb-11	56	59	59	±106
Jun-11	59	61	62	±112
Dec-11	61	70	87	±156
CES	158	70	124	±224

**Based on the highest %Reduction in Table 3c.

Table 5a: Raw liquefaction-related ground surface subsidence for Patch A using original LiDAR points.

	Average Ground Surface Subsidence (mm)		
Earthquake Event(s)	10-m Buffer	20-m Buffer	50-m Buffer
Sep-10	21	21	21
Feb-11	131	131	131
Jun-11	79	79	79
Dec-11	27	26.5	27
CES	258	258	258

Table 5b: Raw liquefaction-related ground surface subsidence for Patch B using original LiDAR points.

	Average Ground Surface Subsidence (mm)		
Earthquake Event(s)	10-m Buffer	20-m Buffer	50-m Buffer
Sep-10	NA	NA	-27
Feb-11	NA	NA	135
Jun-11	NA	NA	86
Dec-11	NA	NA	18
CES	NA	NA	211

Table 5c: Raw liquefaction-related ground surface subsidence for Road using original LiDAR points.

	Average Ground Surface Subsidence (mm)		
Earthquake Event(s)	10-m Buffer	20-m Buffer	50-m Buffer
Sep-10	NA	36	45
Feb-11	NA	75	74
Jun-11	NA	140	126
Dec-11	NA	18	-8
CES	NA	269	238

Table 6a: Corrected liquefaction-related ground surface subsidence for Patch A using original LiDAR points with the calculated adjustments in Table 2.

	Average Calculated Ground Surface Subsidence (mm)		
Earthquake Event(s)	10-m Buffer	20-m Buffer	50-m Buffer
Sep-10	-82 $\pm$ 175	-82 $\pm$ 175	-82 $\pm$ 175
Feb-11	127 $\pm$ 75	127 $\pm$ 75	127 $\pm$ 75
Jun-11	67 $\pm$ 75	67 $\pm$ 75	67 $\pm$ 75
Dec-11	-29 $\pm$ 125	-29 $\pm$ 125	-29 $\pm$ 125
CES	83 $\pm$ 175	83 $\pm$ 175	83 $\pm$ 175

Notes: Plus/minus values are same as those in Table 4a, but rounded to the nearest 25; Positive overall values indicate ground surface subsidence, while negative overall values indicate ground surface uplift.

Table 6b: Corrected liquefaction-related ground surface subsidence for Patch B using original LiDAR points with the calculated adjustments in Table 2.

	Average Calculated Ground Surface Subsidence (mm)		
Earthquake Event(s)	10-m Buffer	20-m Buffer	50-m Buffer
Sep-10	NA	NA	-130$\pm$200
Feb-11	NA	NA	131$\pm$100
Jun-11	NA	NA	74$\pm$100
Dec-11	NA	NA	-37$\pm$150
CES	NA	NA	38$\pm$225

Notes: Plus/minus values are same as those in Table 4b, but rounded to the nearest 25; Positive overall values indicate ground surface subsidence, while negative overall values indicate ground surface uplift.

Table 6c: Corrected liquefaction-related ground surface subsidence for Road using original LiDAR points with the calculated adjustments in Table 2.

	Average Calculated Ground Surface Subsidence (mm)		
Earthquake Event(s)	10-m Buffer	20-m Buffer	50-m Buffer
Sep-10	NA	-67 ± 250	-58 ± 250
Feb-11	NA	101± 100	100 ± 100
Jun-11	NA	98 ± 100	84 ± 100
Dec-11	NA	-37 ± 150	-63 ± 150
CES	NA	95 ± 225	63 ± 225

Notes: Plus/minus values are same as those in Table 4c, but rounded to the nearest 25; Positive overall values indicate ground surface subsidence, while negative overall values indicate ground surface uplift.

Table 7a: Corrected liquefaction-related ground surface subsidence for Patch A using LiDAR DEMs.

	Estimated Ground Surface Subsidence (mm)								
	10-m Buffer			20-m Buffer			50-m Buffer		
Earthquake Event(s)	16th %ile	50th %ile	84th %ile	16th %ile	50th %ile	84th %ile	16th %ile	50th %ile	84th %ile
Sep-10	<50	<50	<50	<50	<50	<50	<50	<50	<50
Feb-11	100	150	150	100	150	150	100	150	150
Jun-11	<50	<50	<50	<50	<50	<50	<50	<50	<50
Dec-11	<50	<50	<50	<50	<50	<50	<50	<50	<50
CES	100	150	150	100	150	150	100	150	150

Note: These percentiles are not the exact statistical measures; they indicate the spatial variability of ground surface subsidence.

Table 7b: Corrected liquefaction-related ground surface subsidence for Patch B using LiDAR DEMs.

	Estimated Ground Surface Subsidence (mm)								
	10-m Buffer			20-m Buffer			50-m Buffer		
Earthquake Event(s)	16th %ile	50th %ile	84th %ile	16th %ile	50th %ile	84th %ile	16th %ile	50th %ile	84th %ile
Sep-10	NA	NA	NA	NA	NA	NA	<50	<50	<50
Feb-11	NA	NA	NA	NA	NA	NA	150	150	150
Jun-11	NA	NA	NA	NA	NA	NA	<50	<50	<50
Dec-11	NA	NA	NA	NA	NA	NA	<50	<50	<50
CES	NA	NA	NA	NA	NA	NA	150	150	150

Note: These percentiles are not the exact statistical measures; they indicate the spatial variability of ground surface subsidence.

Table 7c: Corrected liquefaction-related ground surface subsidence for Road using LiDAR DEMs.

	Estimated Ground Surface Subsidence (mm)								
	10-m Buffer			20-m Buffer			50-m Buffer		
Earthquake Event(s)	16th %ile	50th %ile	84th %ile	16th %ile	50th %ile	84th %ile	16th %ile	50th %ile	84th %ile
Sep-10	NA	NA	NA	<50	<50	<50	<50	<50	<50
Feb-11	NA	NA	NA	100	100	150	100	100	150
Jun-11	NA	NA	NA	<50	<50	<50	<50	<50	<50
Dec-11	NA	NA	NA	<50	<50	<50	<50	<50	<50
CES	NA	NA	NA	150	150	200	150	150	200

Note: These percentiles are not the exact statistical measures; they indicate the spatial variability of ground surface subsidence.

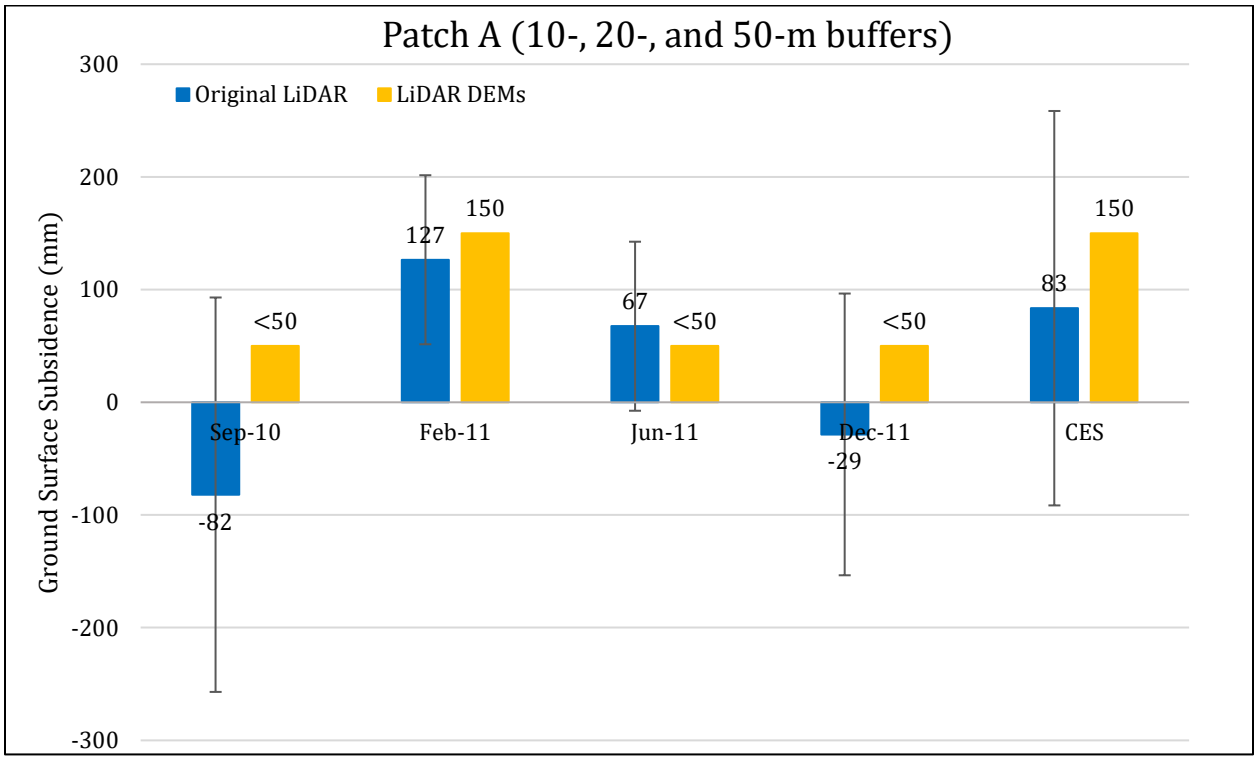

Figure 2: Comparison between ground surface subsidence determined from original LiDAR survey points and ground surface subsidence (50th %ile) estimated using LiDAR DEMs for Patch A.

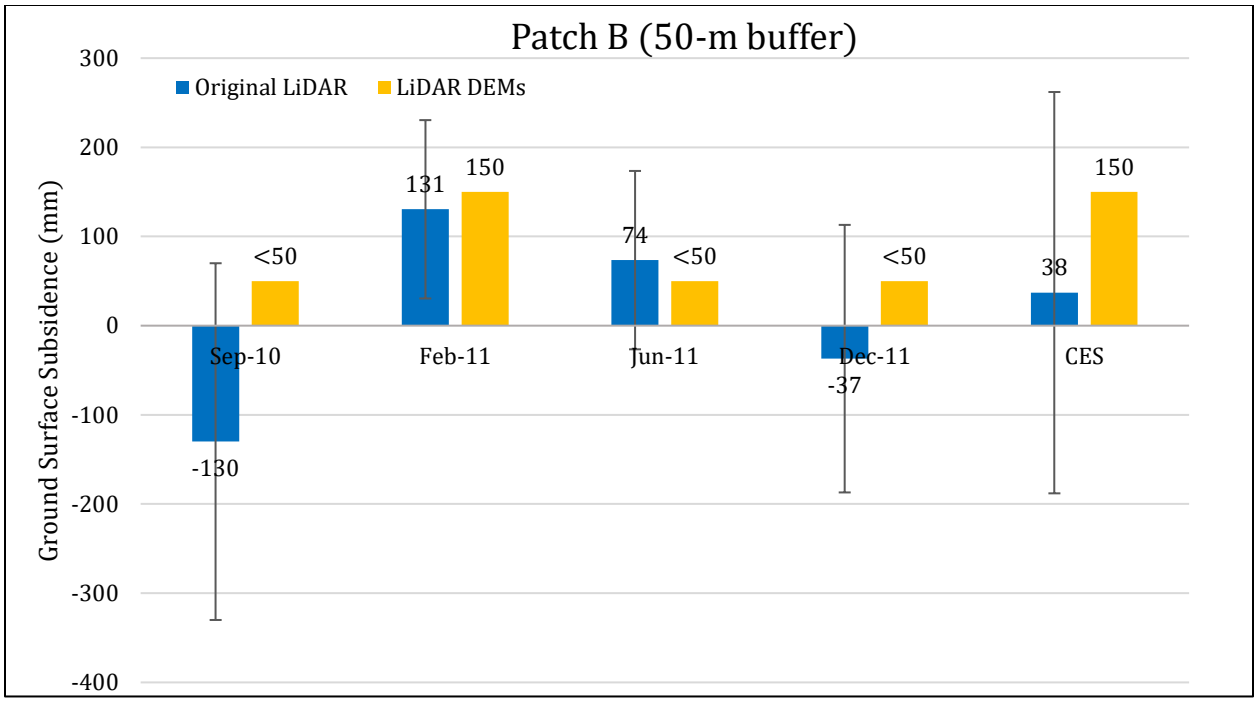

Figure 3: Comparison between ground surface subsidence determined from original LiDAR survey points and ground surface subsidence (50th %ile) estimated using LiDAR DEMs for Patch B.

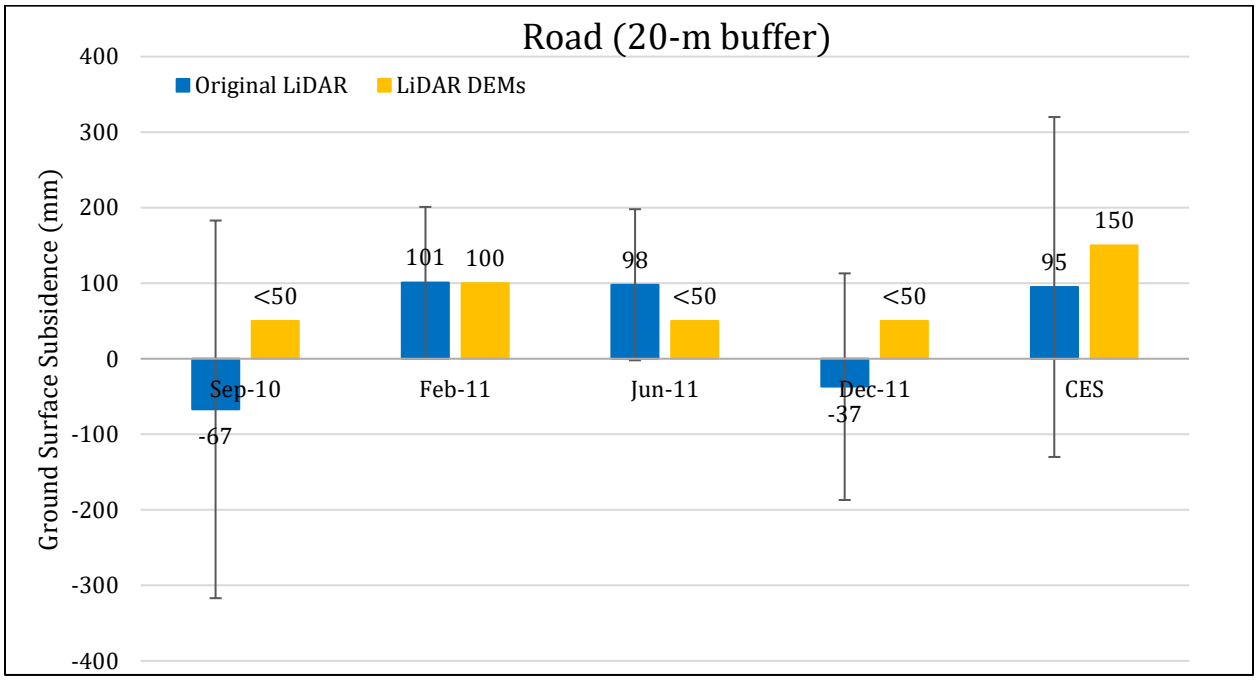

Figure 4: Comparison between ground surface subsidence determined from original LiDAR survey points and ground surface subsidence (50th %ile) estimated using LiDAR DEMs for Road for the 20-m buffer.

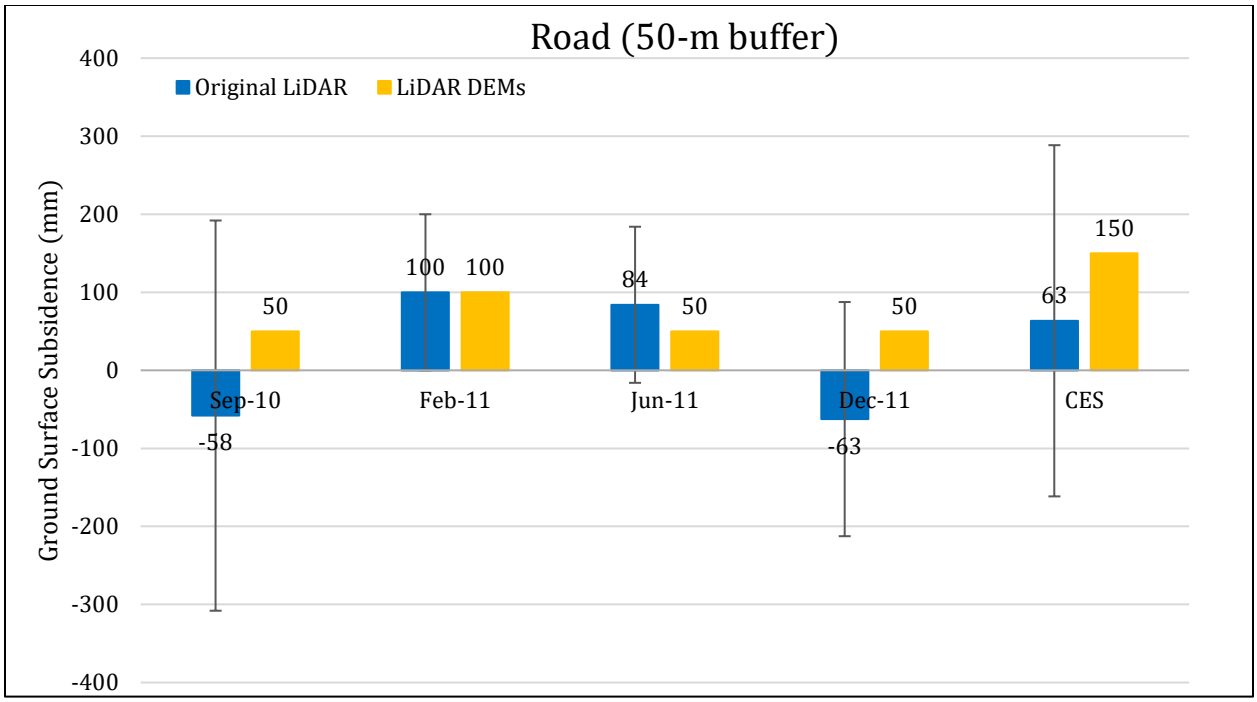

Figure 5: Comparison between ground surface subsidence determined from original LiDAR survey points and ground surface subsidence (50th %ile) estimated using LiDAR DEMs for Road for the 50-m buffer.

Note 2: The ground surface subsidence values determined from original LiDAR survey points are similar to the ground surface subsidence values estimated using LiDAR DEMs for all earthquake events.

Table 8a: Ejecta-Induced settlement for the top 20 m of the soil profile for Patch A for the 50th %ile PGA, P_L=50%, and C_{FC}=0.13 using BI-2014, ZRB-2002, and I_c cutoff of 2.6.

Earthquake Event(s)	M_W	PGA (g)	Depth to Groundwater (m)	S_T (mm)	S_{V1D} (mm)	$S_{E,L}$ (mm)
Sep-10	7.1	0.18	2.5	-82±175	5±20	-87±176
Feb-11	6.2	0.45	2.5	127±75	113±50	14±90
Jun-11	6.2	0.27	2.5	67±75	23±25	44±79
Dec-11	6.1	0.34	2.0	-29±125	64±50	-93±135

Notes: S_T = Total settlement (Table 6); S_{V1D} = Average vertical settlement due to volumetric compression using Boulanger and Idriss (2014) (BI-2014) and Zhang et al. (2002) (ZRB-2002) procedures and de Greef and Lengkeek (2018) thin-layer correction; $S_{E,L}$ = Ejecta-induced settlement as the difference between the LiDAR-based S_T and S_{V1D}; NA = Not available.

Table 8b: Ejecta-Induced settlement for the top 20 m of the soil profile for Patch B for the 50th %ile PGA, P_L=50%, and C_{FC}=0.13 using BI-2014, ZRB-2002, and I_C cutoff of 2.6.

Earthquake Event(s)	M_W	PGA (g)	Depth to Groundwater (m)	S_T (mm)	S_{V1D} (mm)	$S_{E,L}$ (mm)
Sep-10	7.1	0.18	2.5	-130±200	3±20	-133±201
Feb-11	6.2	0.45	2.5	131±100	77±50	54±112
Jun-11	6.2	0.27	2.5	74±100	15±25	59±103
Dec-11	6.1	0.34	2.0	-37±150	43±50	-80±158

Notes: S_T = Total settlement (Table 6); S_{V1D} = Average vertical settlement due to volumetric compression using Boulanger and Idriss (2014) (BI-2014) and Zhang et al. (2002) (ZRB-2002) procedures and de Greef and Lengkeek (2018) thin-layer correction; $S_{E,L}$ = Ejecta-induced settlement as the difference between the LiDAR-based S_T and S_{V1D}; NA = Not available.

Table 8c: Ejecta-Induced settlement for the top 20 m of the soil profile for Road within the 20-m buffer for the 50th %ile PGA, P_L=50%, and C_{FC}=0.13 using BI-2014, ZRB-2002, and I_C cutoff of 2.6.

Earthquake Event(s)	M_W	PGA (g)	Depth to Groundwater (m)	S_T (mm)	S_{V1D} (mm)	$S_{E,L}$ (mm)
Sep-10	7.1	0.18	2.5	-67±250	3±20	-70±251
Feb-11	6.2	0.45	2.5	101±100	77±50	24±112
Jun-11	6.2	0.27	2.5	98±100	15±25	83±103
Dec-11	6.1	0.34	2.0	-37±150	43±50	-80±158

Notes: S_T = Total settlement (Table 6); S_{V1D} = Average vertical settlement due to volumetric compression using Boulanger and Idriss (2014) (BI-2014) and Zhang et al. (2002) (ZRB-2002) procedures and de Greef and Lengkeek (2018) thin-layer correction; $S_{E,L}$ = Ejecta-induced settlement as the difference between the LiDAR-based S_T and S_{V1D}; NA = Not available.

Table 8d: Ejecta-Induced settlement for the top 20 m of the soil profile for Road within the 50-m buffer for the 50th %ile PGA, P_L=50%, and C_{FC}=0.13 using BI-2014, ZRB-2002, and I_C cutoff of 2.6.

Earthquake Event(s)	M_W	PGA (g)	Depth to Groundwater (m)	S_T (mm)	S_{V1D} (mm)	$S_{E,L}$ (mm)
Sep-10	7.1	0.18	2.5	-58±250	3±20	-61±251
Feb-11	6.2	0.45	2.5	100±100	88±50	12±112
Jun-11	6.2	0.27	2.5	84±100	16±25	68±103
Dec-11	6.1	0.34	2.0	-63±150	48±50	-111±158

Notes: S_T = Total settlement (Table 6); S_{V1D} = Average vertical settlement due to volumetric compression using Boulanger and Idriss (2014) (BI-2014) and Zhang et al. (2002) (ZRB-2002) procedures and de Greef and Lengkeek (2018) thin-layer correction; $S_{E,L}$ = Ejecta-induced settlement as the difference between the LiDAR-based S_T and S_{V1D}; NA = Not available.

Note 3: It is uncertain if ejecta from the Feb-11 EQ were removed at the time of the May 2011 LiDAR survey (no photograph for that period was acquired). The ground photograph acquired in Aug 2011 at the time of the LDAT property inspection shows ejecta remnants within Patch B.

Note 4: The uncertainty for volumetric settlement was derived based on the sensitivity of volumetric settlement to PGA, C_{FC}, and P_L for each earthquake event for VsVp 57203 *Shirley Intermediate School* and CC LIQ 1 – CPT 5586 – *Vivian St* sites. Taking the 50th percentile as the baseline case, the minimum and maximum values corresponding to the difference between the 25th percentile and the 50th percentile and the 75th percentile and the 50th percentile were determined. The arithmetic mean of the range of the minimum and maximum difference was evaluated for each patch at the two sites. The maximum arithmetic mean for each earthquake event was rounded to the nearest five and used as the uncertainty value. Accordingly, the 1-D volumetric settlement uncertainties of $\pm$20, $\pm$50, $\pm$25, and $\pm$50 mm for the Sep-10, Feb-11, Jun-11, and Dec-11 earthquake events, respectively, were used for all sites in this study.

Table 9a: Coverage area and height of ejecta estimates for Patch A using aerial and/or ground photographs and engineering judgement.

Earthquake Event	$H_{E,thin}$ (mm)	$A_{E,thin}$ (m^2)	$H_{E,thick}$ (mm)	$A_{E,thick}$ (m^2)	A_T (m^2)
Sep-10	0	0	0	0	85.3
Feb-11	0	0	0	0	85.3
Jun-11	0	0	0	0	85.3
Dec-11	0	0	0	0	85.3

Note: NA = Not available as no aerial and/or ground photograph was acquired for the site; $A_{E,thick/thin}$ = Coverage area of thick/thin ejecta layers; $H_{E,thick/thin}$ = Lower-upper estimate of height of thick/thin ejecta layers; Thin and thick layers correspond to light gray and dark gray colors of ejecta observed in aerial photographs.

Table 9b: Coverage area and height of ejecta estimates for Patch B using aerial and/or ground photographs and engineering judgement.

Earthquake Event	$H_{E,thin}$ (mm)	$A_{E,thin}$ (m^2)	$H_{E,thick}$ (mm)	$A_{E,thick}$ (m^2)	A_T (m^2)
Sep-10	0	0	0	0	47.5
Feb-11	0	0	20-50	20.9	47.5
Jun-11	0	0	0	0	47.5
Dec-11	0	0	0	0	47.5

Note: NA = Not available as no aerial and/or ground photograph was acquired for the site; $A_{E,thick/thin}$ = Coverage area of thick/thin ejecta layers; $H_{E,thick/thin}$ = Lower-upper estimate of height of thick/thin ejecta layers; Thin and thick layers correspond to light gray and dark gray colors of ejecta observed in aerial photographs.

Table 9c: Coverage area and height of ejecta estimates for Road within the 20-m buffer using aerial and/or ground photographs and engineering judgement.

Earthquake Event	$H_{E,thin}$ (mm)	$A_{E,thin}$ (m^2)	$H_{E,prism}$ (mm)	$V_{E,prism}$ (m^3)	$H_{E,cc}$ (mm)	$V_{E,cc}$ (m^3)	A_T (m^2)
Sep-10	0	0	0	0	0	0	271
Feb-11	3-6	31.6	27-290	19.4-24.8	676	0.98	271
Jun-11	2-4	28.4	17-102	0.730-1.46	947	2.64	271
Dec-11	0	0	0	0	0	0	271

Note: $A_{E,thick/thin}$ = Coverage area of thick/thin ejecta layers; $H_{E,thick/thin}$ = Lower-upper estimate of height of thick/thin ejecta layers; $H_{E,prism/pyr}$ = Lower-upper estimate of ejecta height near the curb based on 2-4% cross slope of normal crown; $V_{E,prism+pyr}$ = Lower-upper estimate of total volume of prismatic- and pyramidal-shape ejecta; Thin and thick layers correspond to light gray and dark gray colors of ejecta observed in aerial photographs; $V_{E,cc}$ = Volume of conically shaped ejecta pile components; $H_{E,cc}$ = Lower-upper estimate of height of conically shaped ejecta pile components (based on the repose angle of 30°); A_T= Total assessment area of a buffer being considered.

Table 9d: Coverage area and height of ejecta estimates for Road within the 50-m buffer using aerial and/or ground photographs and engineering judgement.

Earthquake Event	$H_{E,thin}$ (mm)	$A_{E,thin}$ (m^2)	$H_{E,prism}$ (mm)	$V_{E,prism}$ (m^3)	$H_{E,cc}$ (mm)	$V_{E,cc}$ (m^3)	A_T (m^2)
Sep-10	0	0	0	0	0	0	941
Feb-11	3-6	285	16-290	36.7-51.4	676-785	2.50	941
Jun-11	2-4	159	16-102	0.749-1.50	647-947	5.31	922*
Dec-11	0	0	0	0	0	0	941

Note: $A_{E,thick/thin}$ = Coverage area of thick/thin ejecta layers; $H_{E,thick/thin}$ = Lower-upper estimate of height of thick/thin ejecta layers; $H_{E,prism/pyr}$ = Lower-upper estimate of ejecta height near the curb based on 2-4% cross slope of normal crown; $V_{E,prism+pyr}$ = Lower-upper estimate of total volume of prismatic- and pyramidal-shape ejecta; Thin and thick layers correspond to light gray and dark gray colors of ejecta observed in aerial photographs; $V_{E,cc}$ = Volume of conically shaped ejecta pile components; $H_{E,cc}$ = Lower-upper estimate of height of conically shaped ejecta pile components (based on the repose angle of 30°); A_T= Total assessment area of a buffer being considered; * indicates reduction in A_T due to the presence of objects within the assessment area.

Note 5: The values in Table 9 correspond to the coverage area of ejecta outlined in aerial photographs (Figures 70 through 76) and the lower and upper estimates of ejecta height based on geometry, ground photographs (Figures 77 and 78), EQC LDAT property inspection notes (Figure 79) and reports from Aug 2011. The ejecta-induced settlement using photographs and engineering judgment, $S_{E,P}$, is estimated as

$$S_{E,P} = \frac{\sum_{i=1}^{a} A_{E,thick,i} * H_{E,thick,i} + \sum_{j=1}^{b} A_{E,thin,j} * H_{E,thin,j} + \frac{1}{2}\sum_{n=1}^{f} W_{E,prism,n} * H_{E,prism,n} * L_{E,prism,n}}{A_T} + \frac{\frac{1}{3}\sum_{k=1}^{c} A_{E,pile,k} * R_{E,pile,k} * tan30°}{A_T} = \frac{\sum_{i=1}^{a} V_{E,thick,i} + \sum_{j=1}^{b} V_{E,thin,j} + \sum_{n=1}^{f} V_{E,prism,n} + \sum_{k=1}^{c} V_{E,conical\ component,k}}{A_T}$$

where

- $A_{E,thick,i}$ and $H_{E,thick,i}$ are the area and the height of a thick ejecta layer, respectively;
- $A_{E,thin,j}$ and $H_{E,thin,j}$ are the area and the height of a thin ejecta layer, respectively;
- $W_{E,prism,n}$ and $L_{E,prism,n}$ are the width and the length of the coverage area of a prismatically shaped ejecta layer, respectively, and $H_{E,prism,n}$ is the height of a prism-like ejecta layer;
- $A_{E,pile,k}$ and $R_{E,pile,k}$ are the area and the radius of an ejecta pile component, respectively, shaped as a cone with the repose angle of 30°;
- A_T is the total assessment area for a buffer being considered (Figure 1).

Table 10a: Ejecta-induced settlement estimates based on aerial and/or ground photographs.

EQ Event	Patch A (10-, 20-, and 50-m buffers)		Patch B (50-m buffer)	
	$S_{E,P,lower}$ (mm)	$S_{E,P,upper}$ (mm)	$S_{E,P,lower}$ (mm)	$S_{E,P,lower}$ (mm)
Sep-10	0	0	0	0
Feb-11	0	0	9	22
Jun-11	0	0	0	0
Dec-11	0	0	0	0

Note: $S_{E,P,lower}$ and $S_{E,P,upper}$ correspond to lower and upper estimates of $S_{E,P}$, respectively.

Table 10b: Ejecta-induced settlement estimates based on aerial and/or ground photographs.

EQ Event	Road (20-m buffer)		Road (50-m buffer)	
	$S_{E,P,lower}$ (mm)	$S_{E,P,upper}$ (mm)	$S_{E,P,lower}$ (mm)	$S_{E,P,lower}$ (mm)
Sep-10	0	0	0	0
Feb-11	75	96	43	60
Jun-11	13	16	7	8
Dec-11	0	0	0	0

Note: $S_{E,P,lower}$ and $S_{E,P,upper}$ correspond to lower and upper estimates of $S_{E,P}$, respectively.

Table 11a: Best final estimates of ejecta-induced settlement.

EQ Event	Patch A (10-, 20-, and 50-m buffers)			Patch B (50-m buffer)		
	$S_{E,L}$ (mm)	$S_{E,P}$ (mm)	$S_{E,L}$ (mm)	$S_{E,L}$ (mm)	$S_{E,P}$ (mm)	$S_{E,final}$ (mm)
Sep-10	-87±176	0	0	-133±201	0	0
Feb-11	14±90	0	0	54±112	16±6	35±55
Jun-11	44±79	0	0	59±103	0	0
Dec-11	-93±135	0	0	-80±158	0	0

Notes: $S_{E,L}$ = Ejecta-induced settlement based on LiDAR data reported in Table 8; $S_{E,P}$ = Median ejecta-induced settlement for the range of values reported in Table 10; $S_{E,final}$ = Best final estimate of ejecta-induced settlement rounded to the nearest 5; Final plus/minus values are also rounded to the nearest 5.

Table 11b: Best final estimates of ejecta-induced settlement.

EQ Event	Road (20-m buffer)			Road (50-m buffer)		
	$S_{E,L}$ (mm)	$S_{E,P}$ (mm)	$S_{E,L}$ (mm)	$S_{E,L}$ (mm)	$S_{E,P}$ (mm)	$S_{E,final}$ (mm)
Sep-10	-70±251	0	0	-61±251	0	0
Feb-11	24±112	86±10	85±10	12±112	52±8	50±10
Jun-11	83±103	15±1	15±5	68±103	7.5±0.5	10±5
Dec-11	-80±158	0	0	-111±158	0	0

Notes: $S_{E,L}$ = Ejecta-induced settlement based on LiDAR data reported in Table 8; $S_{E,P}$ = Median ejecta-induced settlement for the range of values reported in Table 10; $S_{E,final}$ = Best final estimate of ejecta-induced settlement rounded to the nearest 5; Final plus/minus values are also rounded to the nearest 5.

Note 6:

- $S_{E,final}$ for Patch A for all earthquake events is based solely on $S_{E,P}$.
- $S_{E,final}$ for Patch B is based on $S_{E,P}$ only for all earthquake events except for the Feb-11 EQ, which is a weighted average of $S_{E,L}$ and $S_{E,P}$ with weights of 1/2 and 1/2, respectively.
- For Road, $S_{E,final}$ is equal to $S_{E,P}$ for all earthquake events.
- The uncertainty associated with $S_{E,final}$ is also a weighted average of uncertainties associated with $S_{E,L}$ and $S_{E,P}$ with the same corresponding weights.
- The weights are based on the LiDAR error bands, LPI prediction error (Maurer et al. 2014[3]), presence/absence of ejecta at the site at the time of LiDAR surveys, and completeness of visual evidence (i.e., ground and aerial photographs and EQC LDAT property inspection reports for the site). The Sandown Crescent site is in the apparent zone of higher ground surface subsidence for the Sep-10 EQ (i.e., the overestimate of ground surface elevation by

[3] Maurer, B. W., Green, R. A., Cubrinovski, M., & Bradley, B. A. (2014). Evaluation of the Liquefaction Potential Index for Assessing Liquefaction Hazard in Christchurch, New Zealand. *Journal of Geotechnical and Geoenvironmental Engineering*, 140(7), 04014032-1-11. doi:10.1061/(asce)gt.1943-5606.0001117

July 2003 LiDAR survey). The site is in the zone of accurate LPI prediction to slight LPI overprediction of liquefaction severity for the Sep-10 EQ; it is in the zone of moderate LPI overprediction of liquefaction severity for the Feb-11 EQ. The ejecta appear not to be removed (at least not in its entirety) from the road at the time of the March 2011 (and possibly the May 2011) LiDAR survey. The LDAT property inspection report is available for Patches A and B. There are no ground photographs of the road.

Summary 1:

- **The best estimate of the ejecta-induced free-field ground settlement at the Sandown Crescent site for the SEP 2010, JUN 2011, FEB 2011, and DEC 2011 earthquake is 0 mm, 35±55 mm (range = 0-90 mm, mean = 35 mm), 0 mm, and 0 mm, respectively.**
- **The best estimate of the ejecta-induced free-field ground settlement of the road at the Sandown Crescent site for the SEP 2010, FEB 2011, JUN 2011, and DEC 2011 earthquake is 0 mm, 50±10 mm, 10±5 mm, and 0 mm, respectively.**

Note 7: CPT 15498 was initially named as CC LIQ 11.

Note 8: Patch B was added later hence only Patch A and Road outlines in some of the following figures.

Figure 6: Location of the site.

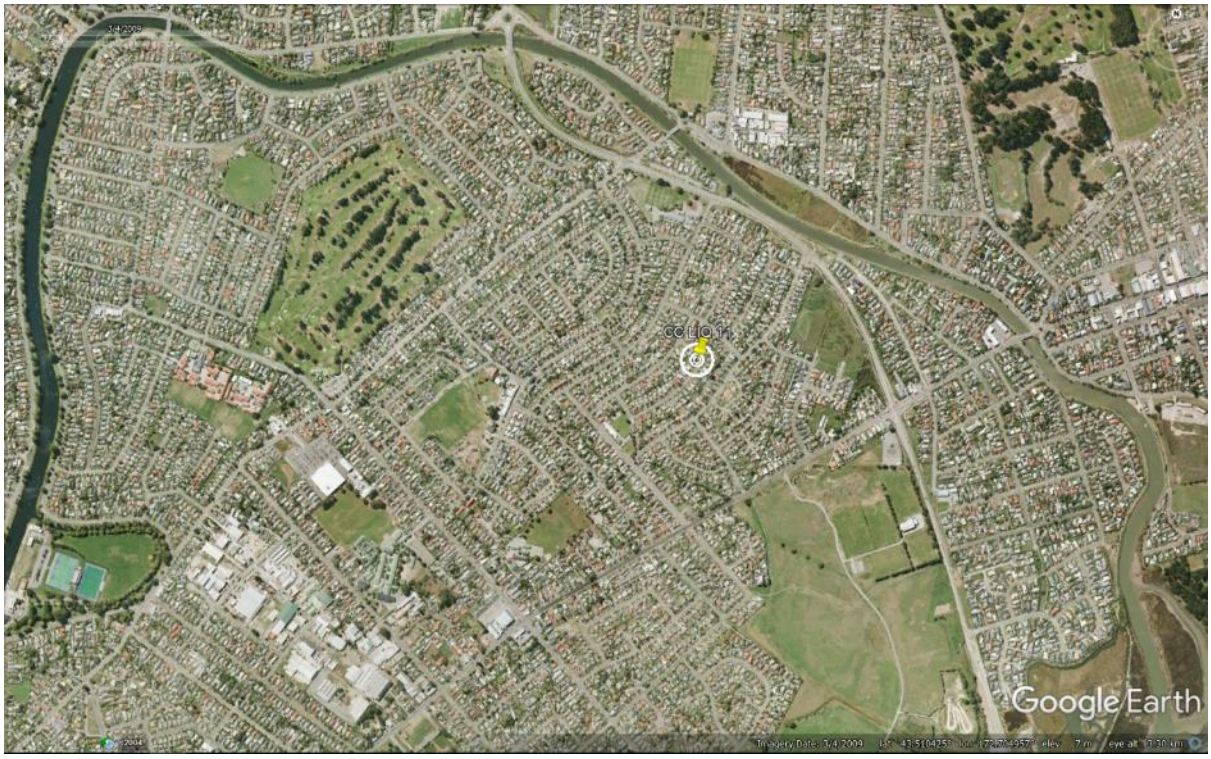

Figure 7: Position of the site relative to nearby buildings, vegetation, and free-face features.

Figure 8: Street view of the site showing flat land.

Figure 9: Satellite image of the site taken in Dec 2004.

Figure 10: Satellite image of the site taken in Mar 2009.

Figure 11: Satellite image of the site taken in Apr 2012.

Figure 12: Satellite image of the site taken in Jan 2015.

Figure 13: Satellite image of the site taken in Jun 2015.

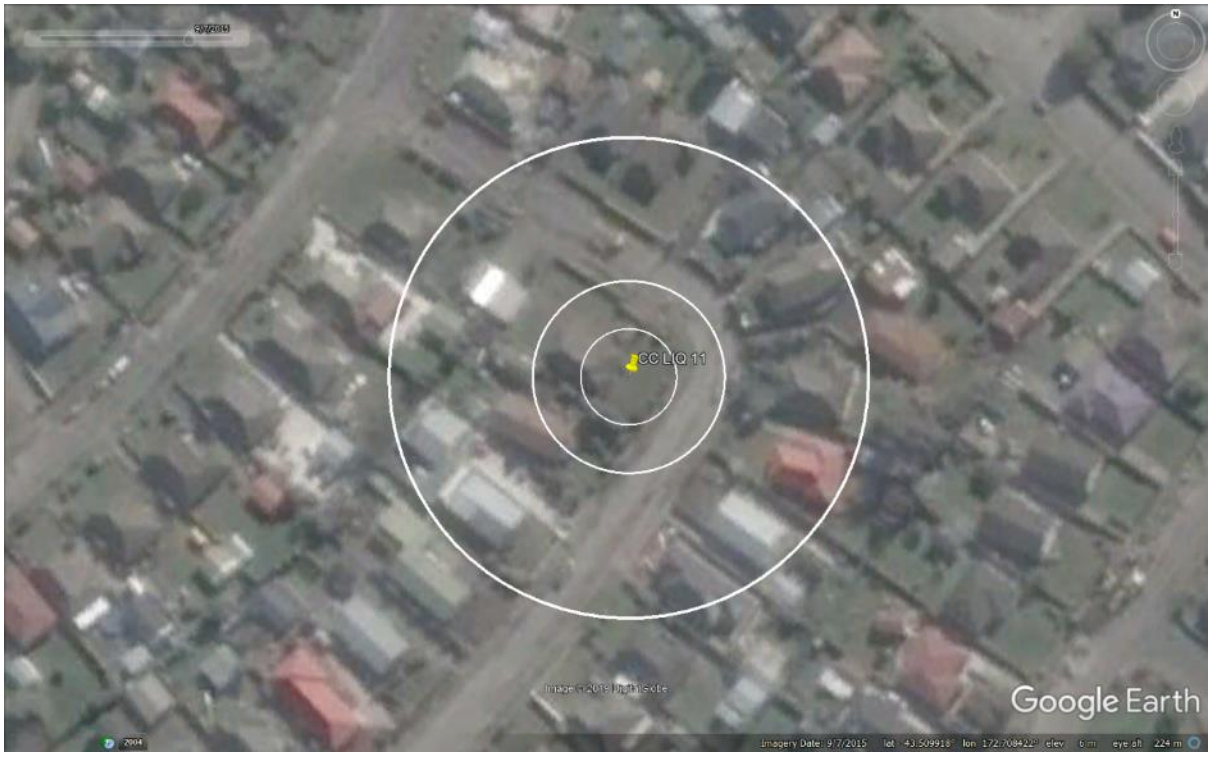

Figure 14: Satellite image of the site taken in Sep 2015.

Figure 15: Satellite image of the site taken in Jan 2016.

Figure 16: Aerial photograph of the site taken on Sep 4, 2010.

Figure 17: Aerial photograph of the site taken on Feb 24, 2011.

Figure 18: Aerial photograph of the site taken on June 16, 2011.

Figure 19: Aerial photograph of the site taken on Dec 24, 2011.

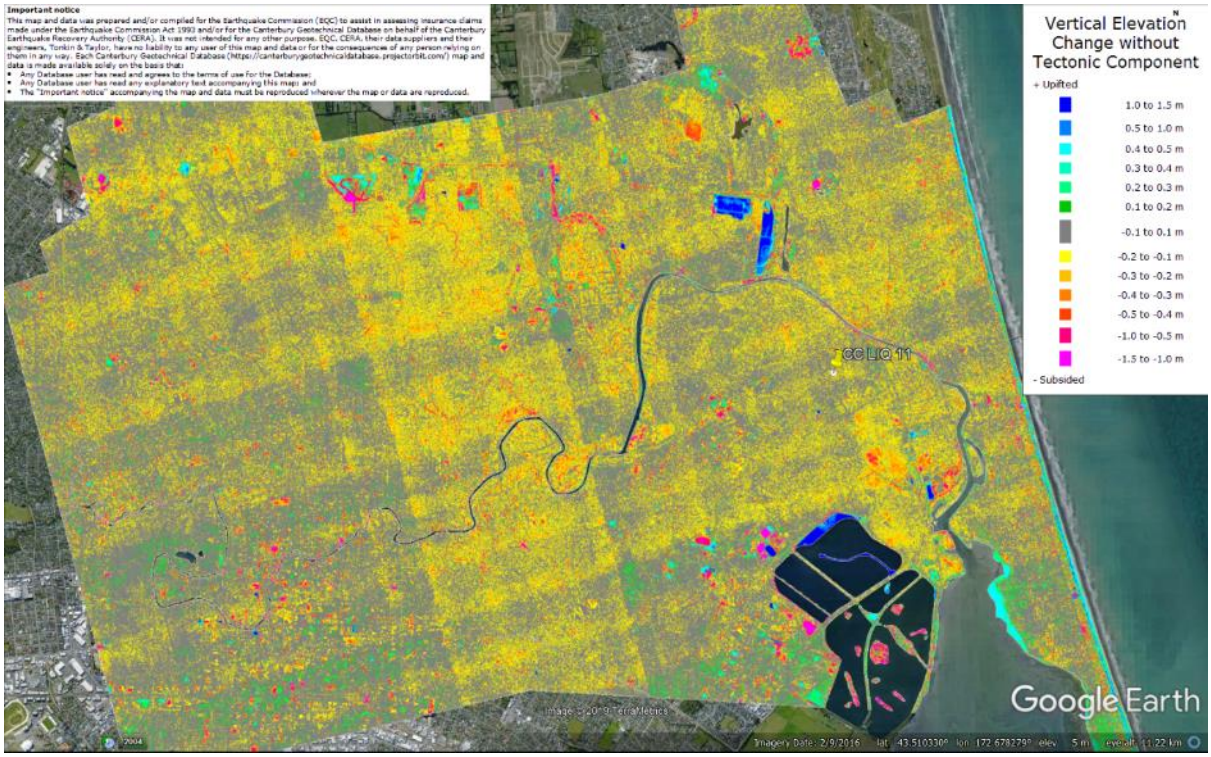

Figure 20: Vertical Ground Movements (Surface – Tectonic) for Sep 2010 Earthquake – the site is in the apparent zone of overestimated ground surface subsidence (e.g., July 2003 LIDAR flight error band).

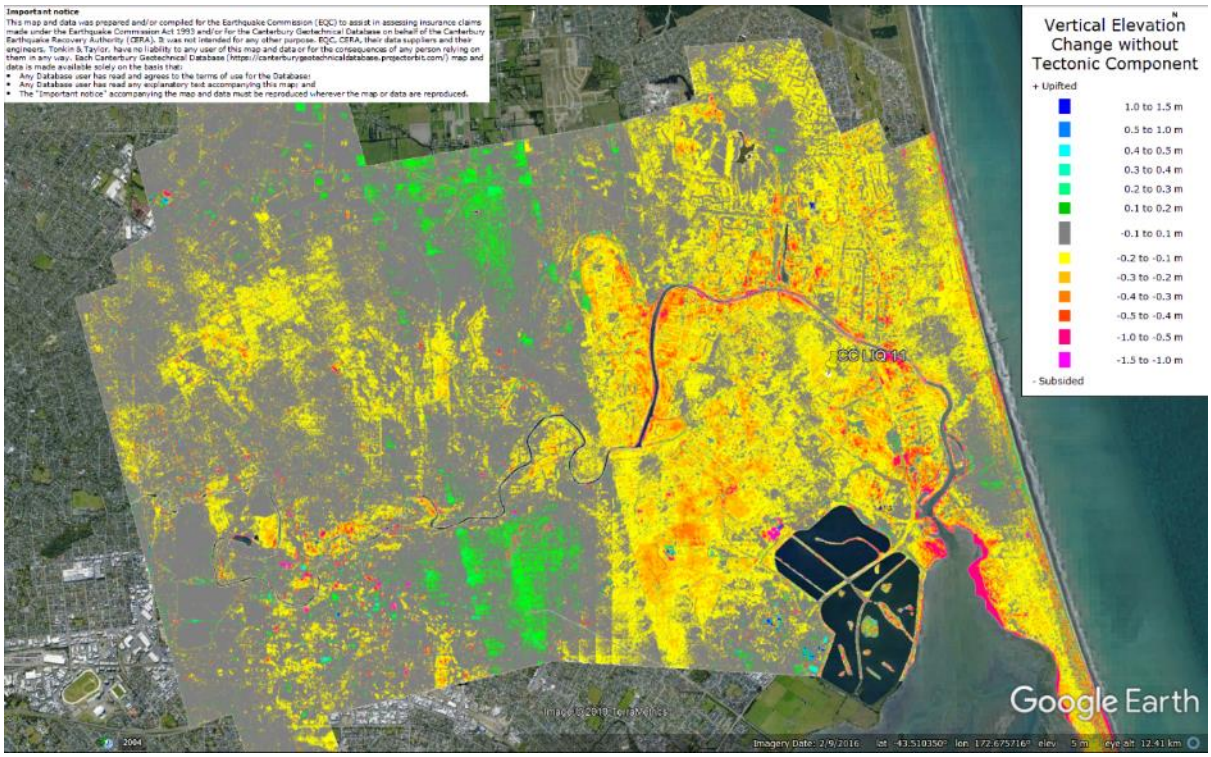

Figure 21: Vertical Ground Movements (Surface – Tectonic) for Feb 2011 Earthquake – the site is not in the apparent zone of underestimated ground surface subsidence.

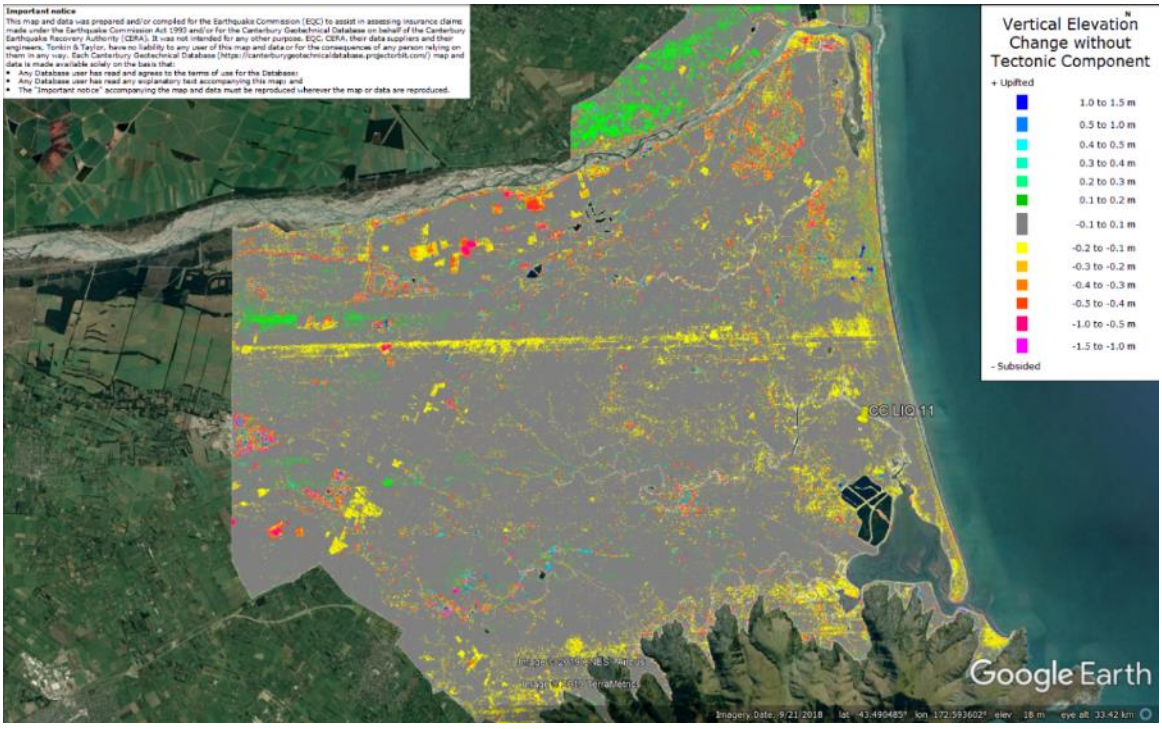

Figure 22: Vertical Ground Movements (Surface – Tectonic) for June 2011 Earthquake – the site is not in the apparent zone of overestimated or underestimated ground surface subsidence.

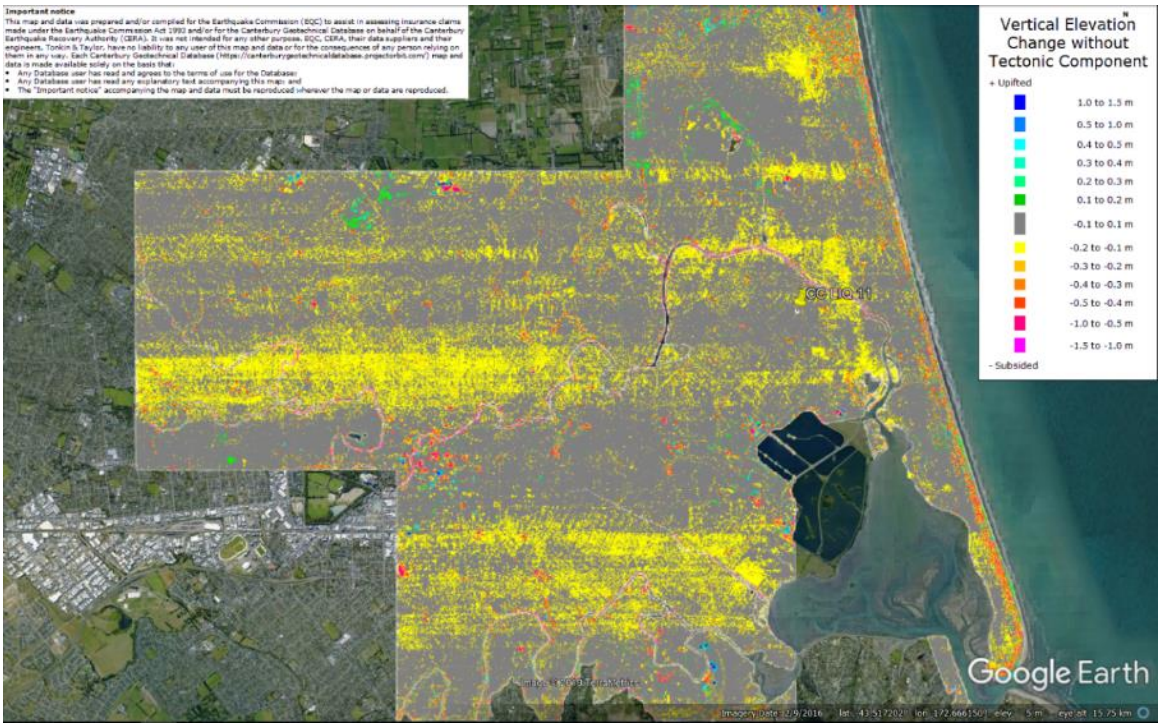

Figure 23: Vertical Ground Movements (Surface – Tectonic) for Dec 2011 Earthquake – the site is not in the apparent zone of overestimated or underestimated ground surface subsidence.

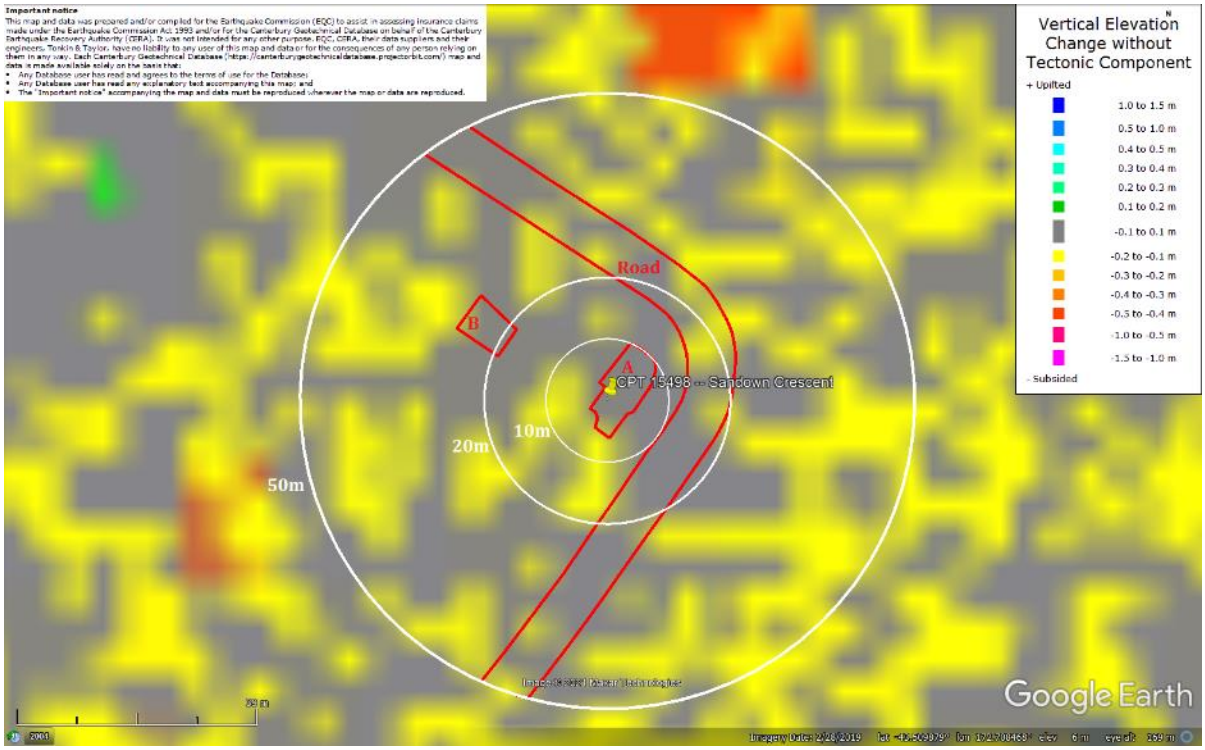

Figure 24: Ground surface subsidence without tectonic component for Sep 2010 Earthquake according to the LiDAR DEM.

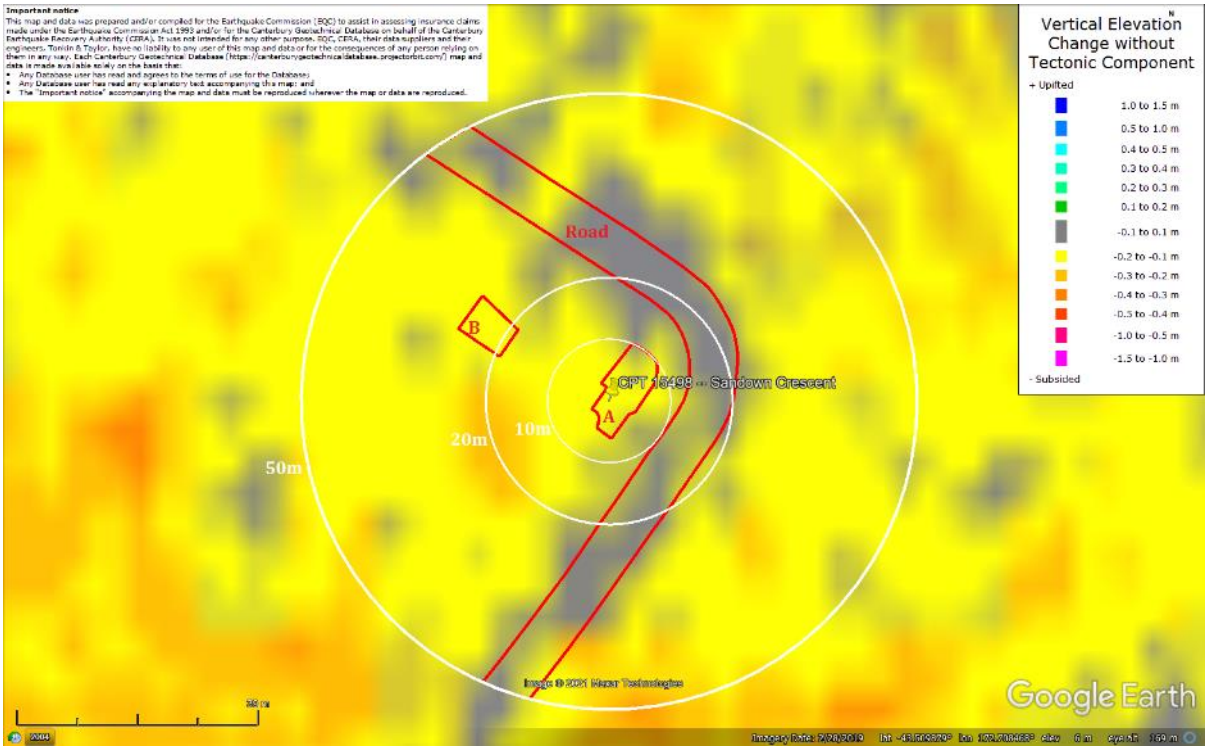

Figure 25: Ground surface subsidence without tectonic component for Feb 2011 Earthquake according to the LiDAR DEM.

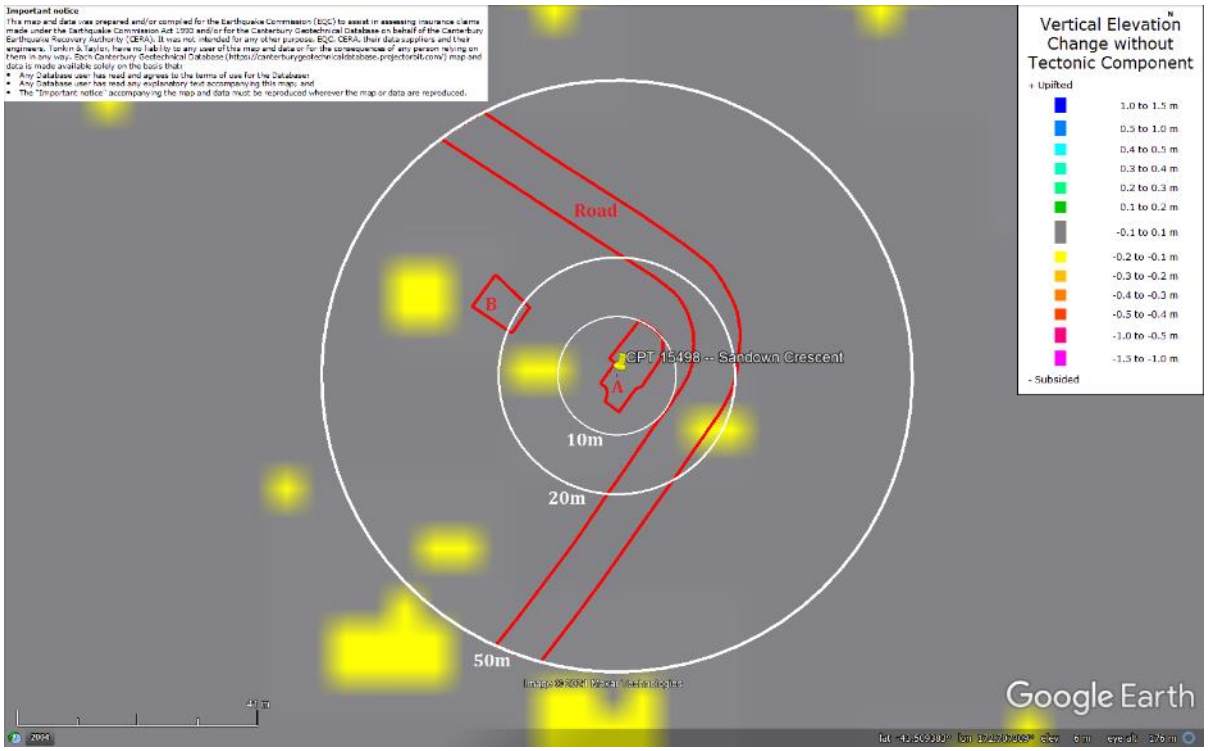

Figure 26: Ground surface subsidence without tectonic component for Jun 2011 Earthquake according to the LiDAR DEM.

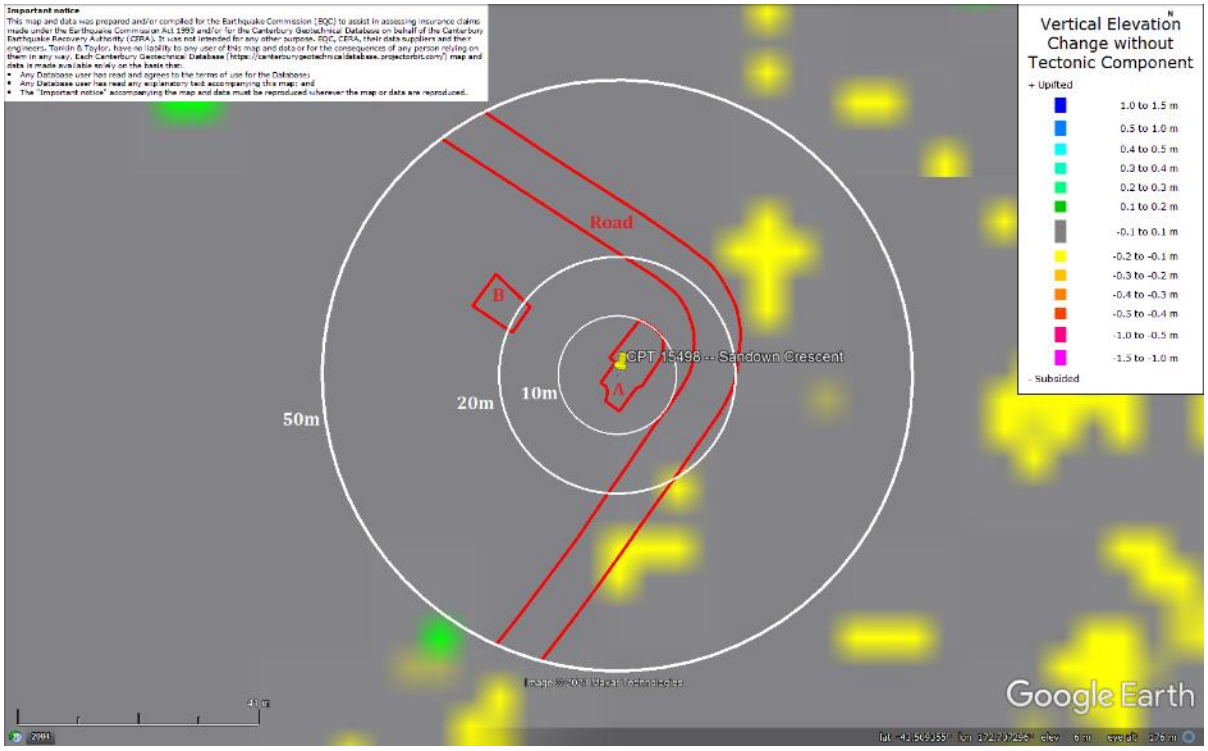

Figure 27: Ground surface subsidence without tectonic component for Dec 2011 Earthquake according to the LiDAR DEM.

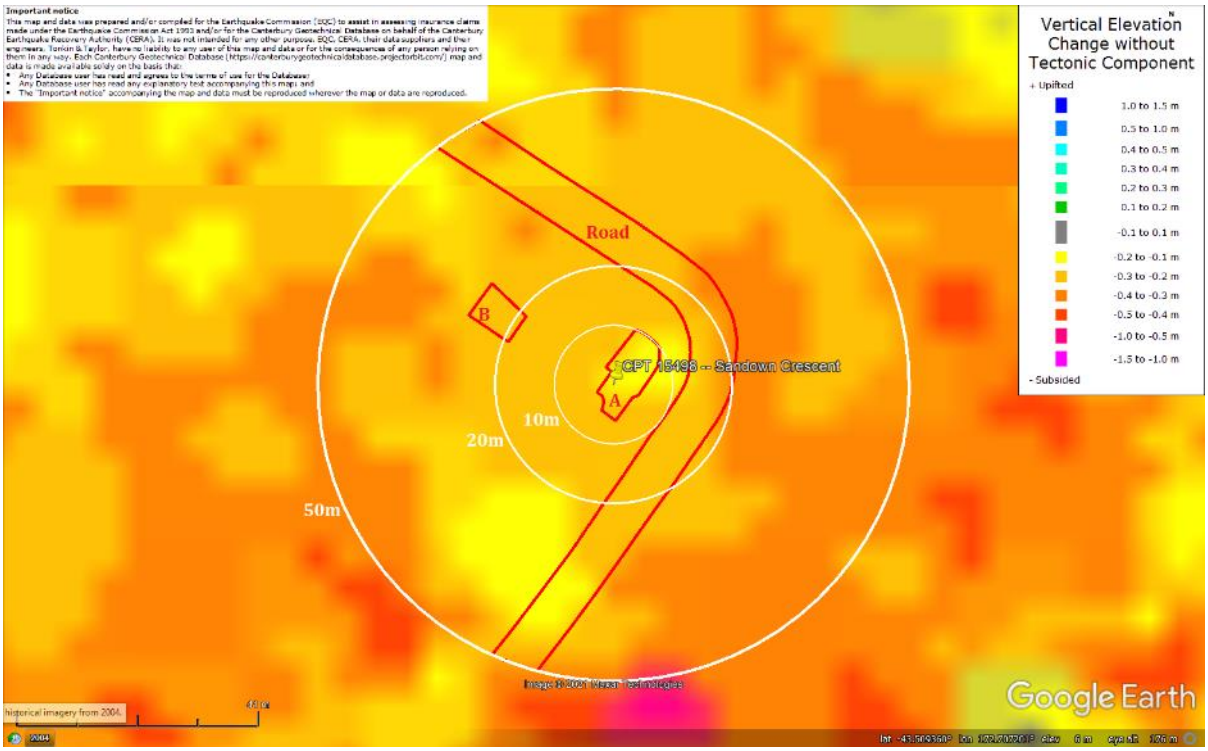

Figure 28: Ground surface subsidence without tectonic component for Canterbury Earthquake Sequence according to the LiDAR DEM.

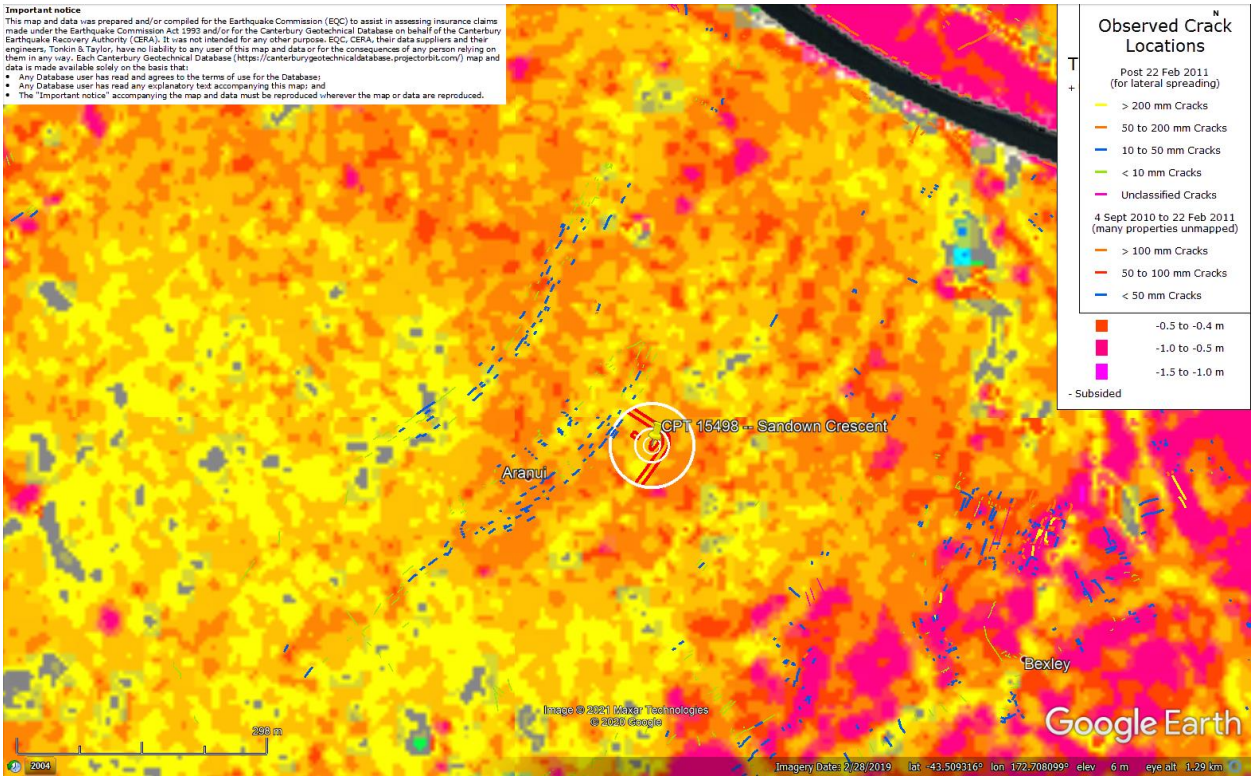

Figure 29: Absence of ground cracks indicates no lateral spreading for Canterbury Earthquake Sequence.

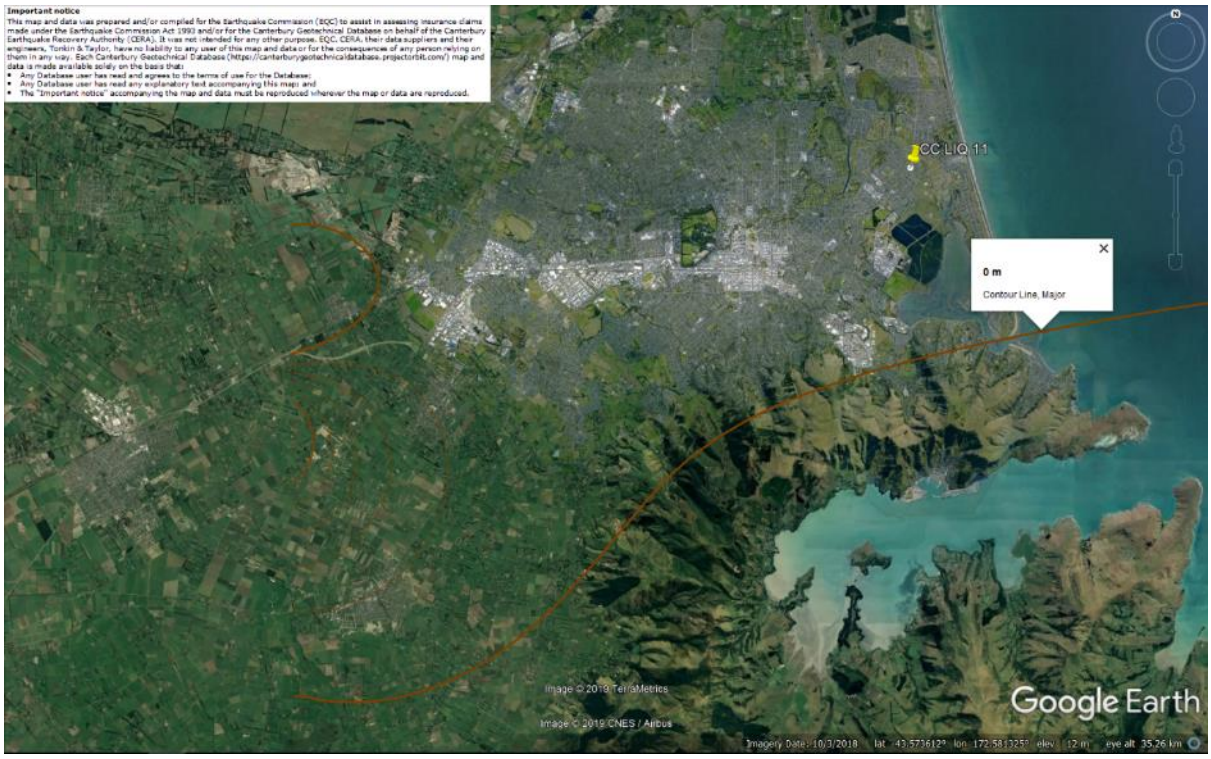

Figure 30: Vertical tectonic movements for Sep 2010 Earthquake.

Figure 31: Vertical tectonic movements for Feb 2011 Earthquake.

Figure 32: Vertical tectonic movements for June 2011 Earthquake.

Figure 33: Vertical tectonic movements for Dec 2011 Earthquake.

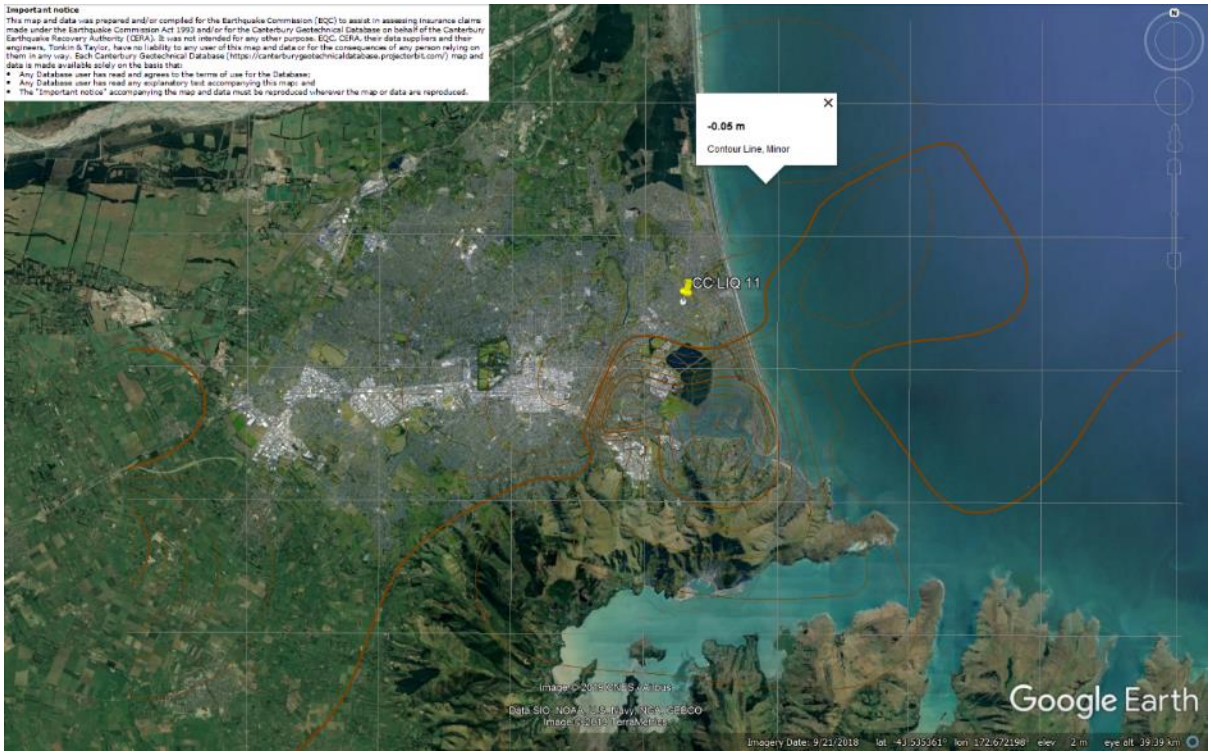

Figure 34: Vertical tectonic movements for Canterbury Earthquake Sequence.

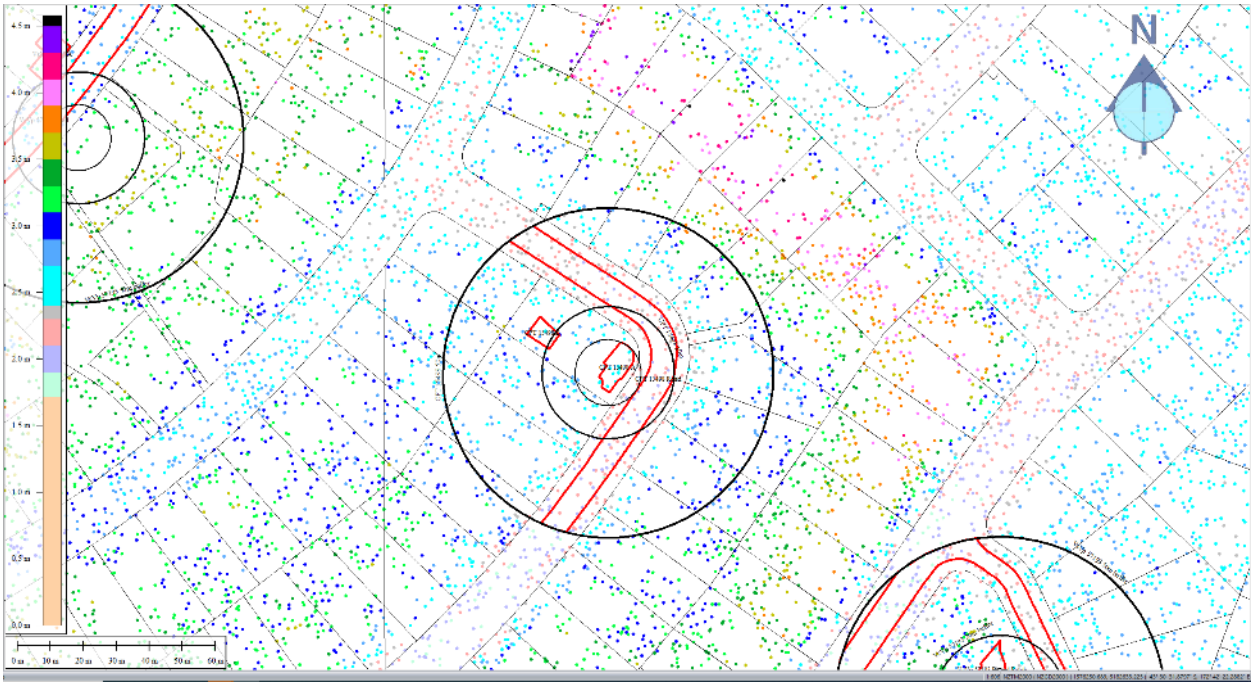

Figure 35: Jul 2003 LiDAR survey.

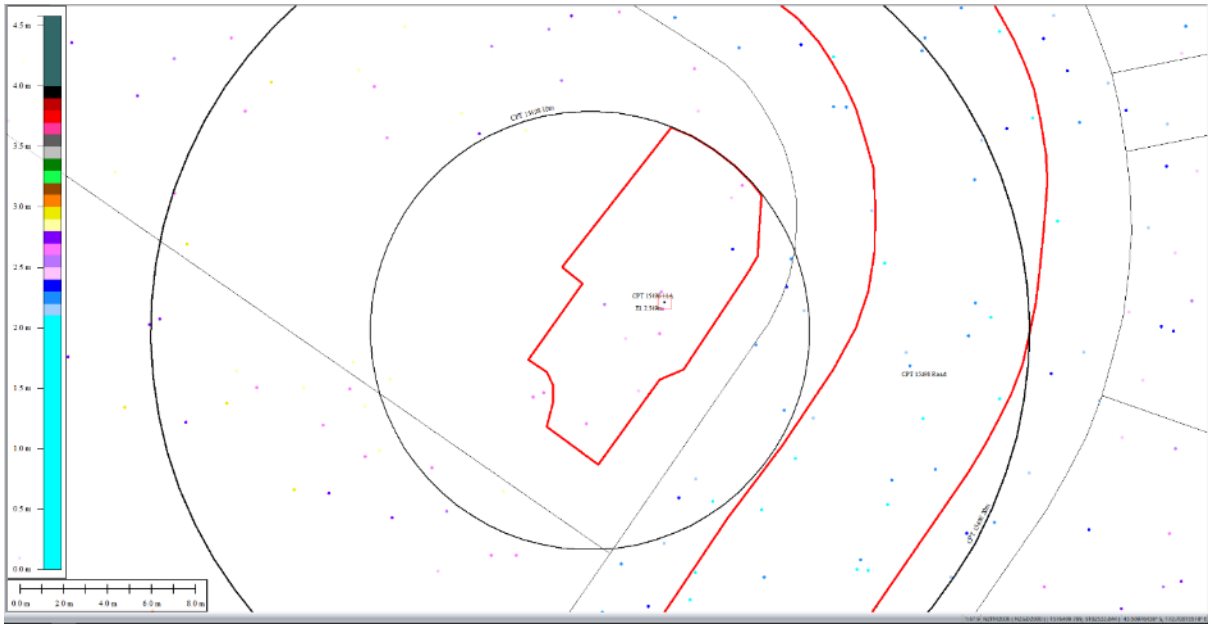

Figure 36: Ground surface elevation for Patch A for Jul 2003 LiDAR survey.

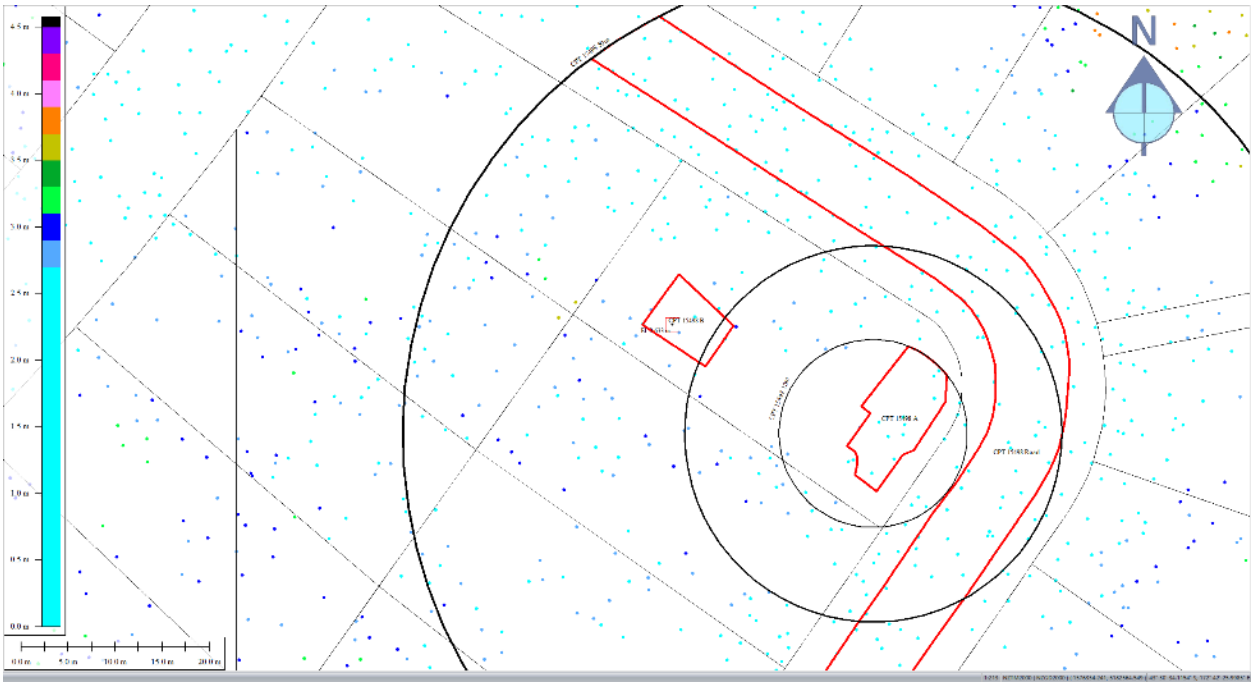

Figure 37: Ground surface elevation for Patch B for Jul 2003 LiDAR survey.

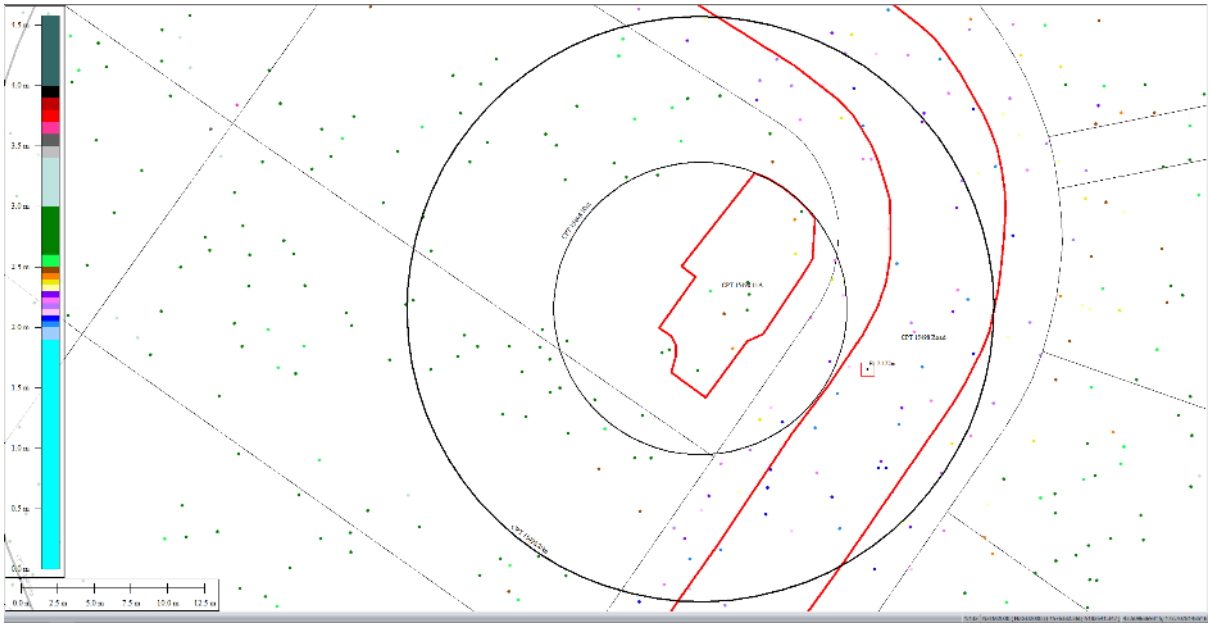

Figure 38: Ground surface elevation averaged over the 20-m buffer for Road for Jul 2003 LiDAR survey.

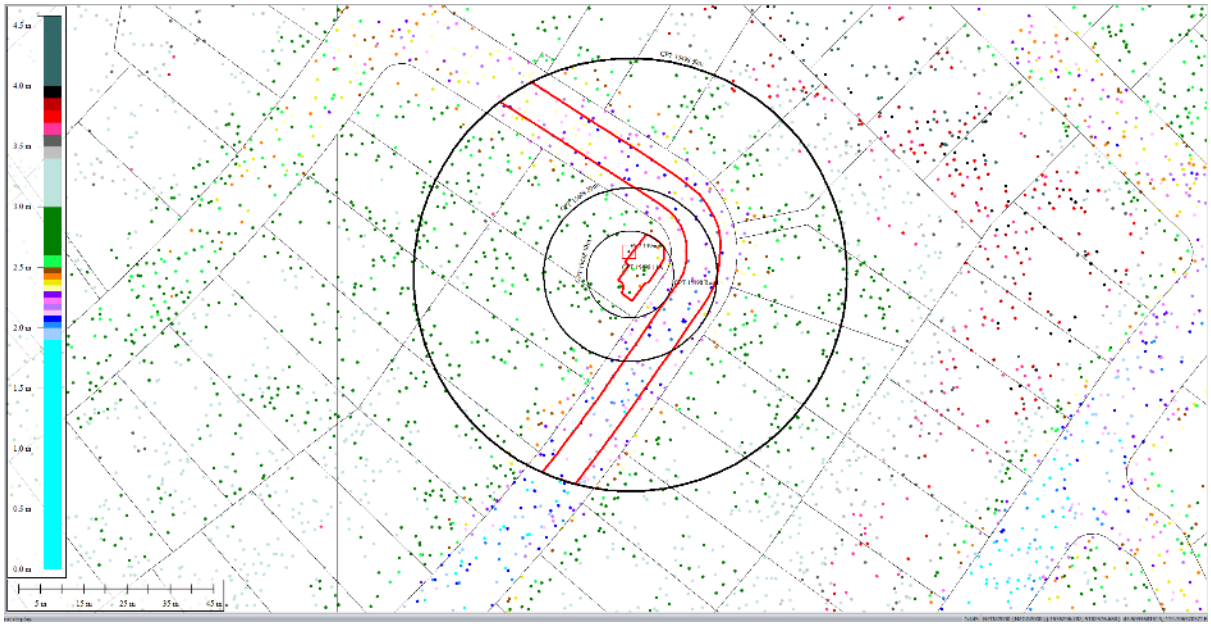

Figure 39: Ground surface elevation averaged over the 50-m buffer for Road for Jul 2003 LiDAR survey.

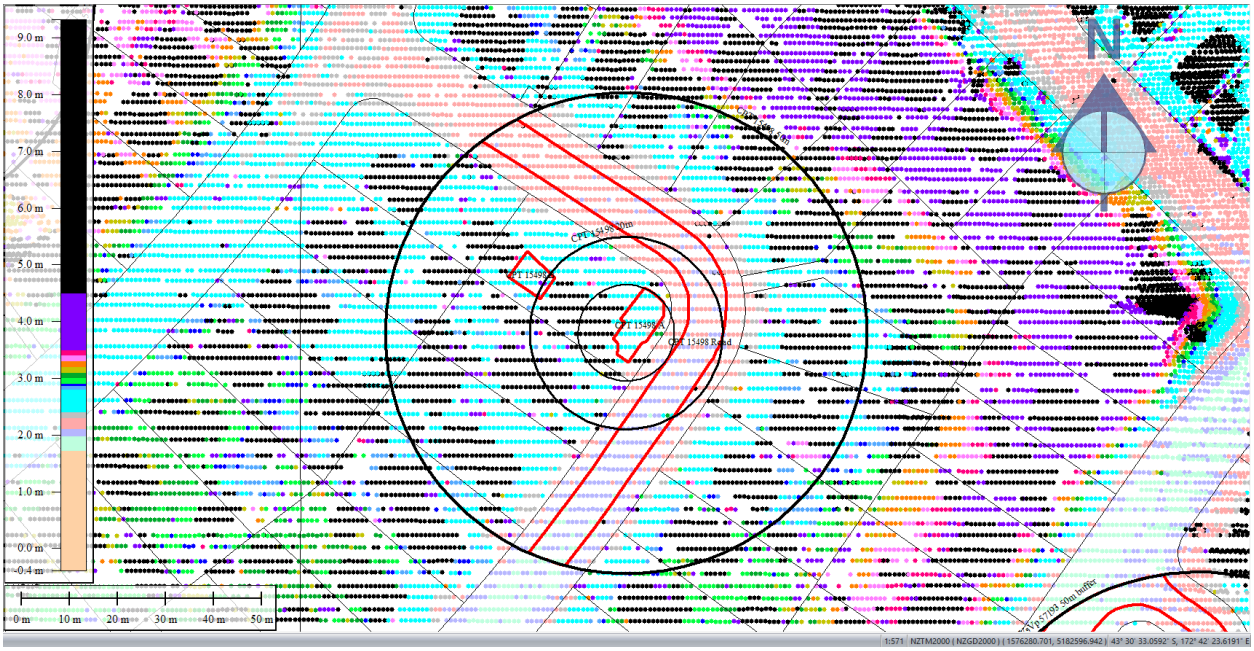

Figure 40: Sep 5, 2010 LiDAR survey.

Figure 41: Ground surface elevation for Patch A for Sep 5, 2010 LiDAR survey.

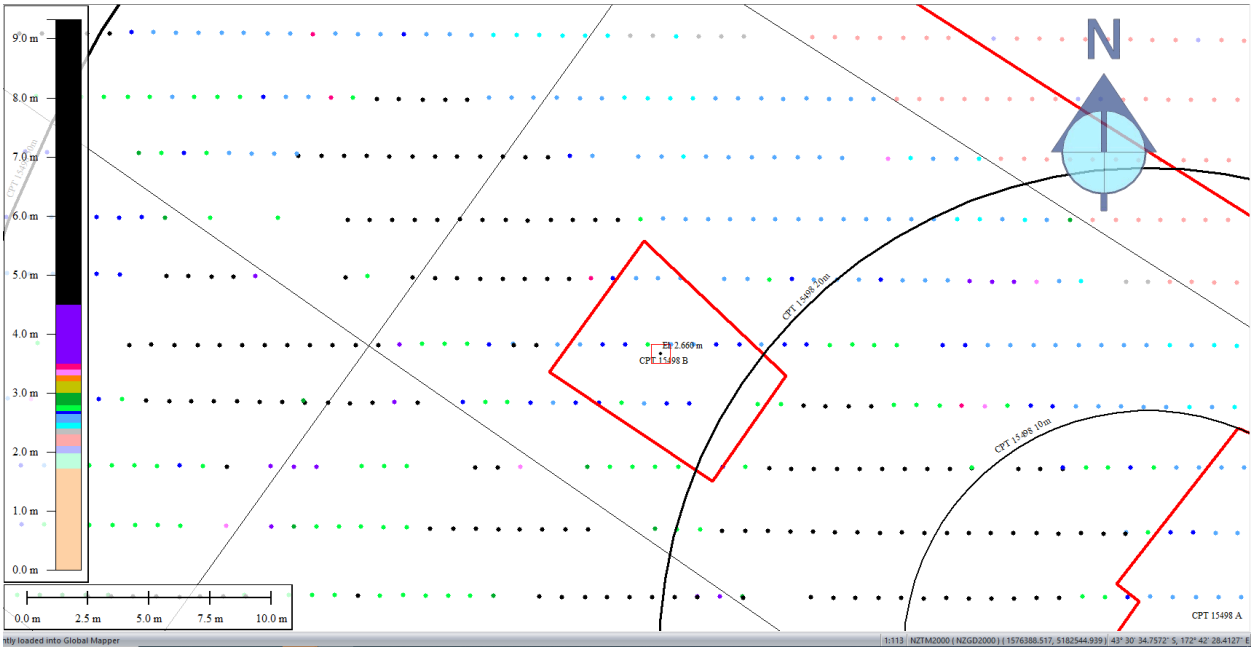

Figure 42: Ground surface elevation for Patch B for Sep 5, 2010 LiDAR survey.

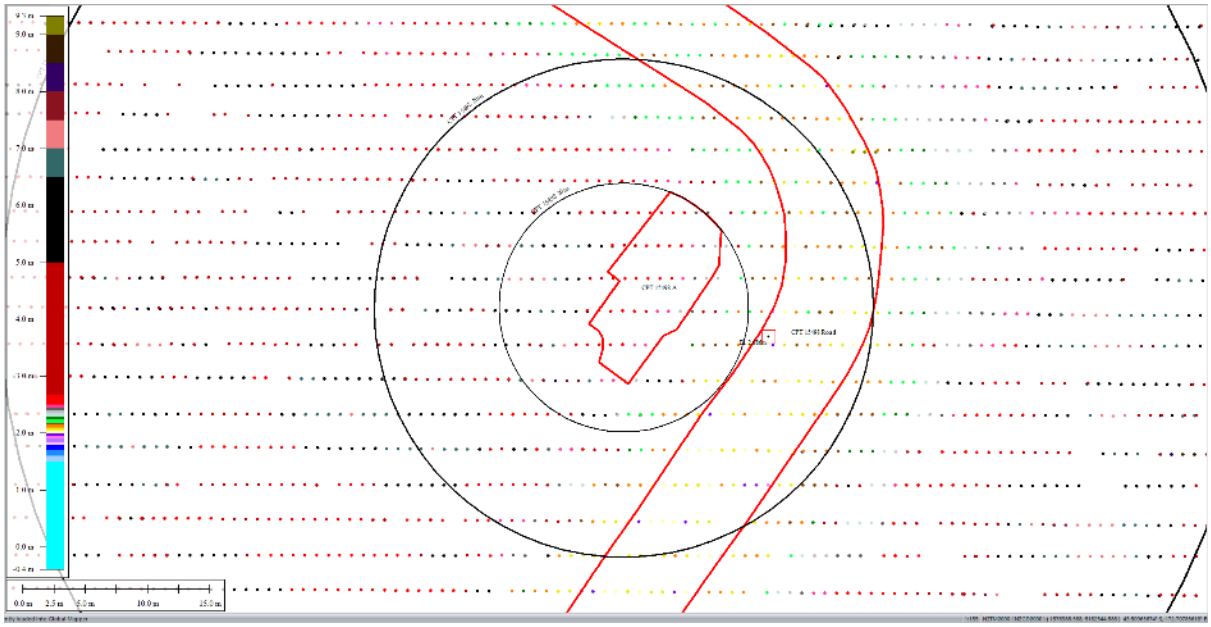

Figure 43: Ground surface elevation averaged over the 20-m buffer for Road for Sep 5, 2010 LiDAR survey.

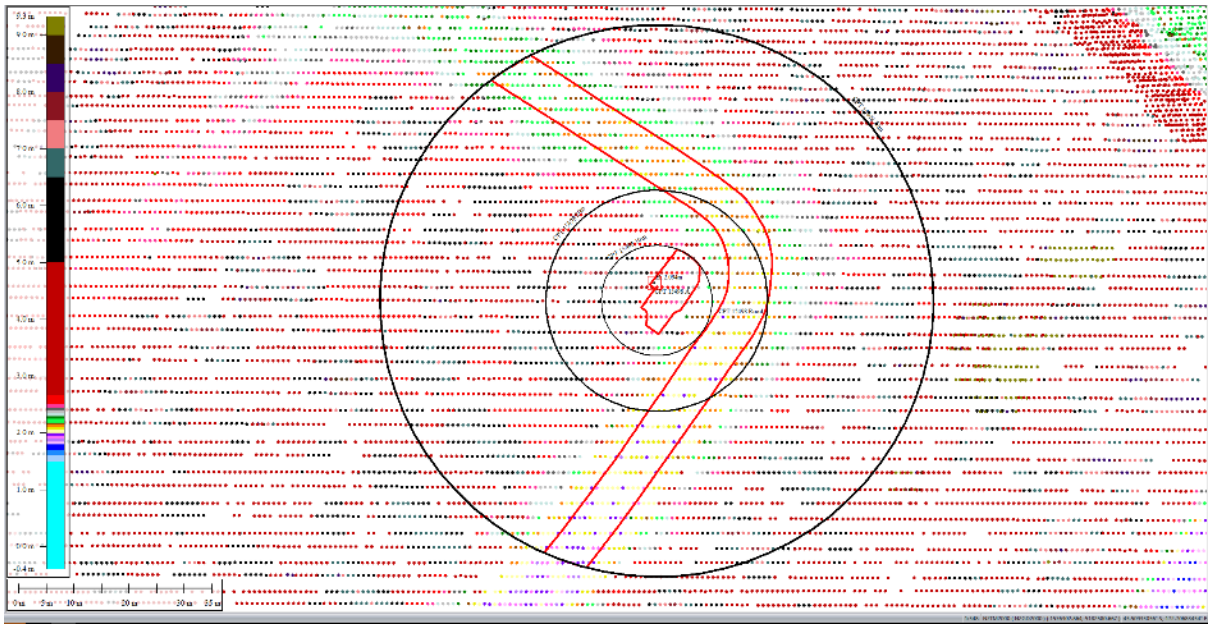

Figure 44: Ground surface elevation averaged over the 50-m buffer for Road for Sep 5, 2010 LiDAR survey.

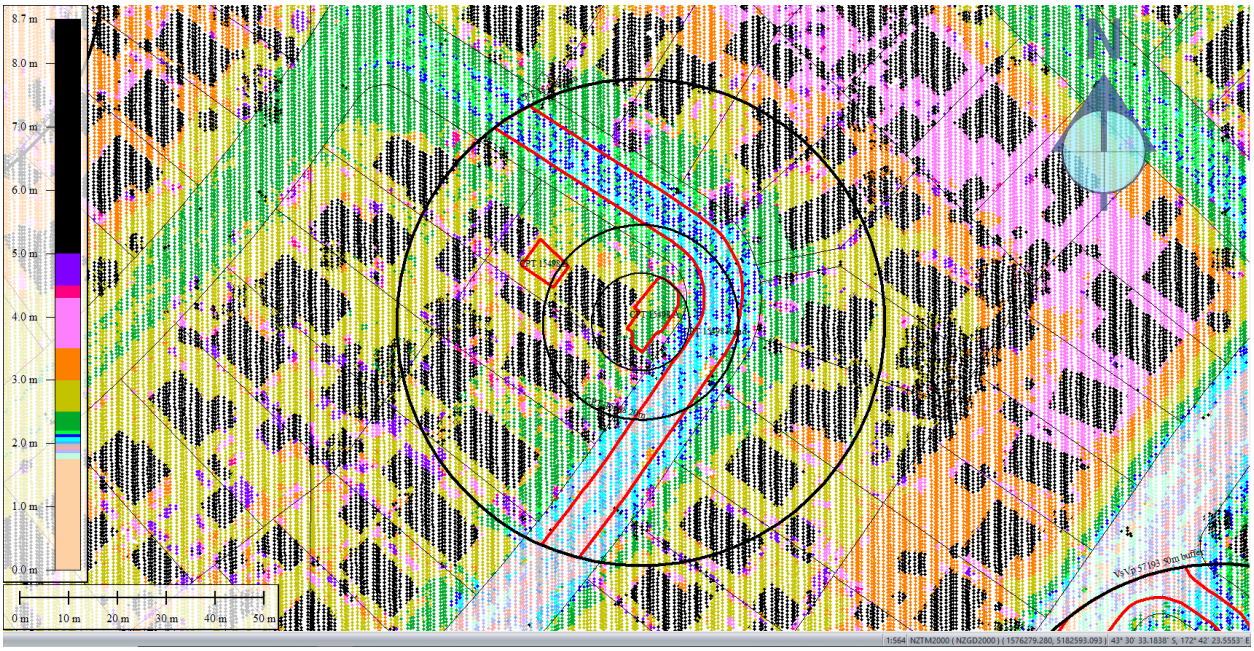

Figure 45: Mar 2011 LiDAR survey.

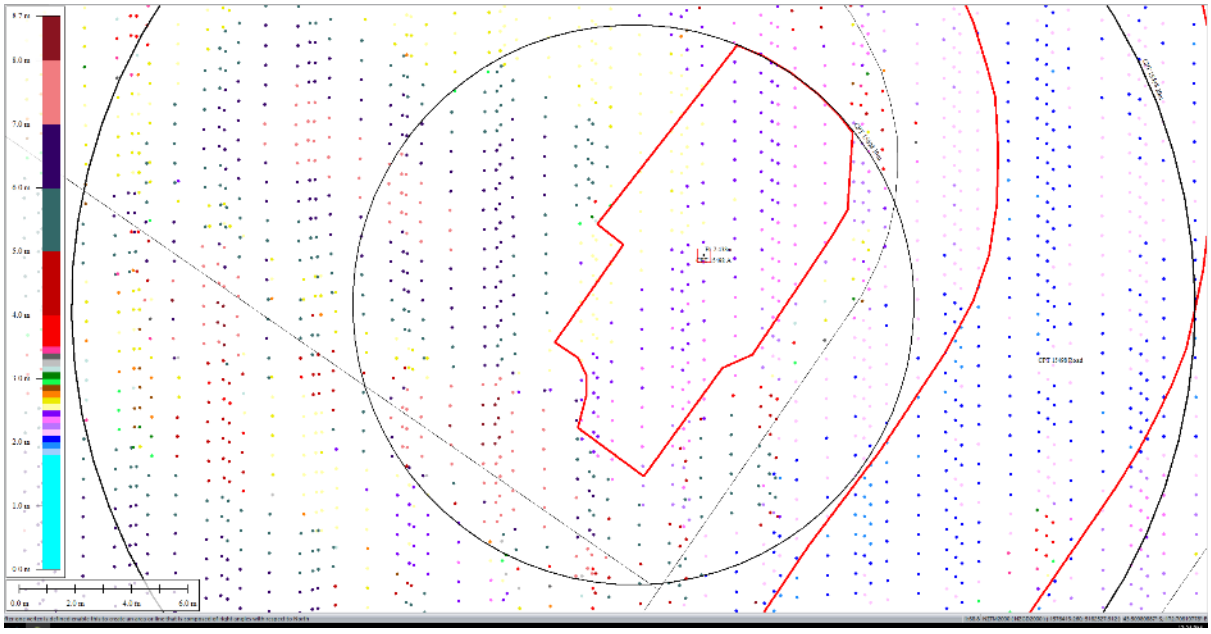

Figure 46: Ground surface elevation for Patch A for Mar 2011 LiDAR survey.

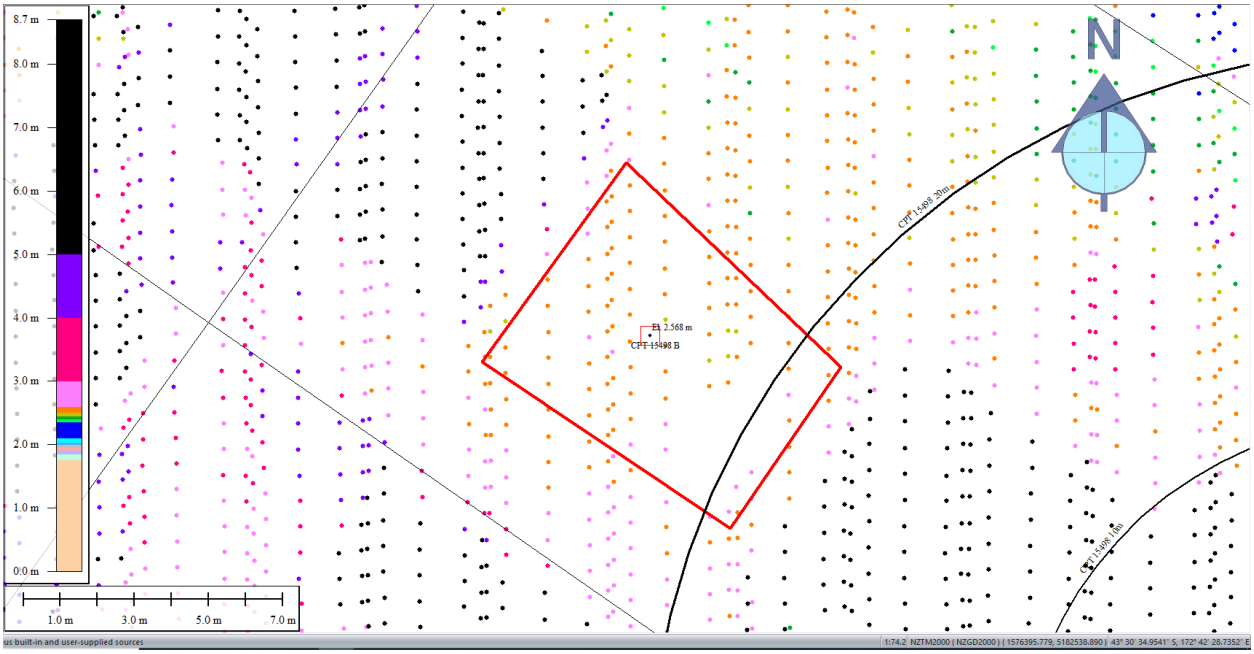

Figure 47: Ground surface elevation for Patch A for Mar 2011 LiDAR survey.

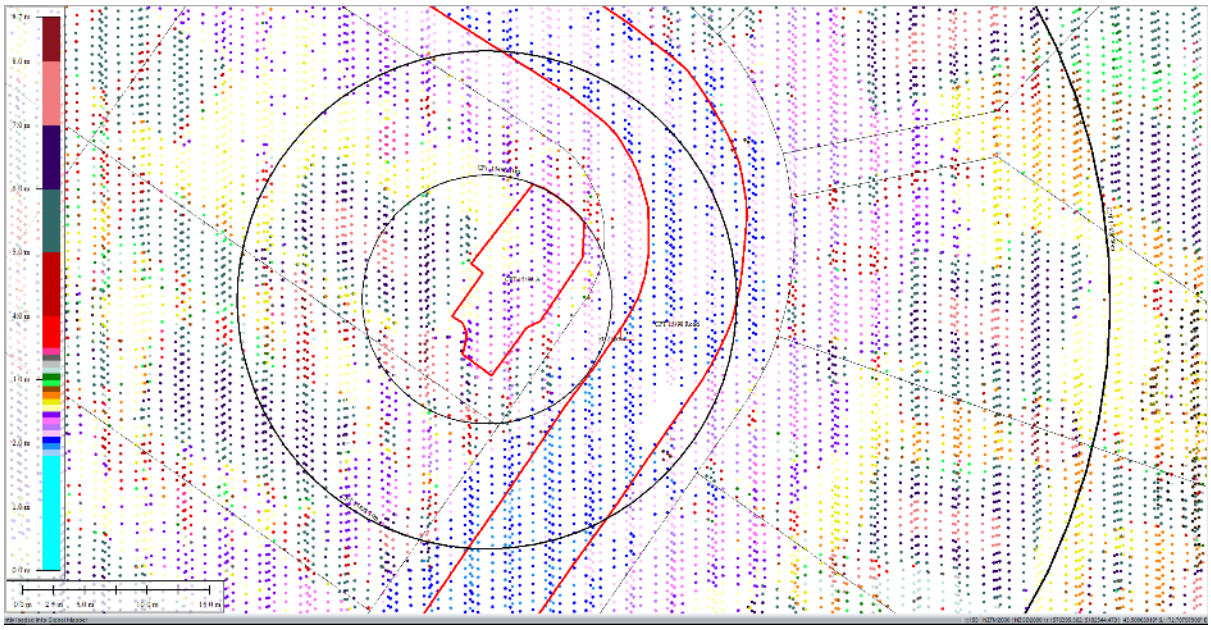

Figure 48: Ground surface elevation averaged over the 20-m buffer for Road for Mar 2011 LiDAR survey.

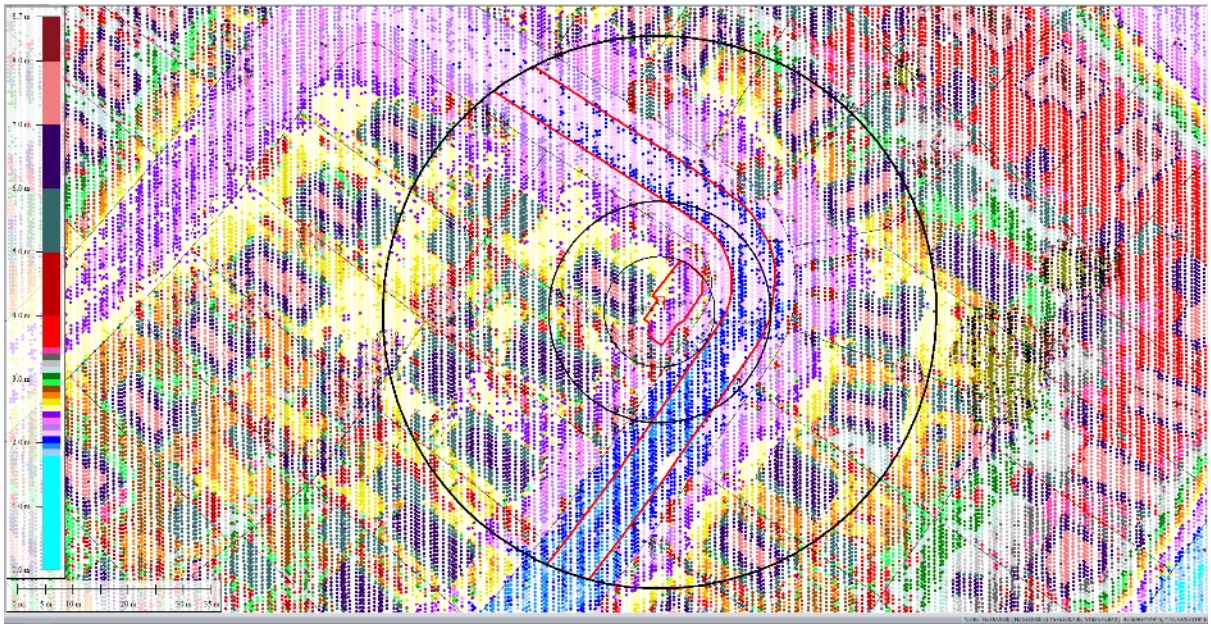

Figure 49: Ground surface elevation averaged over the 20-m buffer for Road for Mar 2011 LiDAR survey.

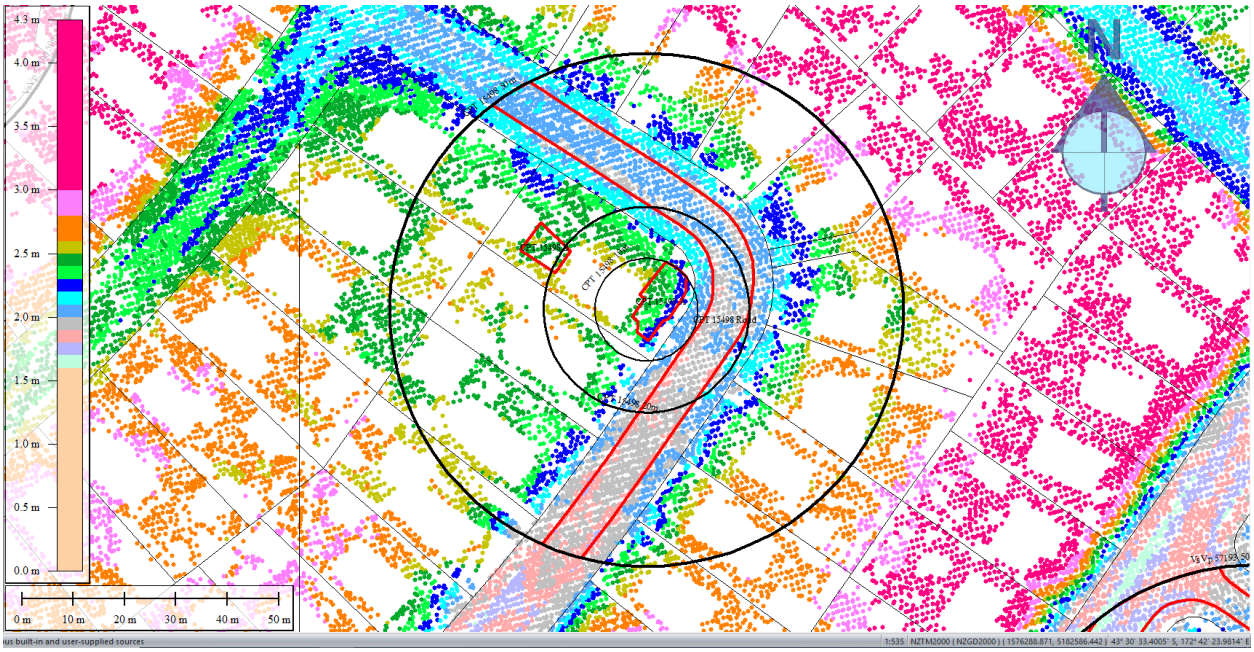

Figure 50: May 2011 LiDAR survey.

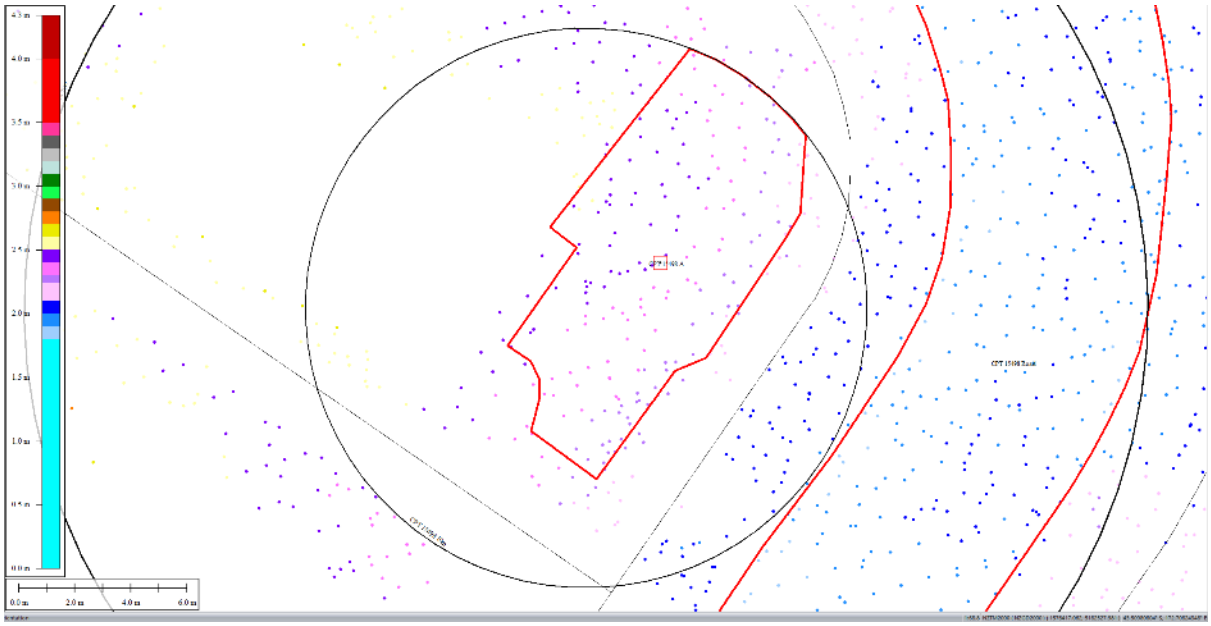

Figure 51: Ground surface elevation for Patch A for May 2011 LiDAR survey.

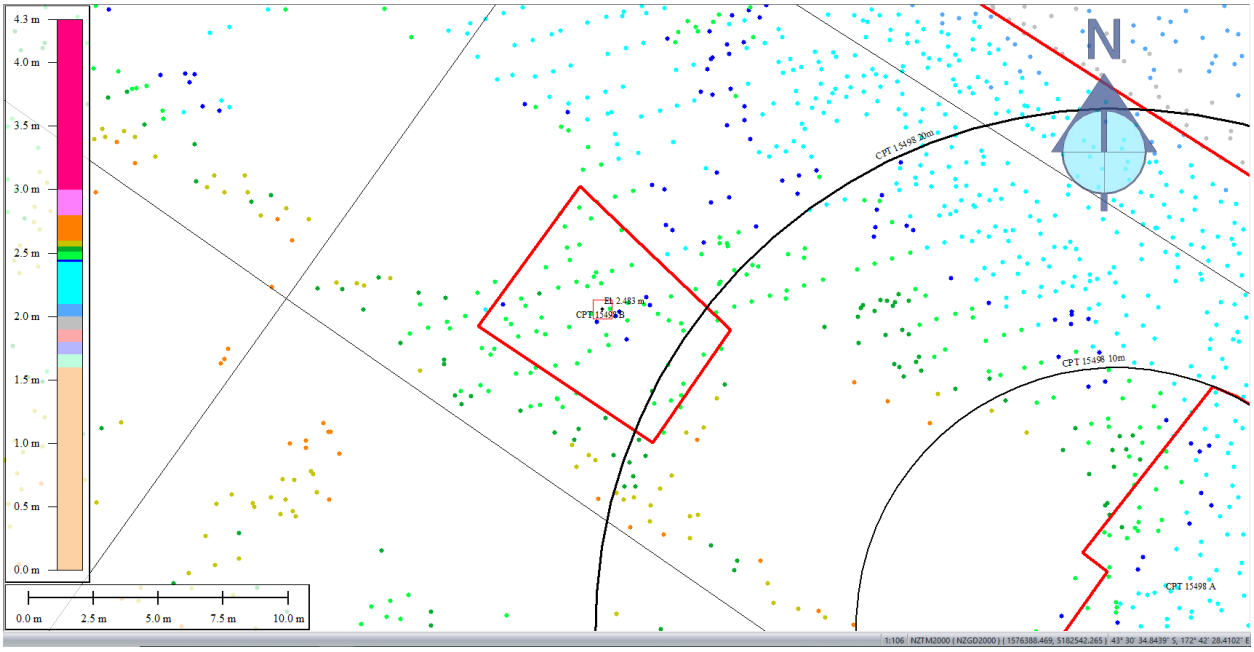

Figure 52: Ground surface elevation for Patch B for May 2011 LiDAR survey.

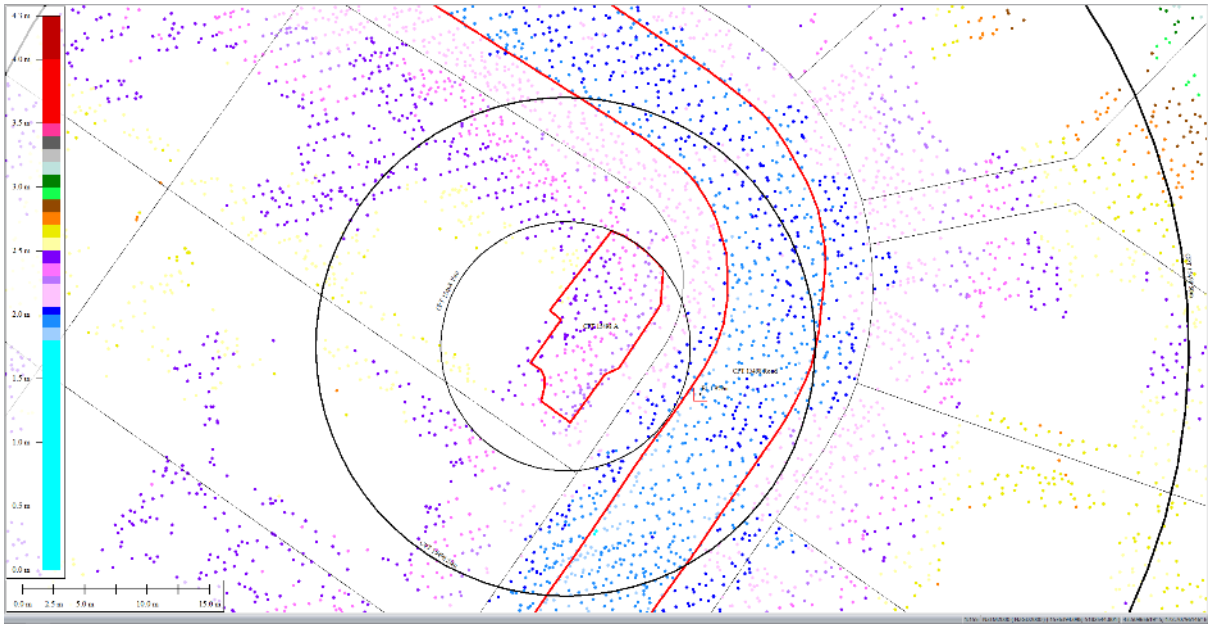

Figure 53: Ground surface elevation averaged over the 20-m buffer for Road for May 2011 LiDAR survey.

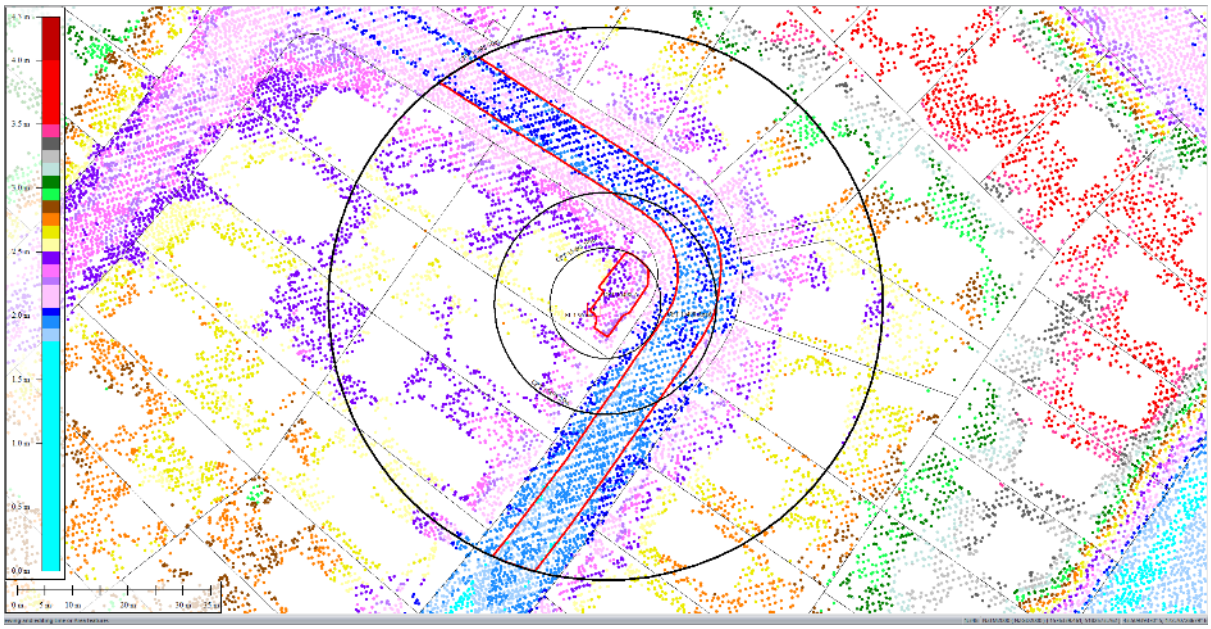

Figure 54: Ground surface elevation averaged over the 50-m buffer for Road for May 2011 LiDAR survey.

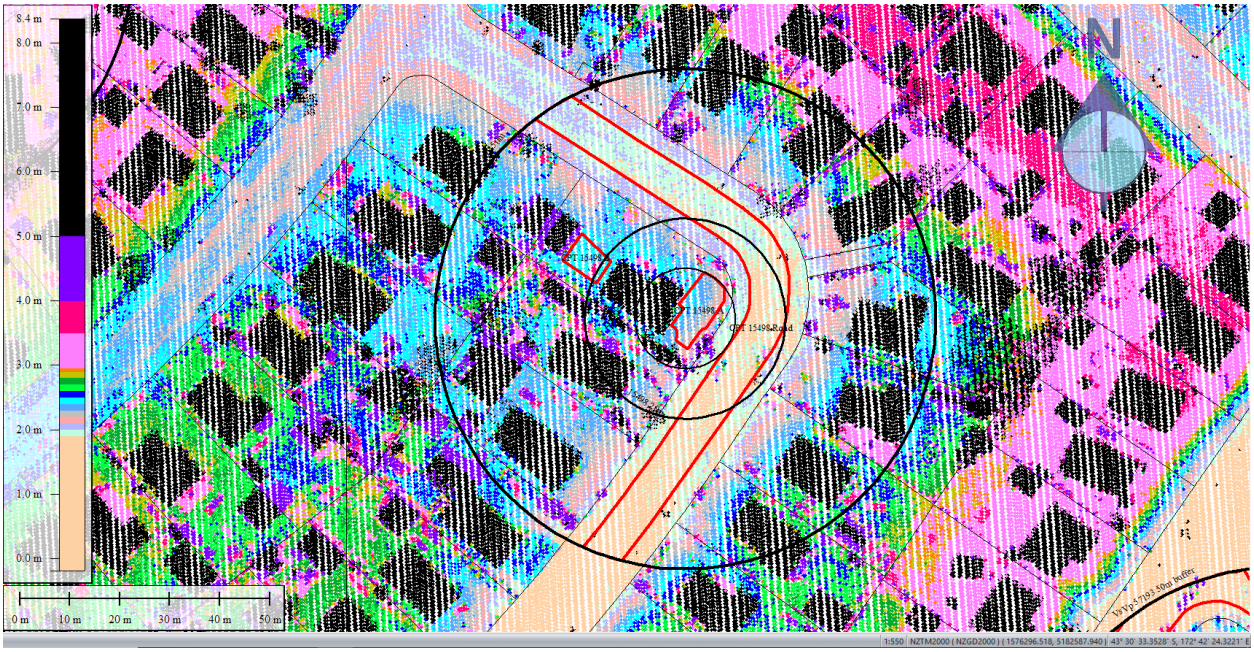

Figure 55: Sep 2011 LiDAR survey.

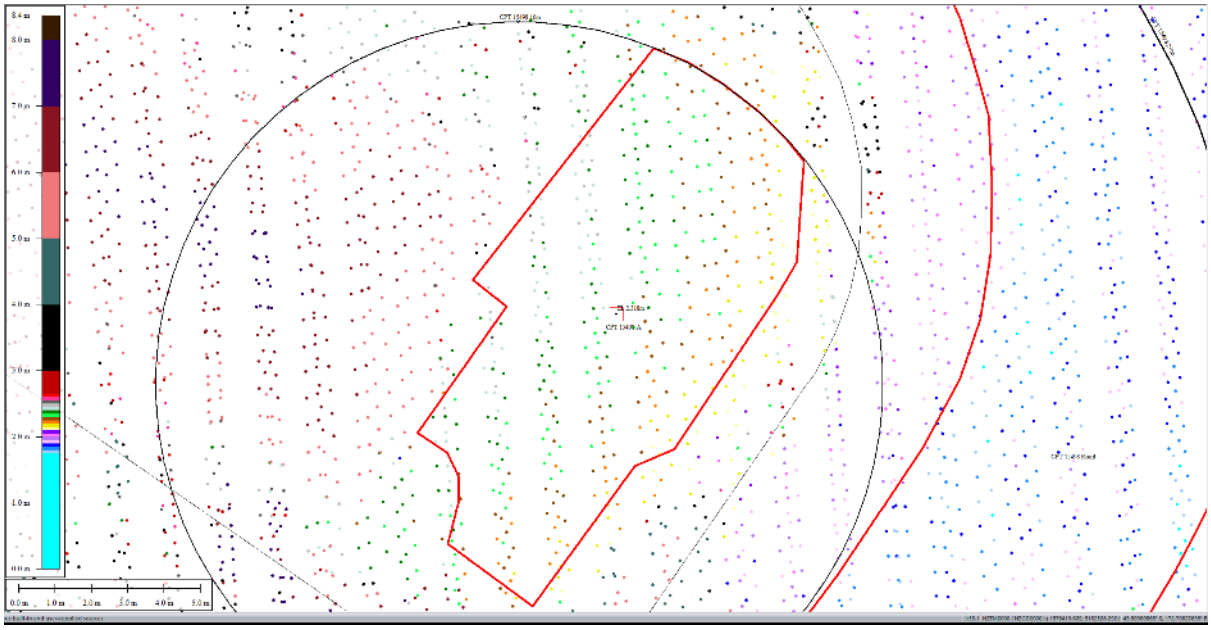

Figure 56: Ground surface elevation for Patch A for Sep 2011 LiDAR survey.

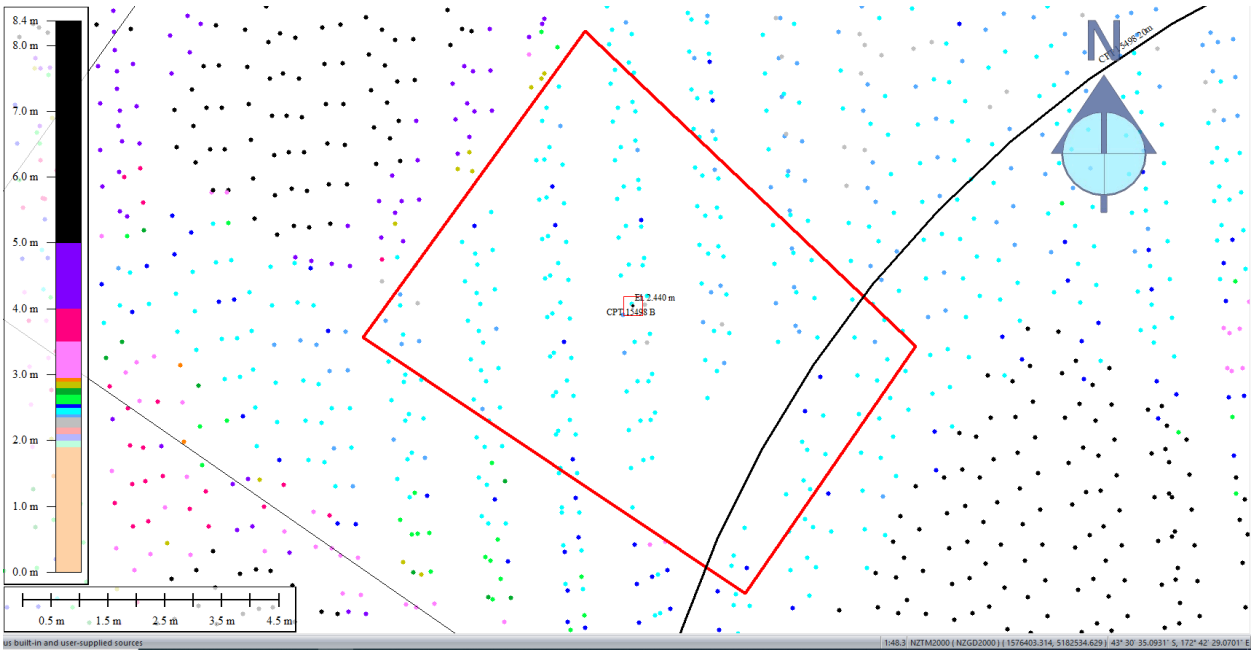

Figure 57: Ground surface elevation for Patch B for Sep 2011 LiDAR survey.

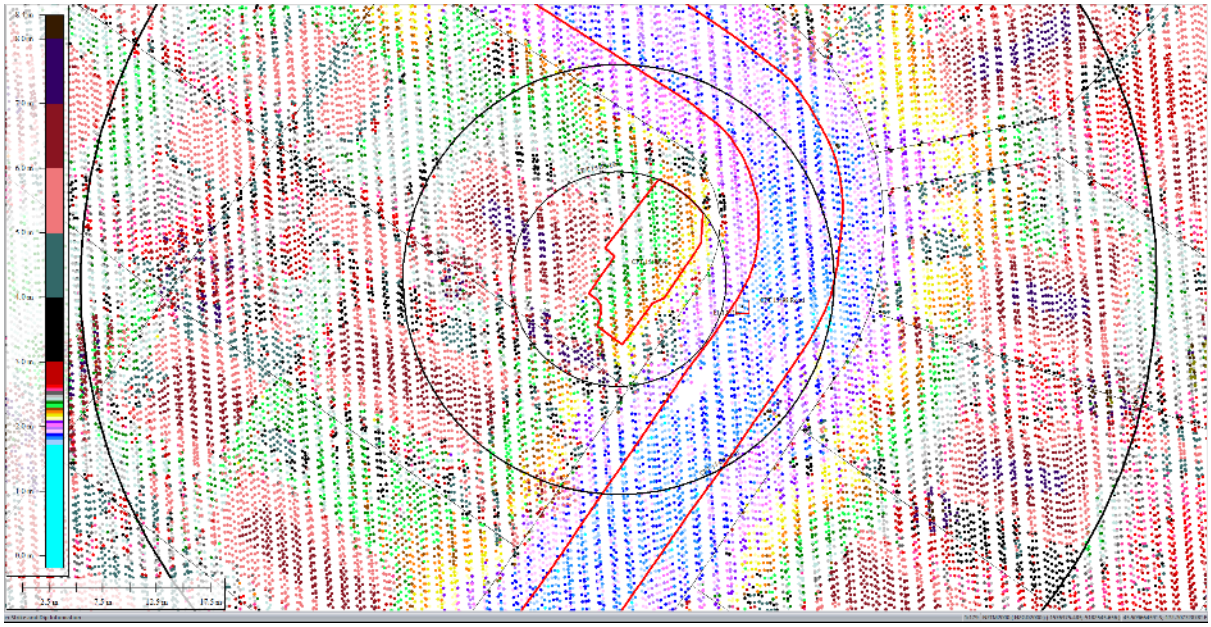

Figure 58: Ground surface elevation averaged over the 20-m buffer for Road for Sep 2011 LiDAR survey.

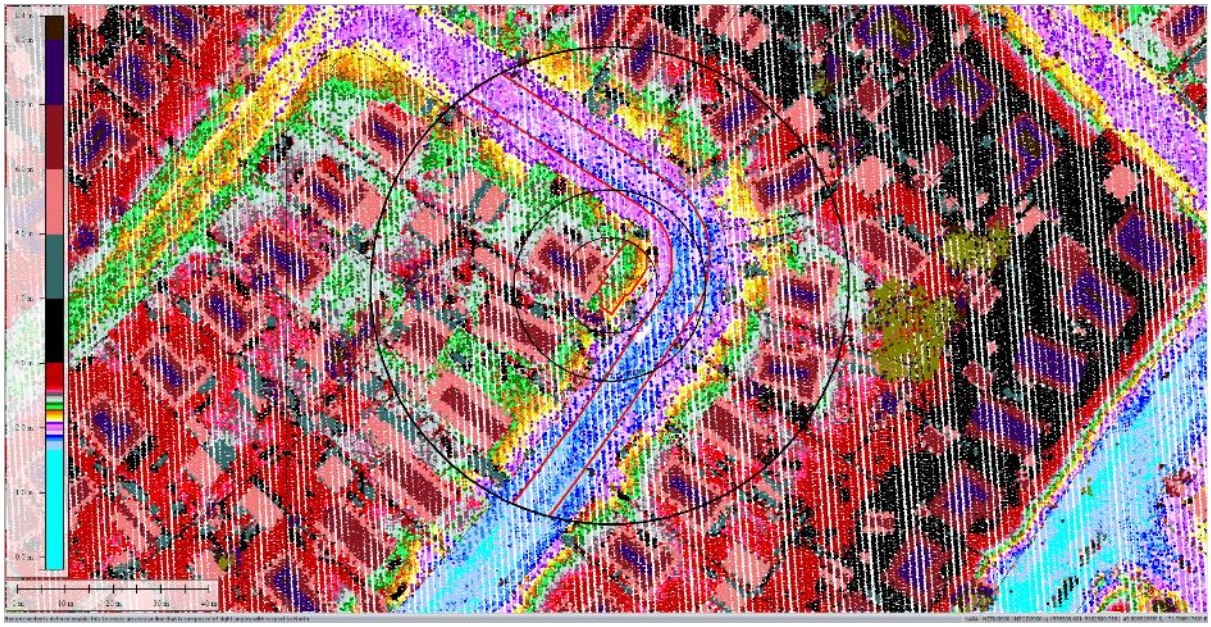

Figure 59: Ground surface elevation averaged over the 50-m buffer for Road for Sep 2011 LiDAR survey.

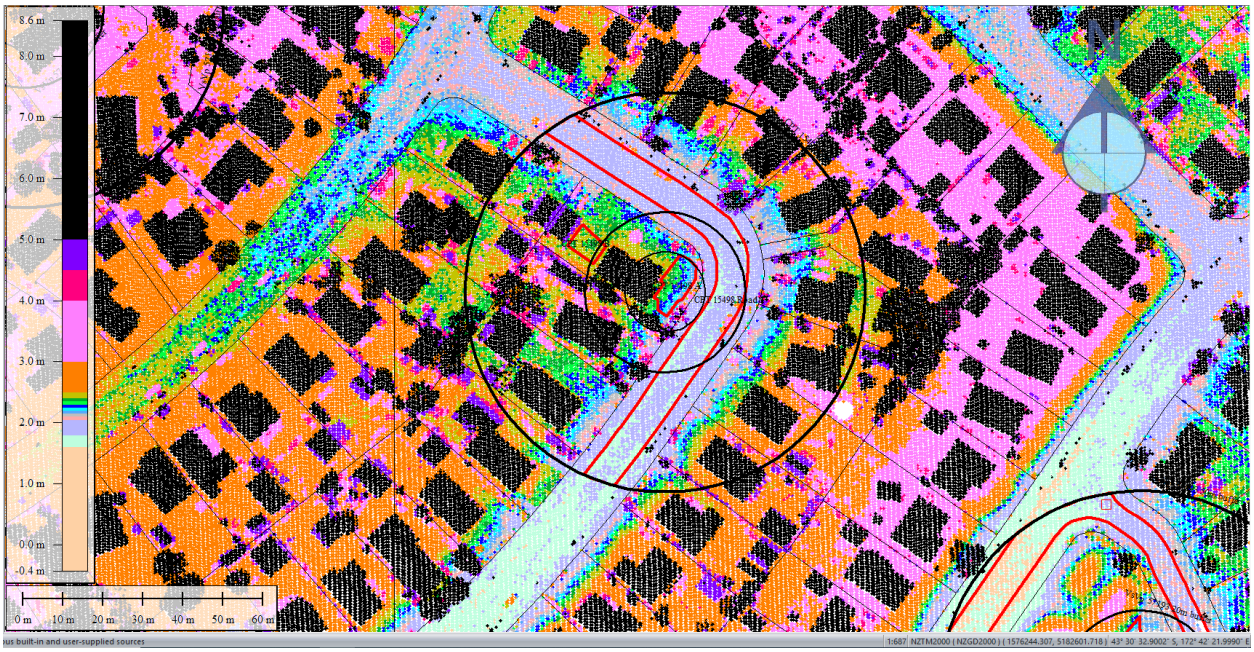

Figure 60: Feb 2012 LiDAR survey.

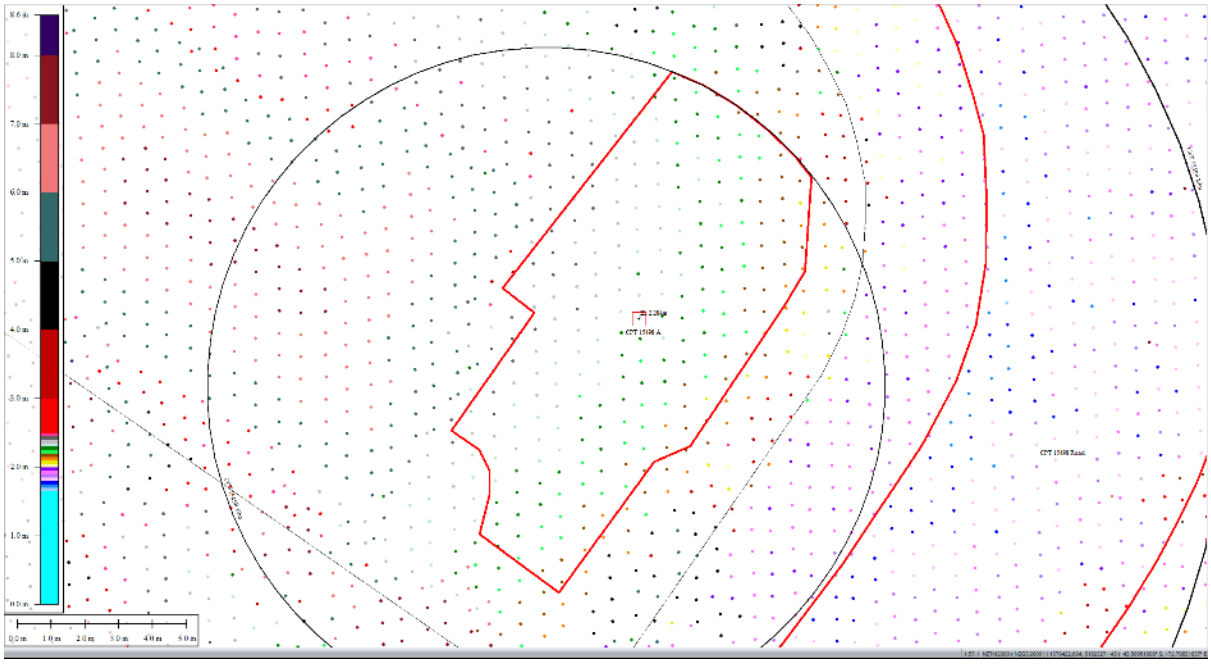

Figure 61: Ground surface elevation for Patch A for Feb 2012 LiDAR survey.

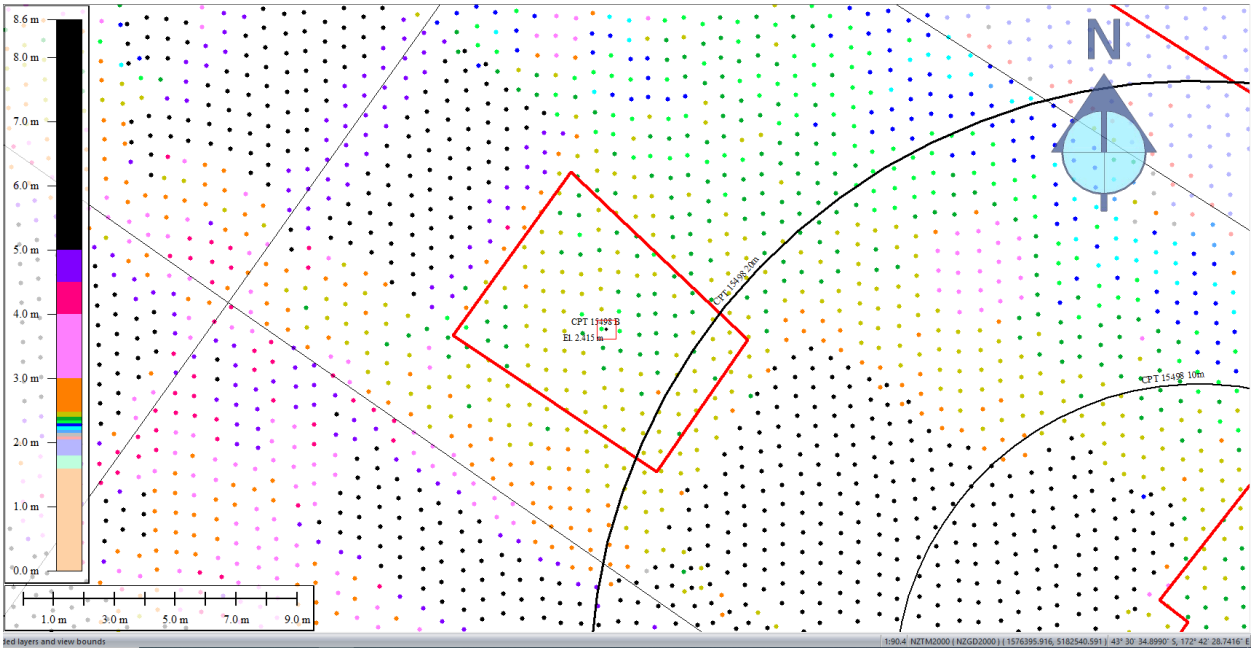

Figure 62: Ground surface elevation for Patch B for Feb 2012 LiDAR survey.

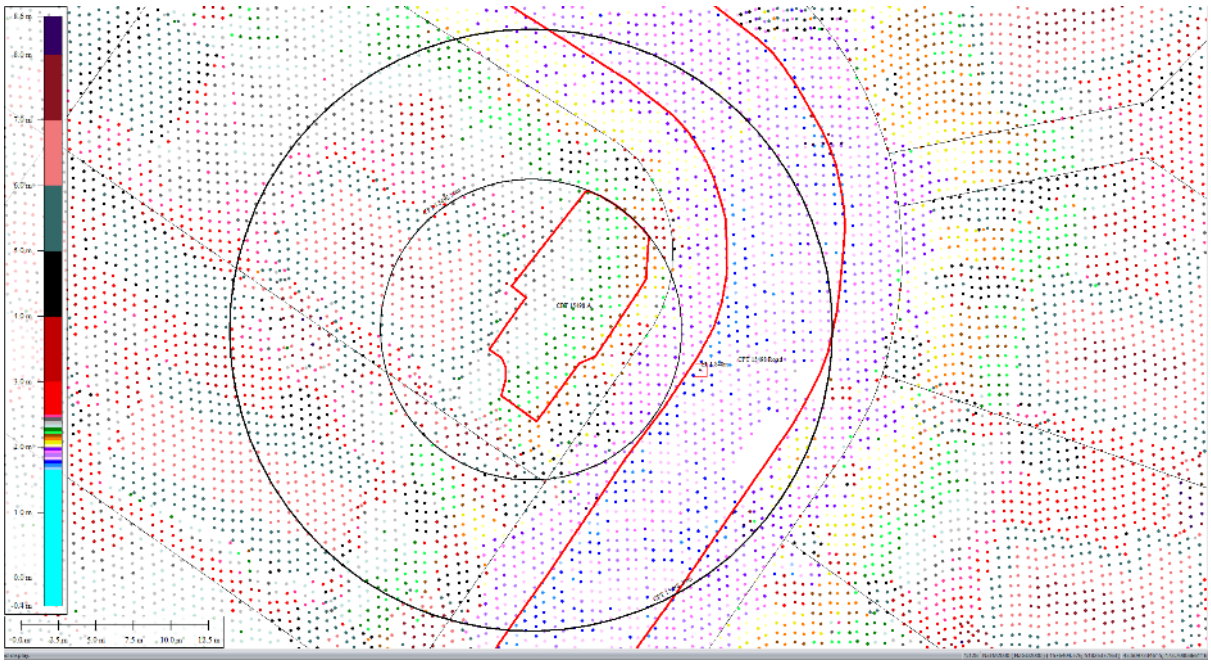

Figure 63: Ground surface elevation averaged over the 20-m buffer for Road for Feb 2012 LiDAR survey.

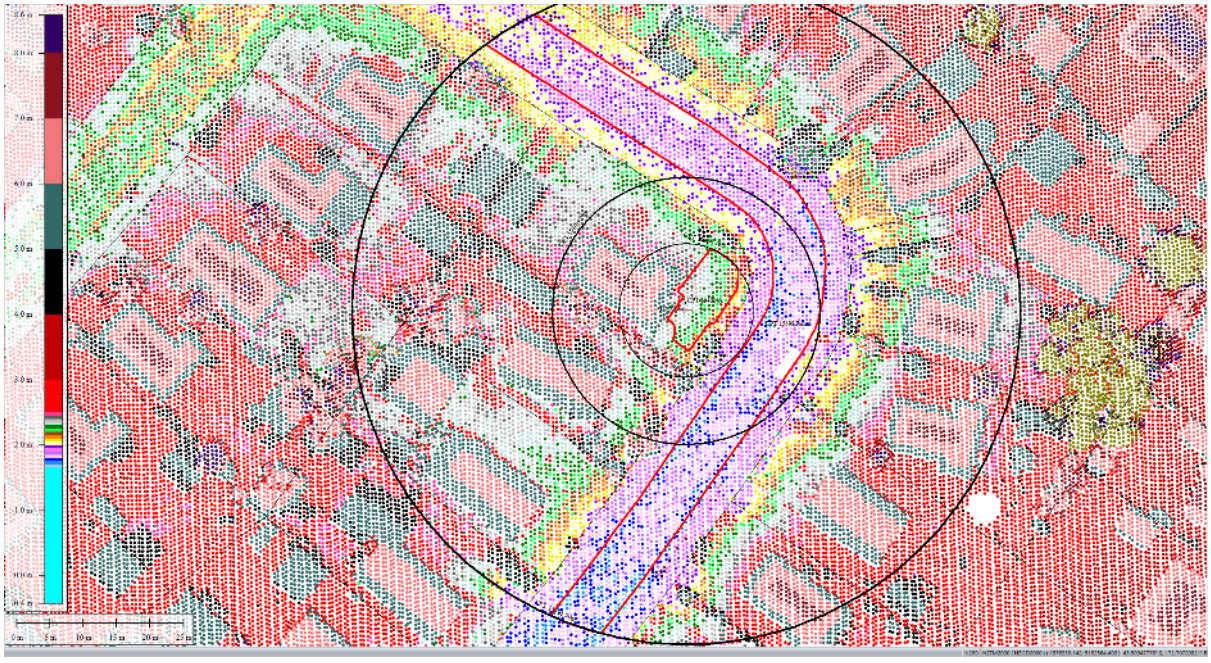

Figure 64: Ground surface elevation averaged over the 50-m buffer for Road for Feb 2012 LiDAR survey.

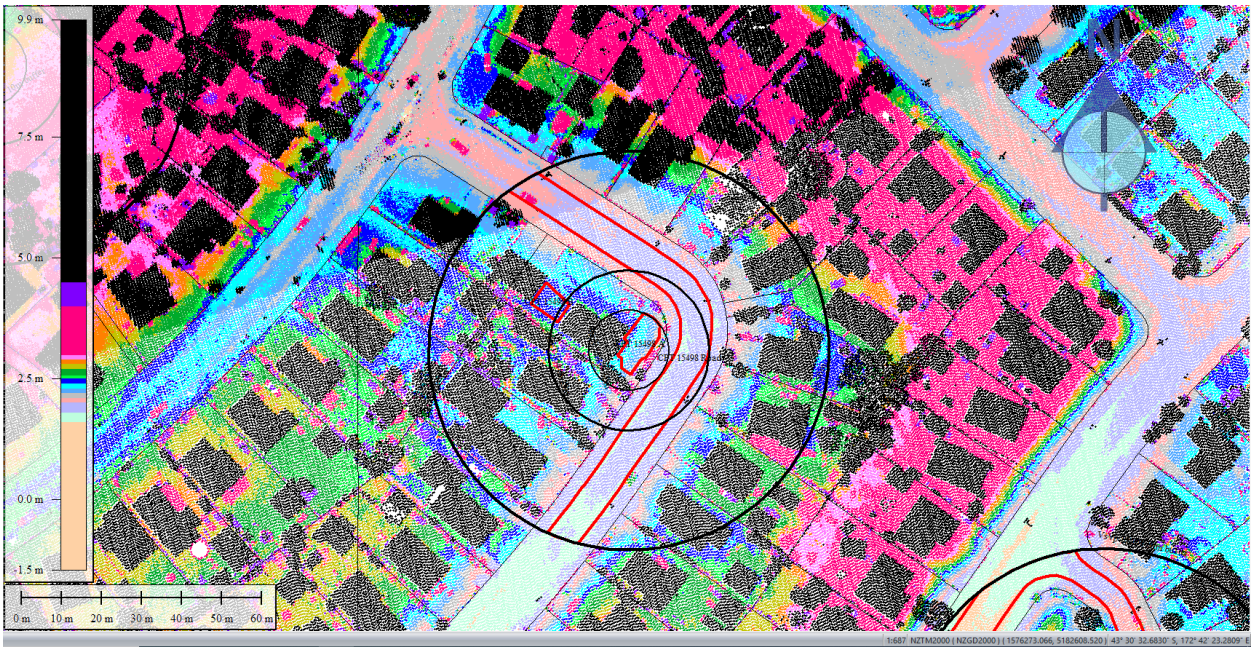

Figure 65: Oct 2015 LiDAR survey.

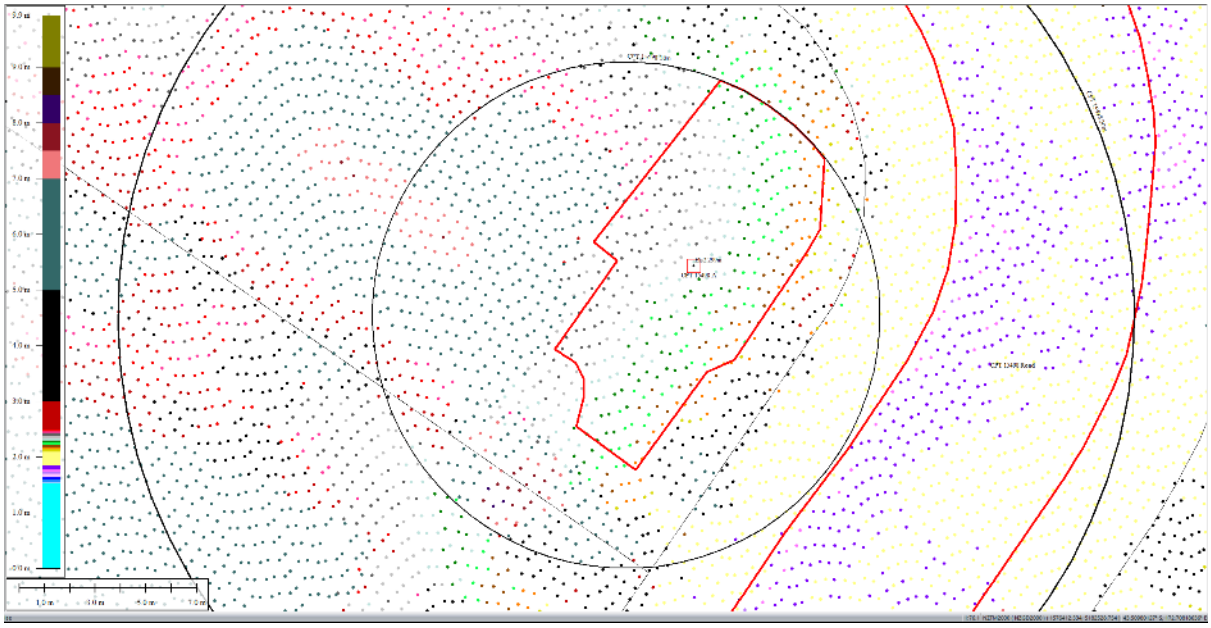

Figure 66: Ground surface elevation for Patch A for Oct 2015 LiDAR survey.

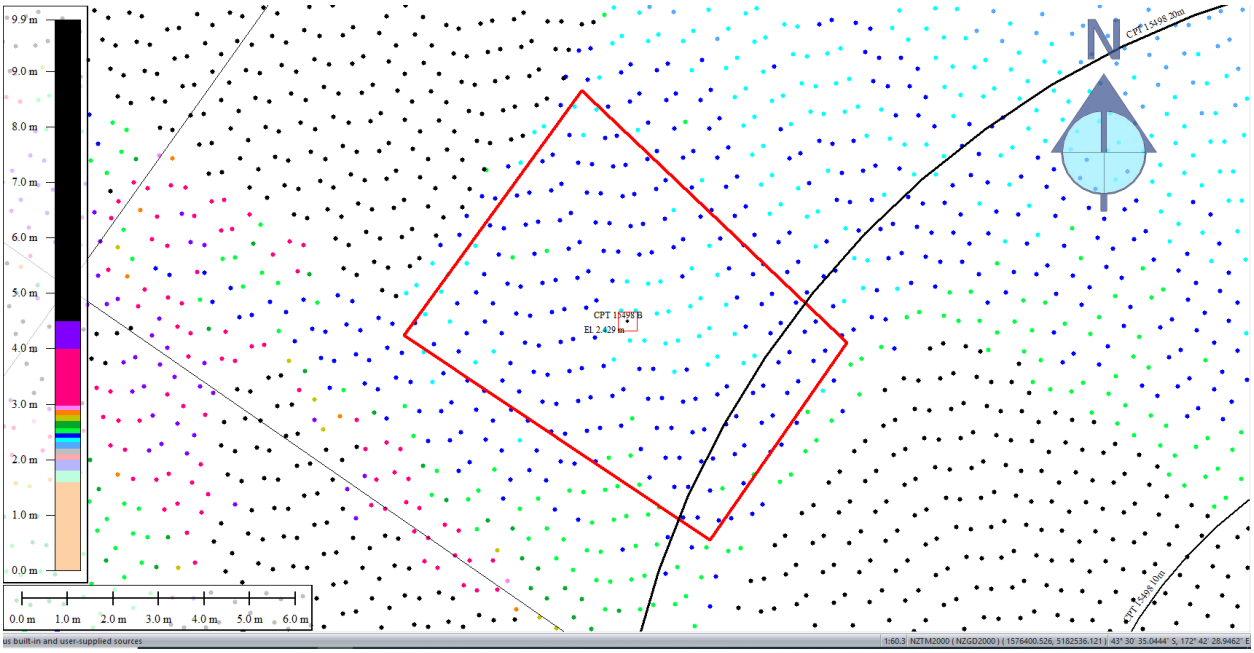

Figure 67: Ground surface elevation for Patch B for Oct 2015 LiDAR survey.

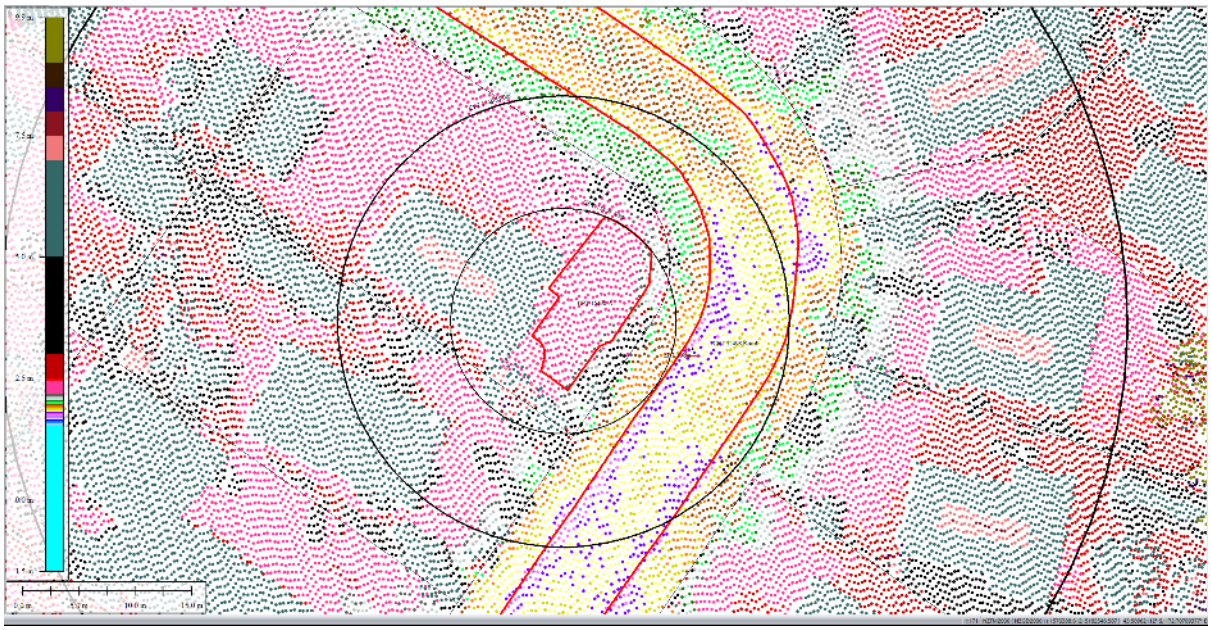

Figure 68: Ground surface elevation averaged over the 20-m buffer for Road for Oct 2015 LiDAR survey.

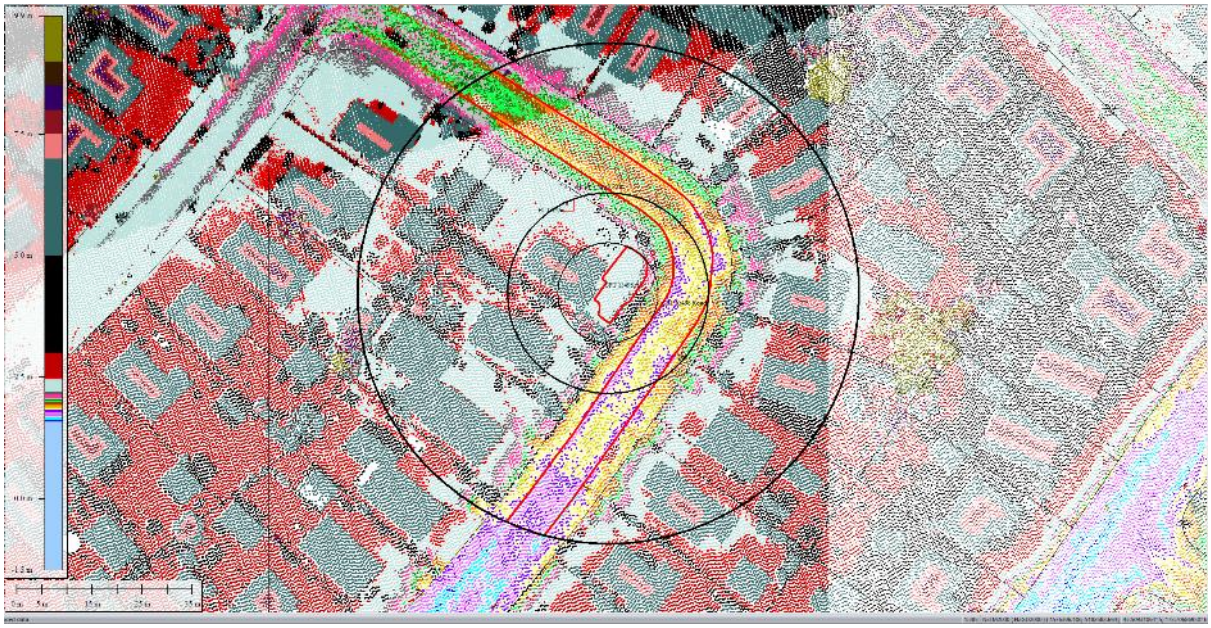

Figure 69: Ground surface elevation averaged over the 50-m buffer for Road for Oct 2015 LiDAR survey.

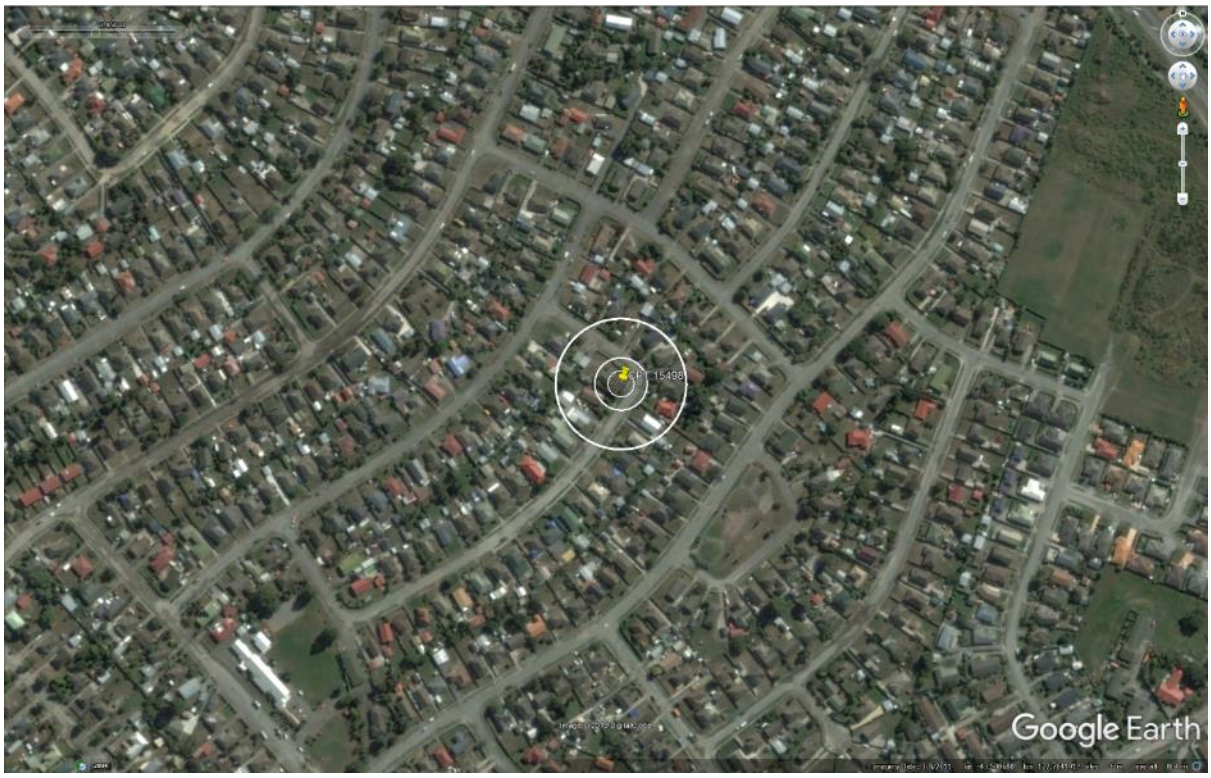

Figure 70: Satellite image taken on Mar 8, 2011 showing evidence of ejecta.

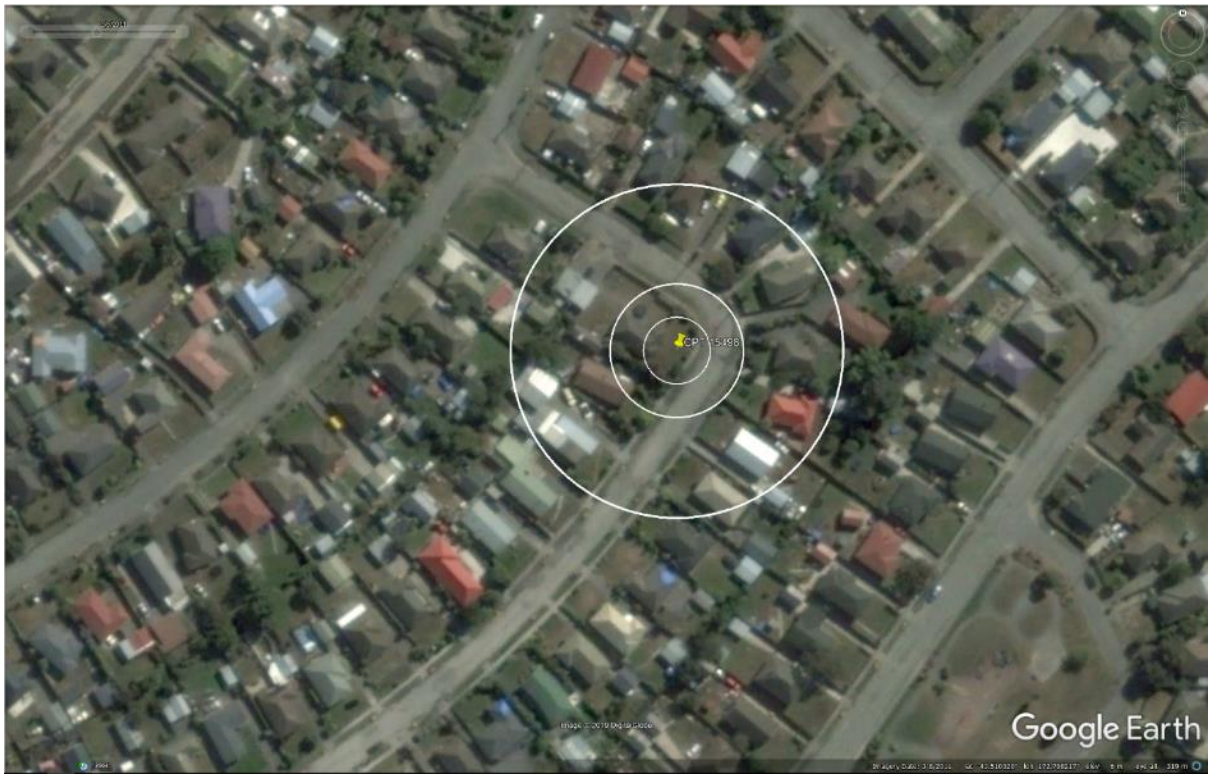

Figure 71: Satellite image taken on Mar 8, 2011 showing evidence of some ejecta remaining on the road at the time of the Mar 2011 LiDAR survey.

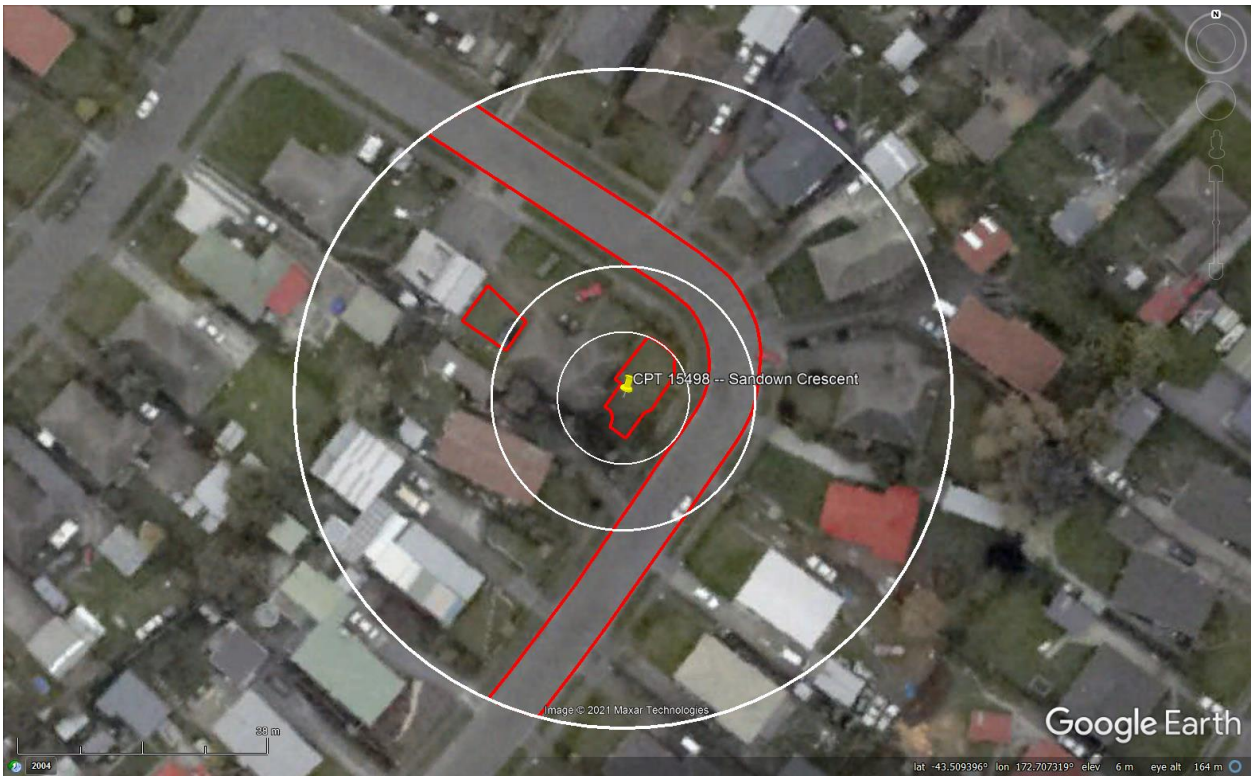

Figure 72: Aerial photograph showing absence of ejecta at the site for Sep-10 EQ.

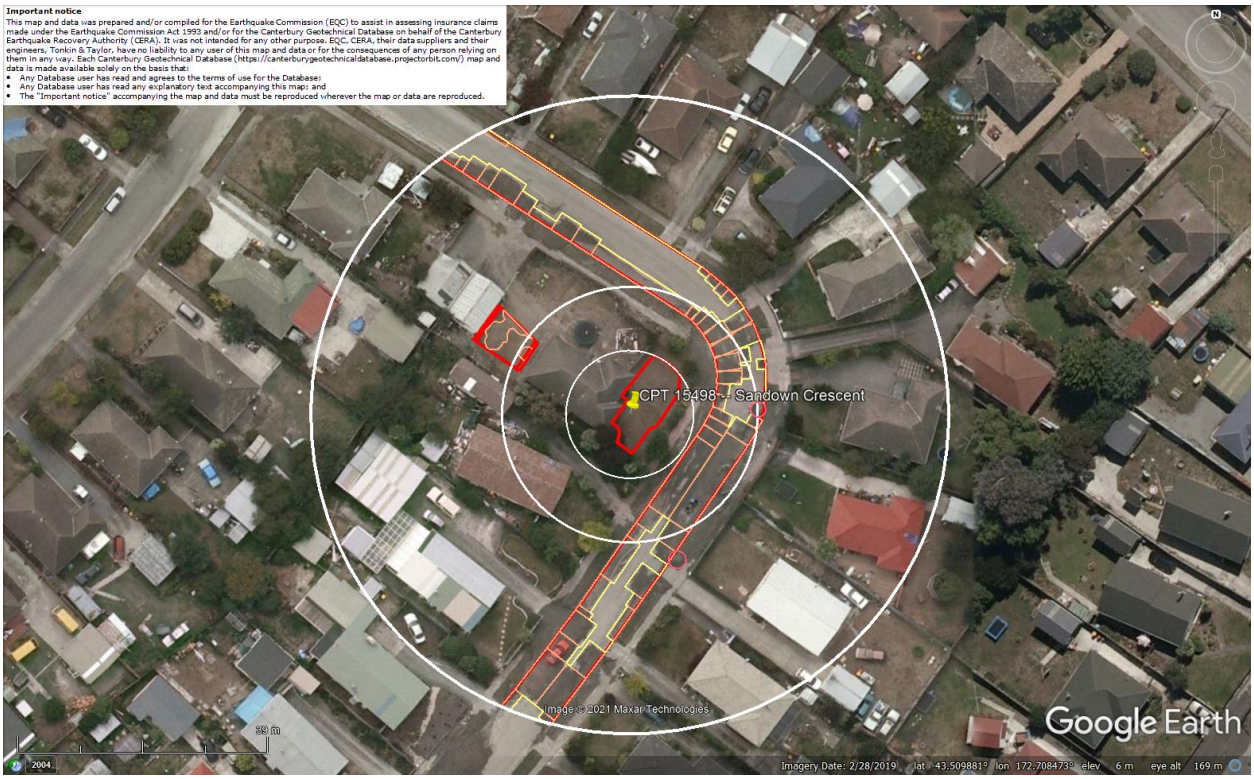

Figure 73: Ejecta outline for Feb-11 EQ.

Figure 74: Satellite image of the site for Feb-11 EQ.

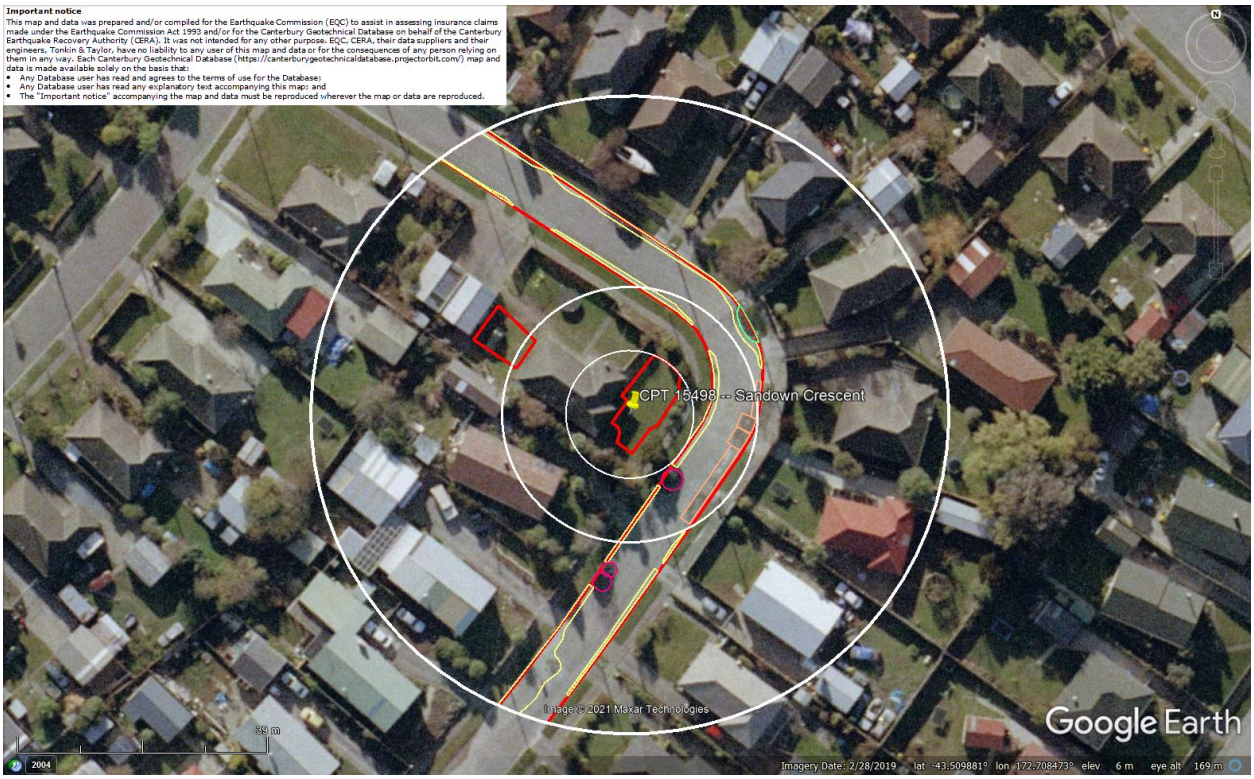

Figure 75: Ejecta outline for Jun-11 EQ.

Figure 76: No ejecta for Dec-11 EQ.

Figure 77: Ground photographs of Patch A.

Figure 78: Ground photographs of Patch B.

Contents of this figure cannot be shared as doing so is restricted by a Non-Disclosure Agreement.

Figure 79: LDAT property inspection notes for Patches A and B.

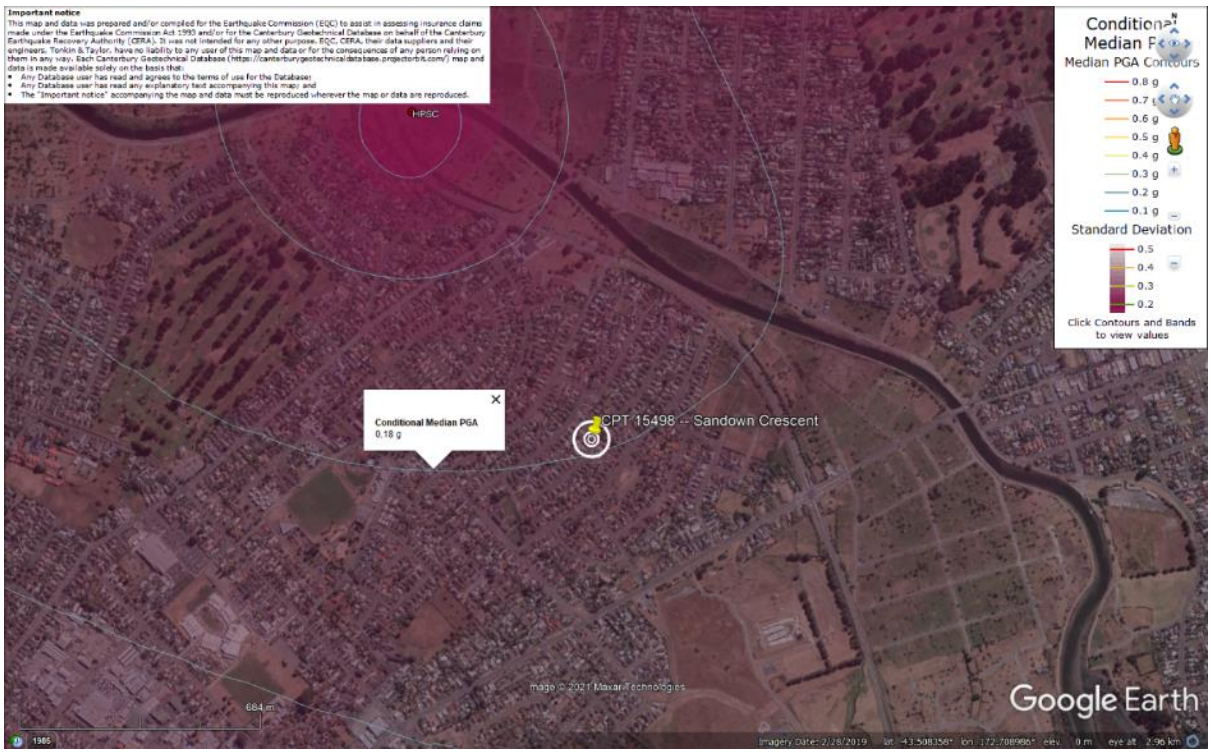

Figure 80: PGA for Sep-10 EQ (st. dev. = 0.300-0.325 ln units).

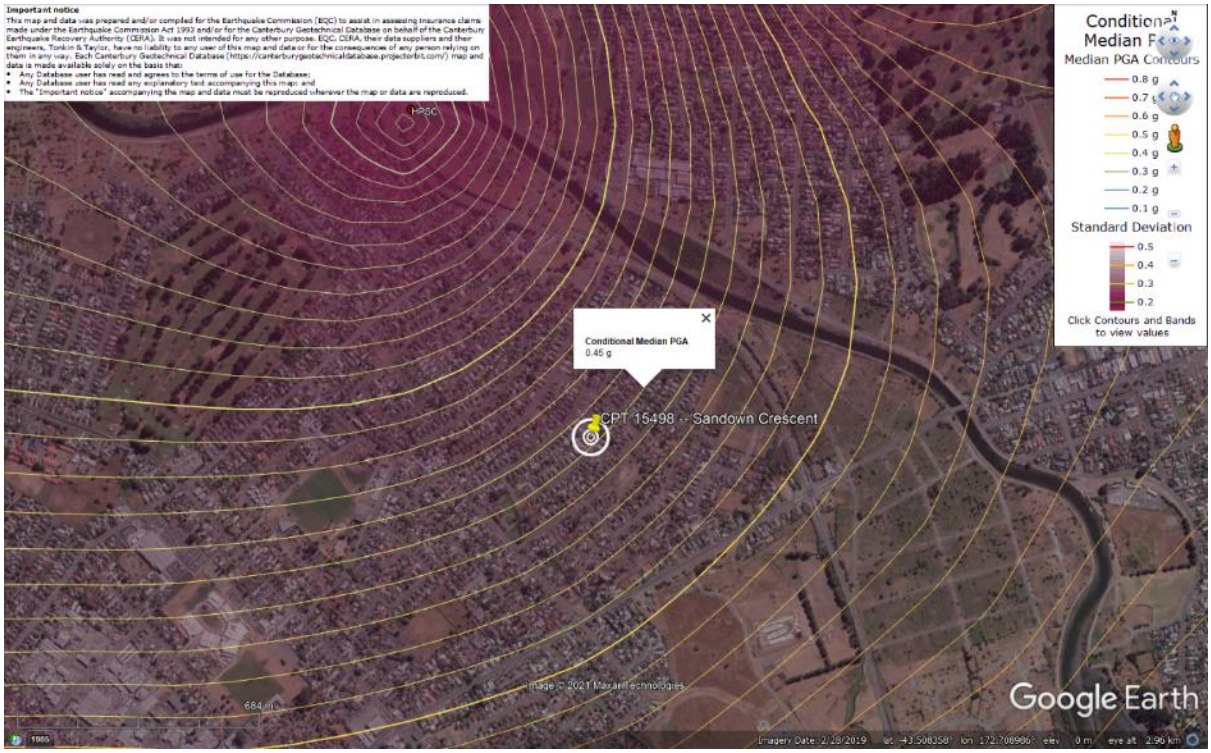

Figure 81: PGA for Feb-11 EQ (st. dev. = 0.325-0.350 ln units).

Figure 82: PGA for Jun-11 EQ (st. dev. = 0.325-0.350 ln units).

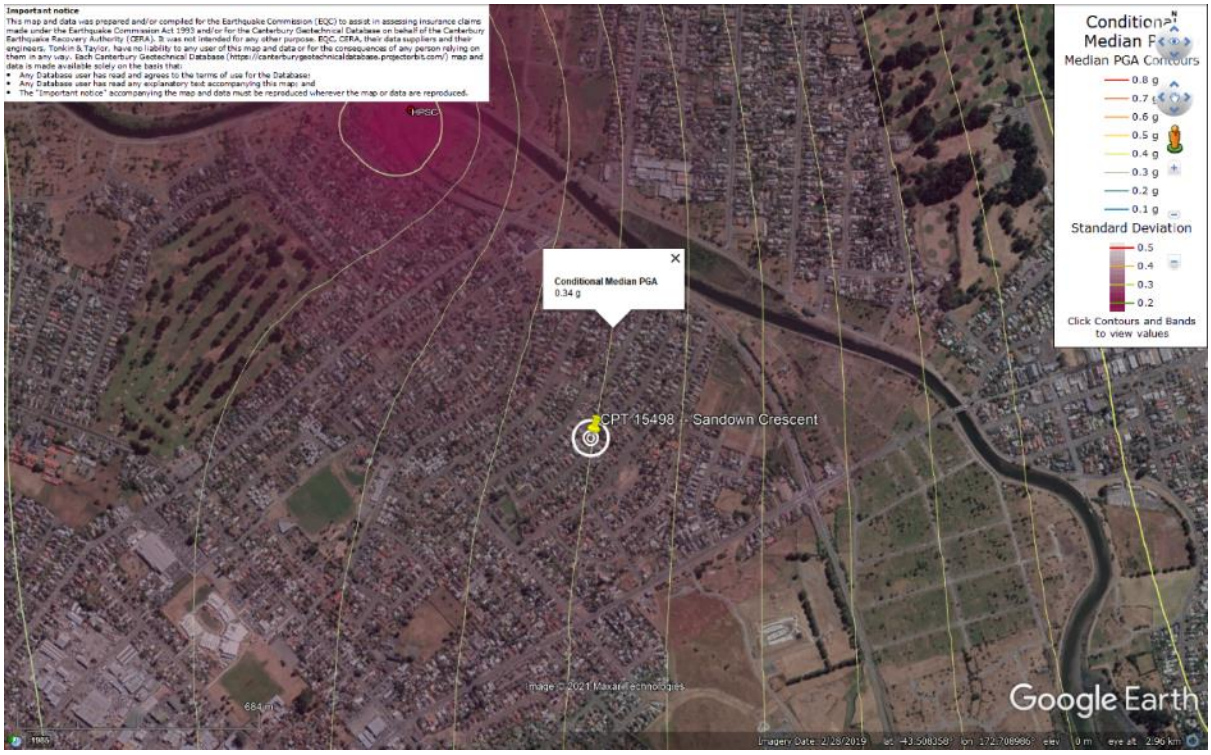

Figure 83: PGA for Dec-11 EQ (st. dev. = 0.350-0.375 ln units).

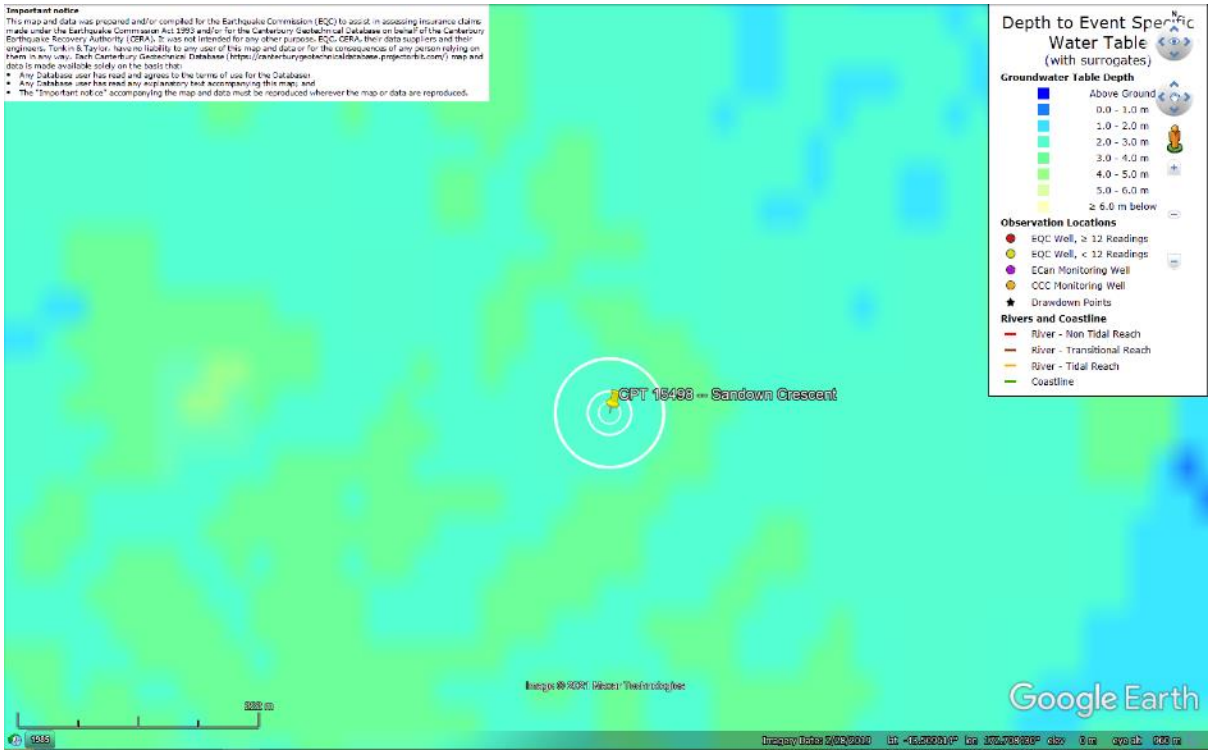

Figure 84: Depth to groundwater table for Sep-10 EQ.

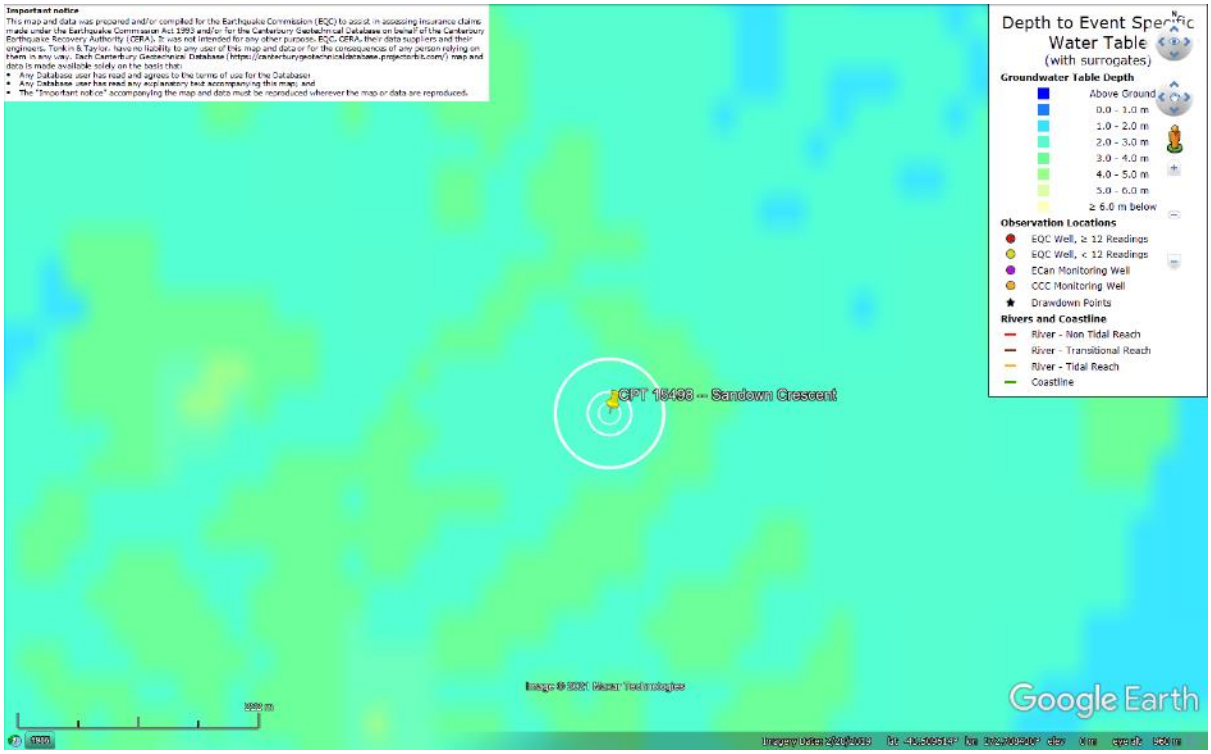

Figure 85: Depth to groundwater table for Feb-11 EQ.

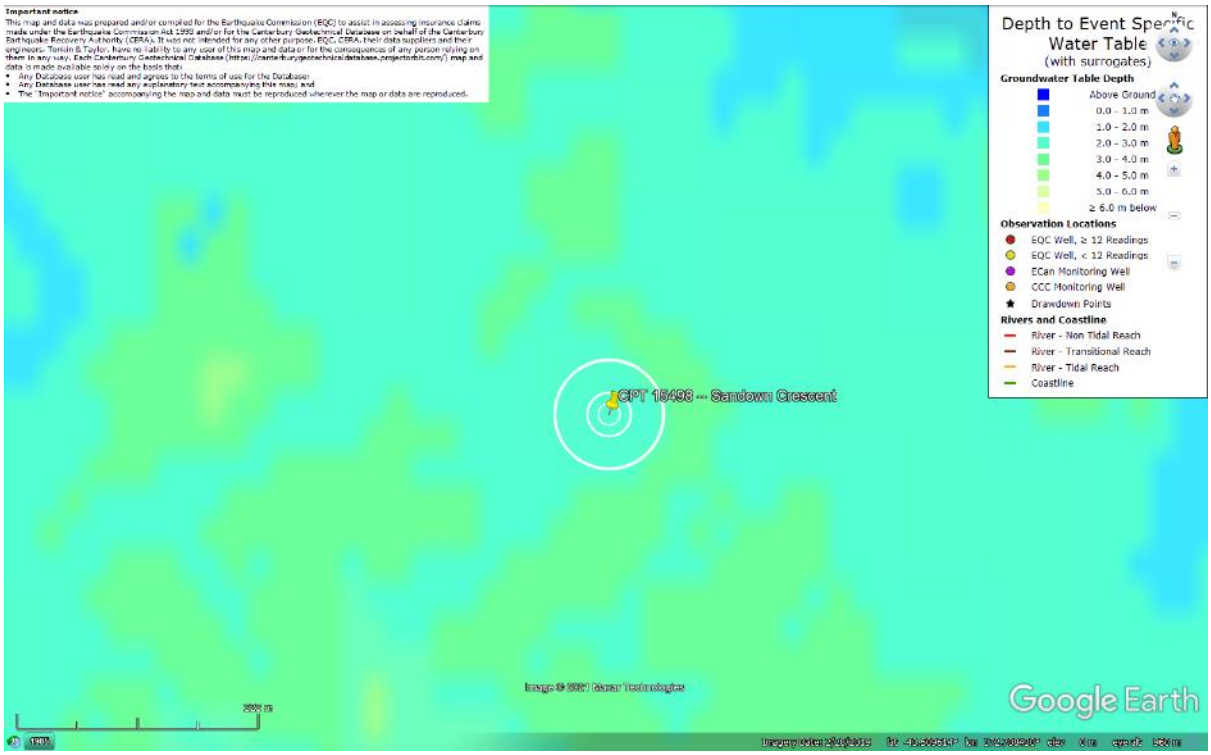

Figure 86: Depth to groundwater table for Jun-11 EQ.

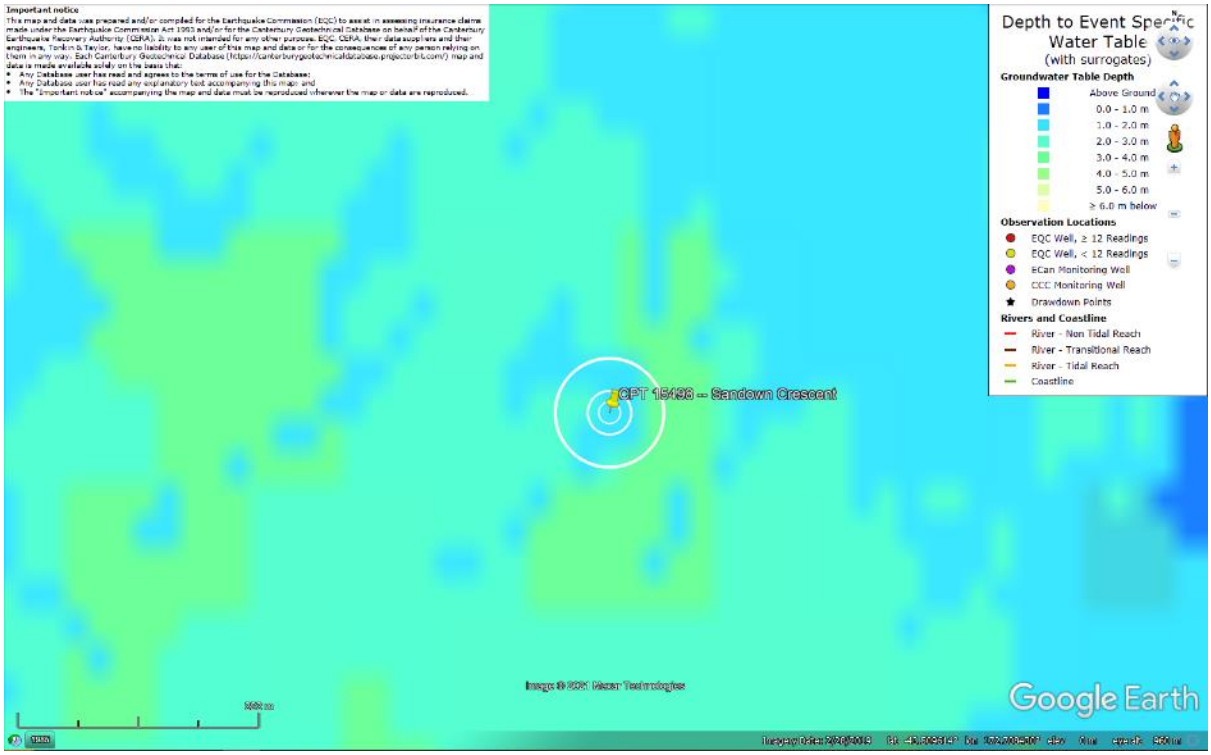

Figure 87: Depth to groundwater table for Dec-11 EQ.

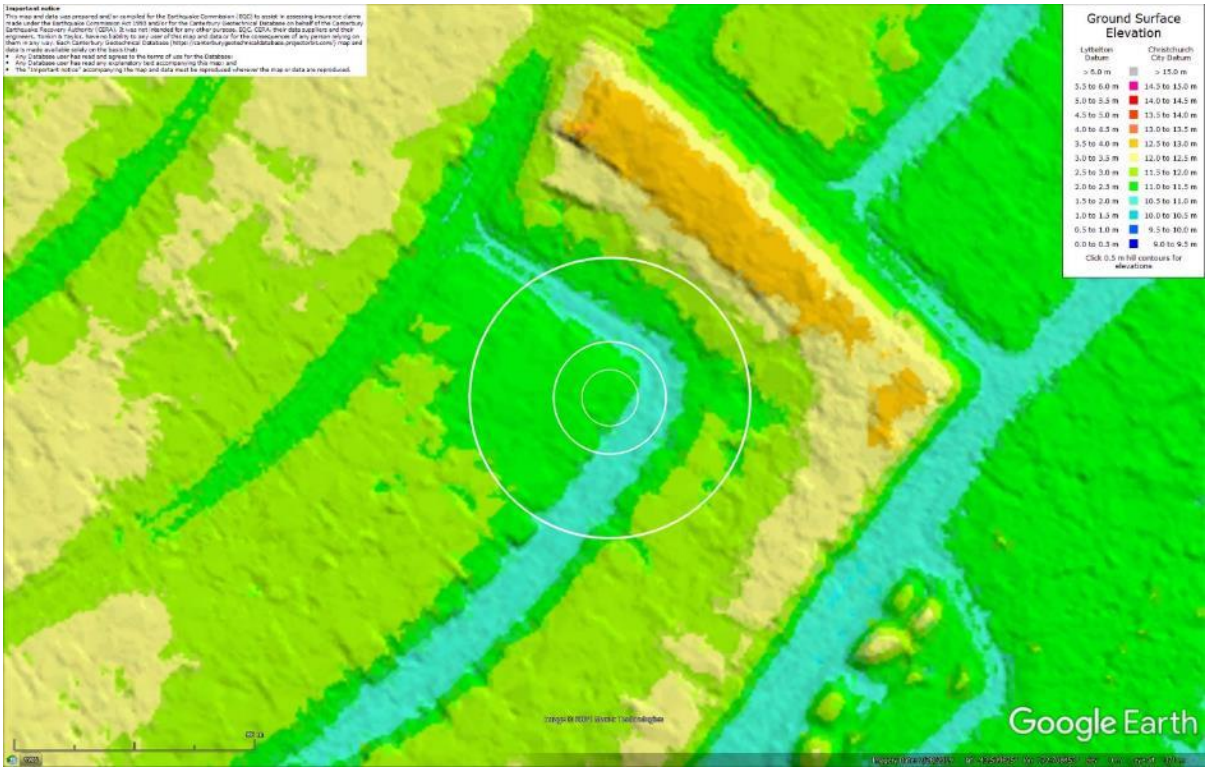

Figure 88: Ground surface elevation according to the Sep-11 LIDAR survey.

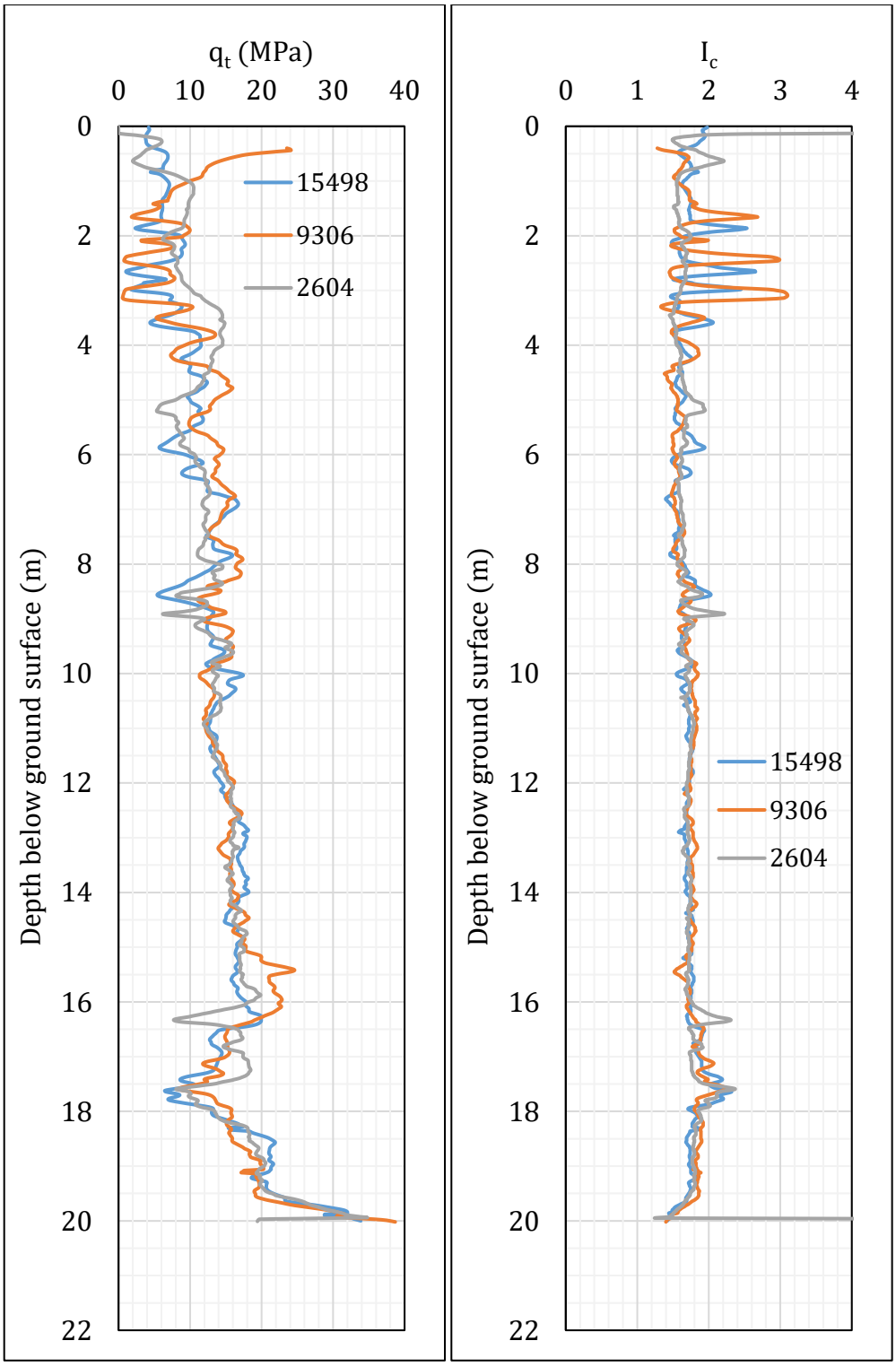

Figure 89: q_t and I_c profiles.

Note 9: The selection of CPTs for the area considered for settlement assessment (Figure 1) is based on the proximity of the CPTs to the considered areas. In accordance with that, the following table shows CPTs that were used for the volumetric settlement analysis in *Cliq v.3.0.3.2*, a CPT soil liquefaction software developed by GeoLogismiki. (The average volumetric settlements were reported in Table 8.)

Table 12: CPT profiles used in volumetric settlement analysis for areas selected for settlement assessment.

CPT ID No.	Patch A	Patch B	Road (20-m buffer)	Road (50-m buffer)
15498	✓	✓	✓	✓
9306		✓	✓	✓
2604				✓

Table 13: CPT-based results.

		CPT ID		
EQ Event	Parameter	15498	9306	2604
Sep-10	S_{V1D} (mm)	5	1	4
	LSN	1	0	1
	LPI	0	0	0
	LPI_{ish}	0	0	0
	$D_{FS<1}$ (m)	undet.	undet.	undet.
Feb-11	S_{V1D} (mm)	113	40	112
	LSN	19	9	15
	LPI	9	3	8
	LPI_{ish}	4	3	5
	$D_{FS<1}$ (m)	2.68	2.52	4.75
Jun-11	S_{V1D} (mm)	23	6	20
	LSN	4	2	3
	LPI	0	0	1
	LPI_{ish}	0	0	0
	$D_{FS<1}$ (m)	undet.	undet.	5.24
Dec-11	S_{V1D} (mm)	64	22	59
	LSN	12	6	10
	LPI	3	1	3
	LPI_{ish}	0	1	0
	$D_{FS<1}$ (m)	2.68	2.50	4.90

Notes: $D_{FS<1}$ = Depth to the first liquefiable layer ($FS_L<1$) that is at least 200-mm thick, as determined by the Boulanger and Idriss (2016) liquefaction-triggering procedure (P_L=50%, C_{FC}=0.13, and $I_{c,cutoff}$ =2.6), and exported from *Cliq v.3.0.3.2*; undet. = the specified soil layer was not detected.

Note 10: Based on the borehole log (BH 4416, Figure 1), the groundwater table is at a depth of 1.8 m below the ground surface. The soil profile consists of (1) topsoil (sandy silt with organics) to a depth of 0.2 m and (2) fine to medium sand, SP, of the Christchurch formation to a depth of 20 m.

Note 11: The ejecta-induced free-field settlement provided in Table 11 is an areal average settlement due to ejecta, which is based on the total settlement assessment area, A_T (provided in Table 9 and repeated in Table 14). However, the considered area was not always covered completely with ejecta; thus, it is important to provide the localized ejecta-induced settlement, too. The localized settlement due to ejecta is estimated using photographic evidence only as

$$S_{E,P\_localized} = \frac{V_E}{A_E}$$

where V_E is the total volume of ejecta within A_T and A_E is the total coverage area of ejecta within A_T. Please note that the areal ejecta-induced settlement provided in Table 14 as S_{E,P_areal} is the same as $S_{E,P}$ in Table 11, which was estimated as

$$S_{E,P\_areal} = S_{E,P} = \frac{V_E}{A_T}$$

where V_E is the total volume of ejecta within A_T and A_T is the total settlement assessment area.

Table 14a: Areal and localized ejecta-induced settlement estimates for Patch B (50-m buffer) based on photographic evidence.

Earthquake Event	A_T (m^2)	A_E (m^2)	V_E (m^3)	S_{E,P_areal} (mm)	$S_{E,P\_localized}$ (mm)
Sep-10	47.5	0	0	0	0
Feb-11	47.5	20.9	0.4-1.1	15±5	35±15
Jun-11	47.5	0	0	0	0
Dec-11	47.5	0	0	0	0

Notes: S_{E,P_areal} = $S_{E,P}$ reported in Table 11 = areal ejecta-induced settlement; $S_{E,P\_localized}$ = localized ejecta-induced settlement; A_T = total settlement assessment area; V_E = total volume of ejecta within A_T; A_E = total area of ejecta within A_T; The estimates of both areal and localized ejecta-induced settlement are rounded to the nearest 5; Final plus/minus values are also rounded to the nearest 5; NA = Not available.

Table 14b: Areal and localized ejecta-induced settlement estimates for Road (20-m buffer) based on photographic evidence.

Earthquake Event	A_T (m^2)	A_E (m^2)	V_E (m^3)	S_{E,P_areal} (mm)	$S_{E,P\_localized}$ (mm)
Sep-10	271	0	0	0	0
Feb-11	271	271	20.4-26.0	85±10	85±10
Jun-11	271	75.3	3.4-4.2	15±5	50±5
Dec-11	271	0	0	0	0

Notes: S_{E,P_areal} = $S_{E,P}$ reported in Table 11 = areal ejecta-induced settlement; $S_{E,P\_localized}$ = localized ejecta-induced settlement; A_T = total settlement assessment area; V_E = total volume of ejecta within A_T; A_E = total area of ejecta within A_T; The estimates of both areal and localized ejecta-induced settlement are rounded to the nearest 5; Final plus/minus values are also rounded to the nearest 5; NA = Not available.

Table 14c: Areal and localized ejecta-induced settlement estimates for Road (50-m buffer) based on photographic evidence.

Earthquake Event	A_T (m^2)	A_E (m^2)	V_E (m^3)	S_{E,P_areal} (mm)	$S_{E,P\_localized}$ (mm)
Sep-10	941	0	0	0	0
Feb-11	941	941	39.0-55.0	50±10	50±10
Jun-11	922	379	6.7-8.1	10±5	20±5
Dec-11	941	0	0	0	0

Notes: S_{E,P_areal} = $S_{E,P}$ reported in Table 11 = areal ejecta-induced settlement; $S_{E,P\_localized}$ = localized ejecta-induced settlement; A_T = total settlement assessment area; V_E = total volume of ejecta within A_T; A_E = total area of ejecta within A_T; The estimates of both areal and localized ejecta-induced settlement are rounded to the nearest 5; Final plus/minus values are also rounded to the nearest 5; NA = Not available.

Summary 2:

- **The best estimate of the localized ejecta-induced free-field ground settlement at the Sandown Cres site for the SEP 2010, FEB 2011, JUN 2011, and DEC 2011 earthquake is 0 mm, 35±15 mm, 0 mm, and 0 mm, respectively.**
- **The best estimate of the localized ejecta-induced settlement of the road at the Sandown Cres site for the SEP 2010, FEB 2011, JUN 2011, and DEC 2011 earthquake is 0 mm, 50±10 mm, 20±5 mm, and 0 mm, respectively.**